受入
'76-3-162
高工研図書室

Ref.TH.2136-CERN

THE ANALYTIC FOUNDATIONS OF REGGE THEORY

Alan R. White
CERN - Geneva

A B S T R A C T

Using Toller variables we write a fixed momentum transfer multi-dispersion relation. A multi-particle amplitude is broken down into spectral components corresponding to the physical region multiple discontinuities. Each component has the physical characteristic that it corresponds to a class of multiple scattering processes with a particular energy flow pattern in one physical region. Processes in different channels are related by signature.

Each spectral component has a unique cross-channel where it has a convergent partial wave expansion. We then show that the partial wave amplitudes can be continued into the complex plane of all total (cross-channel) angular momenta and sub-channel helicities. These continuations are sufficient to write Sommerfeld-Watson representations of all spectral components, and hence of amplitudes, which can be used to study both Regge and helicity pole limits.

We show that the spectral components diagonalize the cross channel unitarity relation asymptotically and so their partial wave continuations are sufficient for a complete analysis of this relation. From two-particle unitarity we show that a Regge pole in the elastic amplitude must be present in the angular momentum and helicity planes of all amplitudes and multi-Regge pole residues must factorize. We then prove the physical region factorization of multi-Regge pole amplitudes and give the structure of vertex functions.

From multi-particle unitarity we prove that multi-Regge cuts appear in all amplitudes. We derive a complete set of discontinuity formulae, which we express as a quasi-unitarity condition on Reggeons treated as non-relativistic quasi-particles.

A graphical analysis relating energy flow scattering diagrams and angular momentum coupling schemes plays a central rôle in the analysis.

Ref.TH.2136-CERN
16 February 1976

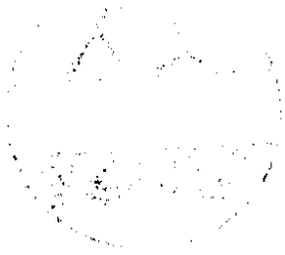

SECTION 1 INTRODUCTION

Regge poles [1] were first introduced into relativistic scattering theory nearly fifteen years ago [2,3]. The necessity for accompanying Regge cuts was discovered within two years [4-6]. The intervening years have seen a gradual improvement of our understanding of Regge theory but, particularly at the multiparticle level, the theory has remained incomplete with its fundamental status unclear. However, on the basis of recent progress, which I shall partially be reporting, I shall, in these lectures*), be able to give a complete and systematic development of the Regge theory of elastic and multiparticle amplitudes. The emphasis will be on the mathematical aspects of the theory. While I cannot strictly claim that the results I shall present are rigorous, I feel that they do provide a framework for a rigorous development of Regge theory. Of course, I also hope that the representations of amplitudes that I shall give will be used for studying the experimental implications of multi-Regge theory and in particular will lead to new experimental predictions.

My starting point will be the analyticity, unitarity, and crossing properties of amplitudes. The fundamental nature of these properties, together with the detailed analytic structure that follows from them, has been extensively discussed in preceding lectures. In particular, Stapp has described the multiparticle dispersion relations that we have derived, which incorporate the multiple discontinuity formulae derived by him and his collaborators. These dispersion relations are a generalization of the fixed momentum transfer dispersion relation for the four-point function.

There are many spectral contributions to each dispersion relation coming from the various multiple discontinuities present in each physical region contributing to the relation. The fundamental new feature of the development of Regge theory that we present here is that (essentially) each spectral component has a distinct Sommerfeld-Watson representation. Each component has a Froissart-Gribov continuation in a distinct set of angular momentum and helicity labels. These continuations are sufficient for the study of the Regge behaviour of all multiparticle amplitudes, since they allow both a complete analysis of the full multiparticle (cross-channel) unitarity relation, and the writing of Sommerfeld-Watson representations for each component.

---

*) The material presented in this paper is all original, although it was prepared in Lecture format to accompany lectures given at the Les Houches Institute of Theoretical Physics, June (1975). It will be published in the proceedings of this institute.

Given the existence of Regge poles in the elastic amplitude we can then prove that all multiparticle amplitudes must be Regge-behaved. Multi-Regge pole residues must factorize and the vertex functions must have a specific structure. Further, in all amplitudes Regge poles must be accompanied by an infinite set of Regge cuts satisfying unitarity-like discontinuity formulae in the angular momentum plane.

These results are most powerful when applied to diffraction scattering -- that is, the Pomeron. In a following series of lectures I shall present the Reggeon Calculus [7] as a field-theoretic technique for obtaining a general solution of the discontinuity formulae for a Pomeron pole with unit intercept. From this can be calculated the shape of the elastic diffraction peak at high energy together with the analogous behaviour of exclusive and inclusive diffraction processes. We can then claim that the diffraction peak has been calculated directly from unitarity, crossing, and analyticity, given only that diffractive processes factorize and that total cross-sections do not go to zero at asymptotic energies. (These two conditions tell us that the Pomeron is a single Regge pole with unit intercept -- we shall argue that it must be one or more poles.)

The layout of these lectures is as follows. I will begin by summarizing the background material that is needed for the rest of the lectures. This will include a brief description of the angular, or Toller variables we use together with their essential properties. I shall also state the results presented in Stapp's lectures in the form that I shall use them. These include the structure of physical region discontinuities and their contribution to the fixed momentum transfer dispersion relation.

Stapp has already described how the analytic properties of amplitudes simplify asymptotically when they are considered as functions of the angular variables with generalized momentum transfer variables held fixed and real. In particular the physical region singularity structure simplifies considerably and only multiple discontinuities in non-overlapping channel invariants contribute to the dispersion relation. Not only is this property apparently preserved in the complex plane, but the complex singularities seem to disappear asymptotically. The result is that we can describe the spectral contributions to the dispersion relation entirely in terms of the physical region structure. The spectral components have a simple physical interpretation in that they correspond to distinct sets of multiple scattering processes characterized by energy flow patterns. Each component also has a natural cross-channel where its multiple partial-wave expansion converges; where a Sommerfeld-Watson representation can be derived; and where the unitarity relation can be analysed. These new physical and mathematical features are compactly summarized by a graphical notation which I shall review, and which plays a central role in my analysis.

I shall describe the definitions of generalized Froissart-Gribov continuations of component partial-wave amplitudes in the relevant cross-channel. In this channel it is the total angular momenta and sub-channel helicities which can be continued into the complex plane. I shall show that we can Sommerfeld-Watson transform the associated sums in the partial-wave expansion while the remaining sub-channel angular momentum sums converge even in multi-Regge limits. The resulting representations can be used to study all Regge (and helicity) limits of the components and hence of complete amplitudes.

I shall then move on to the cross-channel unitarity relation. The central result for our analysis is that, for the particular purpose of discussing singularity structure in the angular momentum and helicity planes, the spectral components effectively diagonalize the unitarity relation. I shall not give a complete proof of this result in these lectures since at present I have only an outline argument. I am still working on the complete proof. Nevertheless, it is clear that the result depends crucially on the preservation of the direct-channel singularity structure in the complex plane referred to above. If true, the result provides an enormous simplification of the multiparticle unitarity equations, which is very naturally described by our graphical notation.

I shall first outline the argument for two-particle unitarity. After partial-wave projection and continuation of the equations, I show that a Regge pole in the elastic amplitude must be present in the angular momentum and helicity planes of the multiparticle component amplitudes. Further, multi-Regge pole residue functions must factorize. Given these results we can prove the Regge behaviour of our components in Regge and helicity limits directy from the Sommerfeld-Watson representations. I shall give the structure of vertex functions and indicate how the physical region factorization of multi-Regge pole amplitudes is proved.

Finally, I shall show why the spectral components should similarly diagonalize the multiparticle unitarity equations by using a generalization of an argument used by Mandelstam in his original discussion of Regge cuts. After partial-wave projection and continuation of these equations, I shall show how Regge cuts are generated and discuss how discontinuity formulae are proved.

Much of the material presented here is new and has not been published previously, although several of the basic ideas are certainly not new. I believe that the most attractive features of the development I shall give are its generality and its completeness. I shall be able to achieve a unification of several important developments in our understanding of the structure of multiparticle amplitudes which have taken place over the last several years. The most significant in my opinion are

a) the derivation of the momentum space analyticity properties of amplitudes which provide our starting point -- the physical region singularity structure has been completely determined by Stapp and collaborators [8] and contact made (via discontinuity formulae) with the Axiomatic Field Theory formalism of Bros, Epstein and Glaser [9];

b) the kinematic development, initiated by Toller [10], which provided the angular variables for an arbitrary amplitude in which we write multi-dispersion relations and describe multi-Regge behaviour;

c) the analysis of multiparticle cross-channel unitarity in the angular momentum plane given by Gribov, Pomeranchuk and Ter-Martirosyan [11].

Logically (c) should have succeeded (a) and (b); historically it came first, and thus suffered from many technical problems. A further technical point which is important in the unified development I shall give, is the discovery that multi-particle amplitudes can be continued in helicity planes when they cannot be continued in the associated angular momentum planes [12].

I shall present all the results from a general point of view to emphasize their completeness. It may help the reader to understand the details to look at as many particular examples as possible.

Finally, I would like to add that the complete picture presented here stems largely from work that I have been doing in collaboration with Henry Stapp. These lectures follow on naturally from his lectures. While I have tried to briefly summarize the essential results for the reader of these notes, a proper appreciation of the solid foundations on which I am building can only be obtained by studying the material in his courses.

I would also like to emphasize that the work I am reporting is still in progress and that there are several places where I would like to be able to give more details of results. Nevertheless, I am confident that the over-all picture that I shall present is correct and will survive the painful process of filling in the details.

SECTION 2 BACKGROUND MATERIAL

2.1 The Angular Variables

For a general N-particle amplitude, we call the set of tree diagrams involving only three-point vertices, the set of Toller diagrams. Each Toller diagram

specifies a complete set of variables for an amplitude. We shall give only brief details of the definition of these variables*). More details can be found in Refs. [10], [13], and [14]. Note that a Toller diagram is not initially drawn in a plane, and no planar ordering of the external particles is implied.

We allow momentum to flow through the tree diagram with momentum conserved at each vertex. We then define a set of three standard frames at each vertex in each of which one of the momenta entering the vertex has a standard form -- P_{i0} for external momenta P_i, Q_{i0} for internal momenta Q_i. We define Lorentz transformations ζ_{ij} linking two such standard frames at the same vertex, and "little group" Lorentz transformations g_i which link the standard frames at adjacent vertices in both of which $Q_i = Q_{i0}$.

To calculate an invariant variable $S_{ij} = (P_i + P_j)^2$ [or $(Q_i + P_j)^2$, or $(Q_i + Q_j)^2$] we start in the standard frame for P_j and transform through the tree diagram to the standard frame of P_i. This gives

$$S_{ij} = (P_{i0} + \xi_{in} g_n \zeta_{n,n-1} \cdots \zeta_{21} g_1 \zeta_{1j} P_{j0})^2 \tag{2.1}$$

The above procedure can be carried out either in a direct channel in which $t_i = Q_i^2 \leq 0 \; \forall \; i$ or in a cross-channel in which $t_i \geq 4m^2, \forall \; i$. (In general, these requirements will only be satisfied in part of a particular physical region.) In a cross-channel the g's are simply rotations. We can place the Q_0's (and P_0's) along the t-axis, define the ζ's to act in the (z-t) plane, and write

$$g_i = u_z(\mu_i) u_x(\theta_i) u_z(\nu_i) \qquad \begin{matrix} 0 \leq \theta_i \leq \pi \\ 0 \leq \mu_i \nu_i \leq 2\pi \end{matrix} \tag{2.2}$$

where u_z, u_x are rotations about the z and x axes, respectively. In a direct channel we would place the Q_0's along the z-axis and the g's would become SO(2,1) transformations. The two sets of variables thus introduced are related by analytic continuation with, for example, $z_i = \cos \theta_i \to \cosh \beta_i$, where β_i parametrizes an SO(2,1) boost.

Since the U_z rotations commute with the ζ-boosts we can reduce the number of azimuthal variables μ_i, ν_i as follows. For an *"i-vertex"* where two external particles enter the tree diagram, the invariants are independent of ν_i if g_i transforms *from* this vertex *to* a neighbouring vertex. For an *"i-j vertex"* where one external particle enters the diagram, the invariants depend only on

---

*) Note that my definition of these variables is slightly different from that used by Stapp in his lectures.

$$\omega_{ij} = \nu_i - \nu_j \ , \tag{2.3}$$

where g_i and g_j again transform *from* the vertex. For an internal or *"i-j-k vertex,* the invariants depend only on

$$\omega_{ij} = \nu_i - \nu_j \ , \quad \omega_{jk} = \nu_j - \nu_k \ , \quad \omega_{ki} = \nu_k - \nu_i \ . \tag{2.4}$$

Note that

$$\omega_{ij} + \omega_{ki} + \omega_{jk} = 0 \ . \tag{2.5}$$

Finally then we have a set of t-variables -- (N-3), one for each internal line; a set of z-variables -- (N-3); and a set of ω-variables -- (N-4) of which are independent, one for each *i-j* vertex and three, satisfying (2.5), for each *i-j-k* vertex. The total number of independent variables is therefore the correct 3N-10. These numbers can easily be checked for individual tree diagrams. For the elastic amplitude the single θ is simply the t-channel centre-of-mass scattering angle. The ω's or "Toller angles" are a feature of multiparticle amplitudes only.

Having selected a particular set of variables we will first discuss a particular direct channel parametrized (in part) by the following. For all internal lines connected only to *i* or *i-j* vertices

$$t_{i,j} < 0 \ , \quad z_{i,j} \geq 1 \ , \quad -1 \leq \cos \omega_{ij} \leq 1, \quad \forall \ \ i,j \ . \tag{2.6}$$

For lines connected to *i-j-k* vertices, there are two possibilities. We define

$$\lambda(t_i,t_j,t_k) = t_i^2 + t_j^2 + t_k^2 - 2t_it_j - 2t_jt_k - 2t_kt_i =$$

$$= (\sqrt{t_i} + \sqrt{t_j} + \sqrt{t_k})(\sqrt{t_i} - \sqrt{t_j} - \sqrt{t_k})(\sqrt{t_j} - \sqrt{t_k} - \sqrt{t_i})(\sqrt{t_k} - \sqrt{t_i} - \sqrt{t_j}) \ . \tag{2.8}$$

If $\lambda > 0$, then

$$t_{i,j,k} < 0 \ , \quad z_{i,j,k} \geq 1 \ , \quad -1 \leq \cos \omega_{ij,jk,ki} \leq 1, \quad \forall \ \ i,j,k \ . \tag{2.9}$$
$$z_{i,j,k} \leq -1$$

If $\lambda < 0$, the kinematics are more complicated [15] and the range of our variables becomes

$$t_{i,j,k} < 0 \ , \quad -\infty \leq i\, z_{i,j,k} \leq \infty \ , \quad |\cos \omega_{ij,jk,ki}| \geq 1, \quad \forall \ \ i,j,k \ . \tag{2.10}$$
$$(1 - z^2_{i,j,k})^{1/2} \geq 1$$
$$\leq -1$$

Formulae (2.6), (2.9), and (2.10) define a single direct channel with all other direct channels reached by changing the sign of one or more of the z's in (2.6) and (2.9), and in (2.10) changing the sign of $(1 - z_i^2)^{1/2}$, say. This transformation is used in the group-theoretic or TCP definition of signature [15]. Our analytic definition of signature will be similar. For this purpose we define a planar Toller diagram in a particular physical region as drawn in a plane with incoming particles entering the diagram from the bottom direction and outgoing particles exiting from the top. The change of sign of z_i [or $(1 - z_i^2)^{1/2}$] in (2.10) can be associated with a twist of one half of the diagram relative to the other about the i^{th} line. Note that for i-j-k vertices there are two planar Toller diagrams associated with a single physical region. They are related by a combination of three twist transformations.

There are also a set of cross-channels associated with a particular coupling scheme. For the moment we note only that these all satisfy

$$t_i \geq 4m^2 , \quad -1 \leq z_i \leq 1 , \quad -1 \leq \cos \omega_{ij} \leq 1, \quad \forall \quad i,j \tag{2.11}$$

and distinguish them only by the relative magnitude of the t's.

As an example of the above we have shown a Toller diagram for the six-point function in Fig. 2.1. The direct channels are represented by planar Toller diagrams shown in Fig. 2.2. The cross-channels are shown in Fig. 2.3. There are also TCP conjugate processes to all those shown.

We list the following properties of the angular variables as particularly useful for us.

a) If we define $v_i = e^{i\theta i}$ and $u_{ij} = e^{i\omega_{ij}}$ then all factors of i coming from the dependence of (2.1) on $\sin \theta_i$ and $\sin \omega_{ij}$ cancel. The relation between the invariants s_{ij} and the u's and v's is real and analytic.

b) When all the v's are large we obtain

$$\frac{s_{ij}}{2m^2} \sim \sinh \zeta_{in}\, v_n(\cosh \zeta_{n,n-1} + \cos \omega_{n,n-1})v_{n-1} \ldots v_2(\cosh \zeta_{21} + \cos \omega_{21})v_1 \sinh \zeta_{1j} . \tag{2.12a}$$

c) Similarly, when all the u's are large we obtain

$$\frac{s_{ij}}{2m^2} \sim \sinh \zeta_{in} \sin \theta_n\, u_{n,n-1}(\cos \theta_{n-1} + 1)u_{n-1,n-2} \ldots u_{32}(\cos \theta_2 + 1)u_{21} \sin \theta_1 \sinh \zeta_{1j} . \tag{2.12b}$$

d) When $z_i = v_i = \pm 1$, $(\theta_i = 0,\pi)$, the associated line can be contracted out of the tree diagram for the purpose of calculating invariants. The Toller angles at the contracted vertices are added or subtracted, according to whether $z_i = \pm 1$.

e) Similarly, when $z_i = \pm 1$, $z_j = \pm 1$, and $\cos \omega_{ij} = \pm 1$, both the i- and j-lines can be contracted from the diagram. Clearly, under analogous conditions any number of lines can be contracted out.

f) If P_i and P_j are separated by one internal line only, then s_{ij} is linearly related to the associated z.

The above properties can easily be verified by direct calculation.

2.2 Dispersion Relations and Physical Region Discontinuities (Stapps' Lectures)

To begin the analysis of an N-particle amplitude, we break the amplitude down into spectral components by writing a multiple dispersion relation.

We fix $t_i < 0, \forall\, i$; for i-j vertices we fix $|\cos \omega_{ij}| \leq 1$, and for i-j-k vertices we fix $\lambda(t_i,t_j,t_k) > 0$ and $|\cos \omega_{ij,jk,ki}| \leq 1$. We then disperse in the v-variables. The use of the v-variables at this stage is simply to avoid kinematic singularities. In defining Froissart-Gribov continuations later we shall essentially redisperse each spectral component that contributes to the present dispersion relation. We shall then use z- and u-variables.

A z_i-plane is covered separately by the regions $|v_i| \geq 1$, and $|v_i| \leq 1$ in the corresponding v_i-plane; $z_i \in (1,\infty)$ maps into $v_i \in (0,1)$, $(1,\infty)$, while $z_i \in (-\infty,-1)$ maps into $v_i \in (-\infty,-1)$, $(-1,0)$. Similarly, of course, the u_{ij}-plane also covers the $\cos \omega_{ij}$ plane twice.

The Bergman-Weil theorem*) tells us that, if the amplitude is polynomially bounded, we can write

$$A_N(\underset{\sim}{v},\underset{\sim}{\omega},\underset{\sim}{t}) = \sum_{\underset{\sim}{D}} (2\pi i)^{-N+3} \int_{\Delta_{\underset{\sim}{D}}} d\underset{\sim}{v}'\rho^{\underset{\sim}{D}}(\underset{\sim}{v}') \times \times \det\left[\underset{\sim}{q}^{D_1}, \underset{\sim}{q}^{D_2}, \ldots, \underset{\sim}{q}^{D_{N-3}}\right] + S \,, \tag{2.13}$$

*) My statement of this theorem is a little different from the more general statement given by Stapp.

where det[ ] denotes the determinant of the matrix formed by the (N-3) row vectors $\underset{\sim}{q}^{D_1}$, ..., $\underset{\sim}{q}^{D_{N-3}}$. The sum over $\underset{\sim}{D}$ is over the sets of (N-3) cuts D_1, ..., D_{N-3}, of the amplitude with non-zero multiple discontinuity (or spectral function) $\rho^{\underset{\sim}{D}}(\underset{\sim}{v})$ defined by

$$\rho^{\underset{\sim}{D}}(\underset{\sim}{v}) = \sum_{B} (-1)^{n_B} A_{NB} \ . \tag{2.14}$$

The sum over B is over all combinations of boundary-values onto the cuts D_1, ..., D_{N-3}, and n_B is the number of positive boundary values (chosen by convention). The $\underset{\sim}{q}^{D_i} = [q^{D_i}_{v_1}(\underset{\sim}{v},\underset{\sim}{v}'), \ldots, q^{D_i}_{v_{N-3}}(\underset{\sim}{v},\underset{\sim}{v}')]$ are generalized dispersion denominators which must only satisfy

$$\underset{\sim}{q}^{D_i} \cdot (\underset{\sim}{v}' - \underset{\sim}{v}) = 1 \quad \forall \quad D_i \tag{2.15}$$

and be analytic as functions of $\underset{\sim}{v}$ in the domain of analyticity of A_N when $\underset{\sim}{v}'$ lies on the D_i cut. S represents the remaining lower dimensional integrals, of the same form as that shown, and subtraction constants that will also be present. The construction of $\underset{\sim}{q}$-functions is generally straightforward, and a detailed discussion for normal threshold cuts can be found in Ref. [16].

From (2.6) and (2.9) we see that the physical regions fill the regions $|z_i| \geq 1 \ \forall i$ and there will be contributions to (2.13) from all possible (N-3) simultaneous discontinuities occurring in the physical regions. However, as Stapp has described, dispersing in the v (or equivalently z)-variables produces a remarkable simplification of the complicated analytic properties of multiparticle amplitudes. To describe these results we need a graphical notation (also used by Stapp) which will be central in our further analysis. We shall concentrate on the asymptotic singularity structure.

From a single planar Toller diagram we construct a set of tree-like diagrams called *"hexagraphs"* as follows. Every vertex in a hexagraph is drawn with 120° angles. An *i*-vertex is drawn with the i-line horizontal. An *i-j* vertex is replaced by two vertices in one of which the i-line is horizontal and in the other the j-line is horizontal. An internal *i-j-k* vertex is similarly replaced by three vertices. The vertices are joined by horizontal lines. External particles are still drawn upwards or downwards according to whether they are outgoing or incoming. We do not destrox the cyclic ordering at any of the vertices. The construction of hexagraphs is illustrated in Fig. 2.4.

From the set of hexagraphs we construct a further set of graphs called *"flow graphs"* as follows. Each vertex of a hexagraph is replaced by *"polygraphs"*, as shown in Fig. 2.5. If the horizontal lines of the hexagraph are contracted and

the adjacent sides of polygraphs sewn together, a unique flow graph results, as is illustrated in Fig. 2.6. In Section 5 we briefly discuss further hexagraphs and flow graphs formed by contracting the present set. The unique correspondence is maintained. We refer to the uncontracted sets of graphs as basic graphs.

A flow graph can be regarded as representing all (on-mass-shell) physical multiple scattering processes in which the energy flow corresponds to positive energy flowing upwards through each line of the flow graph. The individual scattering processes have thresholds which give rise to Landau singularities in the amplitude, including normal thresholds in each channel. We begin our summary of analytic structure by first discussing the normal threshold cuts.

By regarding a flow graph also as a Landau diagram we can associate with it the set of normal threshold cuts whose Landau diagrams can be obtained by contracting the flow graph. The first simplification of the analytic structure in z-space is that many normal threshold cuts coincide asymptotically. From the theorems presented by Stapp, ...

> *the sets of normal threshold cuts contained in the set of flow graphs associated with a Toller diagram are the only independent asymptotic cuts.*

For our purposes we can take the set of flow graphs associated with a Toller diagram to be the combination of sets associated with all the corresponding planar Toller diagrams.

A further simplification occurs because only certain combinations of imaginary parts for the invariant variables can be achieved by giving imaginary parts to the z (or equivalently the v) variables. [This can be verified asymptotically from (2.12), but in general it will hold outside of some finite domain in z-space.] Consequently, "bad invariant boundary-values", in which the analytically continued amplitude does not coincide with the unique functions satisfying the generalized Steinmann relations, are not exposed. As Stapp has described, this implies that

> *only multiple discontinuities (with known discontinuity formulae) from cuts in non-overlapping channels contribute to (2.13).*

This last result does not neglect the complicated Landau singularity structure which does give double discontinuities in overlapping channels in invariant space. It is a special property of using the z-variables.

A further simplification which goes a little beyond the results presented by Stapp is suggested by the simple example of the box diagram for the five-point function. This suggests that the boundary-value limitation also eliminates complex singularities in overlapping channel invariants asymptotically. If present, these would certainly destroy the "no overlapping cuts" physical region structure on which my analysis is based. I shall assume that it is a general result in z-space that double discontinuities in overlapping channels are not present in dispersion relations (outside of some finite domain at least).

Finally we note Stapp's discussion of complex singularities (triangles, for example) depending on non-overlapping channel invariants which disappear asymptotically into the real normal threshold cuts.

All of the above results combine to suggest that the asymptotic cut structure is just that given by the normal threshold cuts of the set of flow graphs. The multiple discontinuities also correspond to the sets of non-overlapping cuts in the flow graphs. Note that these occur in sets of (N-3) in the basic flow graphs, and no two basic flow graphs has a set of (N-3) non-overlapping cuts in common. This implies that the flow graphs classify the spectral components in a well-defined manner if we group together all multiple discontinuities occurring in the same flow graph. [The contracted flow graphs correspond to the lower dimensional integrals in S in (2.13).]

In finite z-space we expect complex cuts to protrude from the normal threshold cuts as illustrated in Fig. 2.7. We expect that these can be associated with a unique spectral component. They disappear asymptotically and lead to only minor modifications of the Froissart-Gribov continuations defined assuming (as we shall do) only the real normal threshold cut structure found in the physical regions.

We shall assume that the above results persist when we continue to positive t's. Again the simple examples support this. The simplification of analytic structure depends on features of the angular variables, such as the boundary-value property, which depend only on the t's being real and not on their sign.

Finally we consider the physical significance of the spectral components. Consider first the bubble diagram scattering expansion of a physical amplitude which is illustrated in Fig. 2.8 and which Stapp derived in his lectures. This expansion is very useful for discussing discontinuity formulae heuristically. It is also useful for intuitive discussions of the spectral decomposition achieved by our dispersion relations. The "structure theorem" given by Stapps and Iagolnitzer tells us that in discussing the physical region "positive-α" Landau singularities

we can ignore the structure of the "minus bubbles" in the bubble diagram functions of the scattering expansion. We can effectively treat them as point interactions. Therefore this expansion provides a direct way of writing an amplitude as a sum over amplitudes for all possible scattering processes in a particular physical region. The dispersion relation breaks an amplitude down into components corresponding to classes of scattering processes (not just in one channel but in all direct channels contributing to the dispersion relation). The spectral component corresponding to a particular flow graph arises from all scattering processes whose bubble diagram can be mapped onto the flow graph topologically. Equivalently, a flow graph corresponds to all scattering processes whose energy flow can be mapped onto the flow graph with positive energy flowing up every line of the flow graph.

The scattering processes picked out by the flow graphs associated with a particular Toller diagram are those whose energy flow is compatible with the kinematics of the associated multi-Regge limit. These are the processes which build up multi-Regge asymptotic behaviour. The remaining scattering processes either give Regge behaviour only in some sub-Regge limit defined by contracting the Toller diagram or in no limit associated with this particular diagram. If such a sub-Regge limit exists, it can be found by contracting the bubble diagram associated with a scattering process until it can be mapped onto a contraction of some flow graph associated with the Toller diagram. The relevant sub-Regge limit is described by similarly contracting the Toller diagram.

By classifying our spectral components by flow graphs, we add together the contributions of multiple discontinuities to (2.13) which are associated with the same flow graph. Intuitively we expect that it would be dangerous to separate them since they occur simultaneously in the bubble diagrams corresponding to many scattering processes. Mathematically the separation also seems dangerous since, as Stapp has described, their separation in (2.13) is a technically complicated procedure involving the artificial introduction of functions defined to satisfy generalized Steinmann relations.

SECTION 3 PARTIAL-WAVE EXPANSIONS, FROISSART-GRIBOV CONTINUATIONS, AND SOMMERFELD-WATSON REPRESENTATIONS

3.1 Partial-Wave Expansions

We begin by noting that each spectral component represented by a basic flow graph can immediately be related to a unique cross-channel. So far we have regarded the associated hexagraph as representing direct-channel scattering in the vertical

direction. However, we can also regard the diagram as representing cross-channel scattering in the horizontal direction with, say, the incoming particles entering from the left and the outgoing particles moving to the right.

We introduce signature by noting that if we twist the set of hexagraphs for a single planar Toller diagram about a particular horizontal line of each graph then we obtain the set of hexagraphs for a new planar diagram. This new set will correspond to a completely new set of flow graphs. However, each twisted hexagraph still corresponds to the same cross-channel. Therefore, when we discuss a particular hexagraph we will implicitly consider simultaneously also all the sets of hexagraphs obtained from the initial graph by the twist operation. The associated spectral regions will lie in different half-planes of the relevant angular variables and so just add signature factors to our Froissart-Gribov continuations and Sommerfeld-Watson representations.

The next point we note is that all the cuts of a basic flow graph are either in momentum transfer variables or cross-energy variables in the associated cross-channel. There are no cuts in sub-energy channels, that is in invariants of the form

$$s_i = \left(\sum_{n_i} P_{n_i} \right)^2 , \tag{3.1}$$

where the P_{n_i} are all incoming or all outgoing momenta. Spectral component amplitudes with just two initial particles in the cross-channel have no cross-energy channels, and so for them we immediately obtain the result that in the cross-channel there are no physical region singularities in the z- or ω-variables. For amplitudes with cross-energy channels we must choose the t-variables more carefully to obtain no physical region singularities. We return to this point later.

In general we shall ignore the contracted flow graphs and hexagraphs. As we have noted they correspond to the term S in (2.13) and they will simply be degenerate cases of the following analysis.

To write a partial-wave expansion for a particular component or hexagraph we shall find it convenient to introduce some new notation. We associate a z_i and conjugate angular momentum j_i with each horizontal line of the hexagraph, and with each sloping line we associate an ω_i and a conjugate helicity n_i. This is done as follows. At i-j vertices we simply associate ω_{ij} with the sloping line, while at i-j-k vertices where i, say, is horizontal, we associate ω_{ij} and ω_{ik} with the j- and k-lines. Examples of this relabelling are shown in Fig. 3.1.

Next we break the hexagraph down into *"sub-graphs"* by cutting each sloping line in the centre. This breaks a hexagraph into sub-graphs of the form T_i, D_i, and V_i shown in Fig. 3.2. The different forms of D_i and V_i that we have shown are simply related by the twist operation. Examples of the breakdown of hexagraphs are shown in Fig. 3.3. Our external particles are spinless and so carry zero helicity, although spinning particles could easily be introduced into the formalism.

To construct partial-wave expansions we note that T_i is analogous to a 2-2 scattering amplitude. If the scattering takes place through a state with angular momentum j_i then

$$T_{j_i} \propto d^{j_i}_{n_{i_1}+n_{i_2},\, n'_{i_1}+n'_{i_2}}(z_i) \equiv d^{j_i}_{n,n'}(z_i) \ , \tag{3.2}$$

where $d^j_{n,n'}(z)$ is the usual SO(3) representation function. Similarly D_i is analogous to a transition (or decay!) from a state with helicity n_{i_1} into a two-particle state with helicities n'_{i_1} and n'_{i_2}, and we write

$$D_{j_k} \propto u^{n_1}_k \, d^{j_k}_{n_{k_1},\, n'_{k_2}+n'_{k_3}}(z_k) \equiv u^n \, d^{j_k}_{n,n'}(z_k) \ . \tag{3.3}$$

Finally, V is like a virtual transition, and we write

$$V_{j_\ell} \propto u^{n_{\ell_1}}_{\ell_1} \, d^{j_\ell}_{n_{\ell_1},\, n'_{\ell_1}}(z_\ell) u^{n'_{\ell'_1}}_{\ell'_1} \equiv u^n \, d^{j_\ell}_{n,n'}(z_\ell) u'^{n'} \ . \tag{3.4}$$

We have indicated an economy of notation in (3.2)-(3.4), which we shall follow. We omit suffixes from n's, u's, and ω's when the context makes the suffixes obvious.

To write the complete partial-wave expansion for a spectral component A_s, we first write the decomposition of A_s into sub-graphs symbolically. (Note that we shall use a single hexagraph to represent A_s although we are now grouping all the hexagraphs related by twisting together.) For example, if A_s is represented by the first hexagraph of Fig. 3.2, we write

$$A_s = TDD \ . \tag{3.5}$$

Then using (3.2)-(3.4) we write, suppressing t-labels,

$$A_s(\underset{\sim}{z},\underset{\sim}{u}) = \sum_{\underset{\sim}{j},\underset{\sim}{n}} T_{j_1} D_{j_2} D_{j_3} f_{\underset{\sim}{j}\underset{\sim}{n}} \ , \tag{3.6}$$

where $\underset{\sim}{j} = (j_1,j_2,j_3)$, and in this case (referring to Fig. 3.1 for notation) we see that $\underset{\sim}{n} = (n_1,n_2)$ and

$$T_{j_1} = d^{j_1}_{0n_1}(z_1) \ , \quad D_{j_2} = u_1^{n_1}\, d^{j_2}_{n_1n_2}(z_2) \ , \quad D_{j_3} = u_2^{n_2}\, d^{j_3}_{n_2,0}(z_3) \ ; \tag{3.7}$$

$f_{\underset{\sim}{j}\underset{\sim}{n}} = f_{j_1j_2j_3n_1n_2}$ is the "partial-wave" amplitude for the combination of processes $T_{j_1}, D_{j_2} D_{j_3}$.

The partial-wave expansion for a general hexagraph is constructed by first writing it in a symbolic form analogous to (3.5) and then converting to an explicit form using (3.2)-(3.4). Since our spectral components have no (cross-channel) physical region singularities in the z or ω variables, these expansions will certainly converge in some domain in the product of the $\underset{\sim}{z}$ and $\underset{\sim}{\omega}$ planes which includes the physical region.

We next define projection operators

$$\int T^{-1}_{j_i} = \frac{1}{2(2j_i+1)} \int_{-1}^{+1} dz_i \; d^{j_i}_{n'n}(z_i) \ , \tag{3.8}$$

$$\int D^{-1}_{j_k} = \frac{1}{4\pi(2j_k+1)} \int_{-1}^{+1} dz_k \; d^{j_k}_{n'n}(z_k) \int_{|u|=1} du\; u^{-n-1} \ , \tag{3.9}$$

$$\int V^{-1}_{j_\ell} = \frac{1}{8\pi(2j_\ell+1)} \int_{\substack{|u|=1\\|u'|=1}} du\, du'\; u^{-n-1}\, u'^{-n'-1} \int_{-1}^{+1} dz_\ell \; d^{j_\ell}_{n'n}(z_\ell) \ . \tag{3.10}$$

The general projection formula for a partial-wave amplitude can then be written in the form

$$f_{\underset{\sim}{j}\underset{\sim}{n}} = \prod_i \int T^{-1}_{j_i} \prod_k \int D^{-1}_{j_k} \prod_\ell \int V^{-1}_{j_\ell} \; A_s(\underset{\sim}{z},\underset{\sim}{u}) \ . \tag{3.11}$$

For the particular case of (3.6) we obtain

$$f_{\underset{\sim}{j}\underset{\sim}{n}} = \int T^{-1}_{j_1} \int D^{-1}_{j_2} \int D^{-1}_{j_3} \; A_s(\underset{\sim}{z},\underset{\sim}{u}) \ . \tag{3.12}$$

3.2 Froissart-Gribov Continuation

Next we sketch the definition of a generalized Froissart-Gribov continuation of a partial-wave amplitude $f_{\underset{\sim}{j}\underset{\sim}{n}}$. This is a particularly technical subject, but since

the rest of our analysis depends on the existence of these continuations, we shall try to give a detailed enough treatment to show that the method we outline is completely general.

As we have said, we group together all spectral components with hexagraphs related by twisting, and use only one hexagraph to represent each set. Beyond this, each spectral component has a Froissart-Gribov continuation in a different subset of the $\underset{\sim}{j}$ and $\underset{\sim}{n}$ labels. This subset can be read off from the hexagraph as follows.

In each $V^{-1}_{j_\ell}$ [appearing in (3.11)] we can take n_{ℓ_1} complex with $(j_\ell - n_{\ell_1})$ and $(n_{\ell_1} - n_{\ell_1'})$ held fixed at integer values. In each $D^{-1}_{j_k}$ we can take n_k and $n_{k'}$ $(= n_{k_1'} + n_{k_2'})$ complex with $(j_k - n_k)$ fixed at an integer. In each $T^{-1}_{j_i}$ we can take all three of j_i, n_i, and n_i' complex. (Note that each n-label appears in two sub-graphs, although the corresponding u is associated with only one sub-graph.) In other words, the helicity labels, which are attached to sloping lines of the hexagraph, are always coupled (that is, differ only by an integer) to the angular momentum associated with the corresponding horizontal line of the hexagraph.

It is interesting to note that the continuations we make correspond, in the case when no V's are present in the hexagraph, to continuing the total cross-channel angular momentum to complex values together with all the helicities of (cross-channel) sub-channels. In no case is the angular momentum of a sub-channel continued separately from the helicity. When V's are present the total angular momentum of the cross-channel is not used as a variable. Instead, the scattering can be regarded as made up of sub-processes for which the total angular momenta and sub-channel helicities are analytically continued.

We shall make all our continuations from positive values of the n-labels. Continuations from some negative n can always be achieved by essentially taking the corresponding $u \to 1/u$ in the following.

We shall treat each spectral component as if it has only the real normal threshold cuts obtained by contracting the flow graph (or equivalently normal thresholds in those channels which appear when horizontal cuts are made through the flow graph). As we have said, we believe this is the correct asymptotic singularity structure and the presence of complex singularities in some finite domain will not significantly alter our results.

Comparing (2.12a) and (2.12b), we see that the asymptotic singularity structure in the u-planes will be very similar to that in the v-planes and we shall exploit this. Our Froissart-Gribov continuations will be defined (essentially) by dispersing

a spectral component in the z_i's associated with the T_i's, the u_k's associated with the D_k's, and the products $u_{\ell_1}u_{\ell_1'}$ for each of the V_ℓ's. In terms of the original dispersion variables we simply replace some z's by associated u's and so we still disperse in (N-3) variables. From inspection of the flow graph it can also be checked that the cuts of a spectral component A_s occur (asymptotically) in the variables $z_i, u_k z_k$, and $u_{\ell_1}u_{\ell_1'}z_\ell$ only. Consequently the theorems given by Stapp, which we reviewed in the last section, apply directly when we disperse in the z_i's, the u_k's and the $u_{\ell_1}u_{\ell_1'}$'s.

Whenever it is necessary to locate the positions of cuts in our manipulations we shall proceed as follows. Since there are no cuts in the physical region $|u| = 1$, $-1 \leq z \leq 1$ $\forall$ z,u, we can show from property 2(a) that all intersections of real cuts in the invariant variables that we consider occur at real values of the relevant angular variables. By starting with the simplest invariant and working upwards, we can show that such intersections are confined to the product of either the left- or right-hand axes of each variable. Whether the left- or the right-hand axis is involved can be determined from the asymptotic formulae (2.12a) and (2.12b). Since the absence of physical region singularities is important in this procedure, we must return to the problem of singularities in cross-energy channels.

Cross-energy channel invariants can always be regarded as generalized momentum transfer variables for an unequal mass four-point function. This is illustrated in Fig. 3.4. The "masses" are determined by both angular variables and t's in our case. However, it is a well-known property of unequal mass kinematics that the positive physical-range of a momentum transfer variable (S_c) shrinks to zero as the total energy (t in Fig. 3.4) is increased. Therefore, by increasing the total cross-channel energy relative to the other t-variables we can always separate the cross-energy cuts so that they lie entirely on the right- or left-hand axes of our variables (which is sufficient to define Froissart-Gribov continuations satisfying the Carlson condition and to Sommerfeld-Watson transform the partial-wave expansion) or we can remove them from the physical region altogether.

Finally we begin the construction of our Froissart-Gribov amplitudes. We shall concentrate on the V's first, then the D's, and finally the T's. The V's can be associated with *"V-lines"* in the flow graph that cut the graph into two *"pieces"*. Examples are shown in Fig. 3.5. This result is a simple consequence of the "sewing" procedure that we used to form the flow graphs. Each "piece" contains one T and in general many D's.

We first define a new amplitude $\tilde{A}_s$ by performing the z_ℓ integrations in each of the $\int V^{-1}$ projections; that is, we write

$$\tilde{A}_s(\underset{\sim}{z}_i,\underset{\sim}{z}_k,\underset{\sim}{u}) = \int_{-1}^{+1} d\underset{\sim}{z}_\ell \, A_s(\underset{\sim}{z}_i,\underset{\sim}{z}_k,\underset{\sim}{z}_\ell,\underset{\sim}{u}) \ . \tag{3.13}$$

The cuts of $\tilde{A}_s$ will include those cuts of A_s which are independent of $\underset{\sim}{z}_\ell$, together with cuts from collisions of the cuts of A_s with the end-points $\underset{\sim}{z}_\ell = (\pm 1, \pm 1, \ldots)$. (Note that A_s has no cuts depending on $\underset{\sim}{z}_\ell$ only, and it can be shown that all cuts from pinches of the $\underset{\sim}{z}_\ell$-integration lie within the cuts associated with end-point collisions.) From property 2(d) of the angular variables the "end-point" cuts can be located by simply contracting the ℓ-lines out of the Toller diagram. All such cuts will be functions of the variables $u_\ell = u_{\ell_1} u_{\ell_1'}$ or $u_{\ell'} = u_{\ell_1}/u_{\ell_1'}$ associated with each ℓ. Also, a cut which is a function of u_ℓ, say, has no double discontinuity with a cut which is a function of the corresponding $u_{\ell'}$. This is because the first cut is generated by a collision at the $z_\ell = +1$ end-point, while the latter cut is generated at $z_\ell = -1$.

Since $\tilde{A}_s$ has no cuts depending on just u_{ℓ_1} or $u_{\ell_1'}$ (for any ℓ), if we write

$$\int_{\substack{|u_{\ell_1}|=1 \\ |u_{\ell_1'}|=1}} du_{\ell_1} \, du_{\ell_1'} \, u_{\ell_1}^{-n_{\ell_1}-1} \, u_{\ell_1'}^{-n_{\ell_1'}-1} \, \tilde{A}_s = \tag{3.14}$$

$$= -\frac{1}{2} \int_{\substack{|u_\ell|=1 \\ |u_{\ell'}|=1}} du_1 \, du_{\ell'} \, u_\ell \frac{-(n_{\ell_1}+n_{\ell_1'})-1}{2} \times u_{\ell'} \frac{-(n_{\ell_1}-n_{\ell_1'})-1}{2} \tilde{A}_s$$

we can move either the u_ℓ or the $u_{\ell'}$ contour out to infinity and wrap it around the cuts of $\tilde{A}_s$ as in Fig. 3.6. We cannot move both contours out, since there is no relevant double discontinuity. In this case we anticipate that the amplitude $\tilde{A}_s$ will not be Regge behaved as $u_\ell, u_{\ell'} \to \infty$ and so the behaviour at ∞ will prevent simultaneous manipulations of both the u_ℓ and $u_{\ell'}$ contours.

To define a continuation of $\int V_{j_\ell}^{-1}$ from integer $n_{\ell_1}, n_{\ell_1'} > 0$ to complex $n_{\ell_1}, n_{\ell_1'}$ with $N_{\ell_1} = j_\ell - n_{\ell_1'}$ and $N_\ell = n_{\ell_1'} - n_{\ell_1}$ held fixed, we move the u_ℓ contour out and hence write

$$\int V^{-1}_{\tau_\ell \underset{\sim}{N}_\ell}(n_{\ell_1}) = \frac{1}{8\pi}\left\{\int_{\Delta_R} du_\ell\, u_\ell^{-n_{\ell_1}-1} - \tau_\ell \int_{\Delta_L} du_\ell\, (-u_\ell)^{-n_{\ell_1}-1}\right\}\times \tag{3.15}$$

$$\times \frac{1}{(2n_{\ell_1} + 2N_\ell + 1)} \int_{|u_{\ell'}|=1} du_{\ell'}\, u_{\ell'}^{-N_\ell-1} \int_{-1}^{+1} dz_\ell\, d^{n_{\ell_1}+N_{\ell_1}}_{n_{\ell_1},n_{\ell_1}-N_\ell}(z_\ell)\ ,$$

where Δ_R and Δ_L indicate integrations around the cuts of $\tilde{A}_s$ in the right- and left-half u_ℓ-planes, respectively. We emphasize that the z_ℓ integration must be performed before the u_ℓ contour is determined; τ_ℓ is of course a signature label which is ± 1 according to whether n_ℓ is even or odd.

If (3.15) is used to replace $\int V^{-1}_{j\ell}$ in (3.11) then the resulting expression defines a continuation of $f_{j\underset{\sim}{n}}$ to complex n_{ℓ_1} with N_{ℓ_1} and other differences of helicities and angular momenta held fixed. The Carlson condition for uniqueness,

$$f_\tau(n) \underset{\substack{n\to\infty \\ \text{Re } n>0}}{\lesssim} e^{\theta|n|} \qquad \theta < \pi/2\ , \tag{3.16}$$

is satisfied by $f_{j\underset{\sim}{n}\tau_\ell}(n_{\ell_1})$ by virtue of the asymptotic results,

$$u^{-n-1} = e^{(-n-1)\log u} \underset{n\to\infty}{\to} 0, \qquad u > 1 \tag{3.17}$$

and

$$d^{n_1+N}_{n_1,n_1-M}(z) \underset{n_1\to\infty}{\sim} e^{n_1\left[\ln\,(1-z^2/4)\right]} \to 0, \qquad -1 \le z \le 1\ . \tag{3.18}$$

The absence of double discontinuities in u_ℓ and $u_{\ell'}$ also implies that if we define

$$A_{s\underset{\sim}{\ell}} = \prod_\ell \int V^{-1}_{\tau_\ell \underset{\sim}{N}_\ell}(n_{\ell_1})\, A_s \tag{3.19}$$

then there will be no pinching of the integration contours, and $A_{s\underset{\sim}{\ell}}$ will have cuts in only those invariant variables which are independent of both $u_{\underset{\sim}{\ell}}$ and $u_{\underset{\sim}{\ell}'}$. Therefore we can discuss the cut structure of $A_{s\underset{\sim}{\ell}}$ entirely in terms of the cut structure of the *"pieces"* of the flow graph separated by V-lines. That is, only normal threshold cuts associated with cuts through a single "piece" are present in $A_{s\underset{\sim}{\ell}}$.

Each piece has a general "spike-like" shape, of which some examples are shown in Fig. 3.7 together with their associated hexagraphs. Each piece now contains one T and in general many D's. Our next task will be to deal with the D's. We shall

illustrate this with the simplest piece -- the simple *spike* shown in Fig. 3.7. From the hexagraphs we can see that the most complicated piece has chains of D's which split, attached to each leg of the T. The spike has just two chains which do not split. However, the general method should be clear.

For a general cut through a spike, for example S_{ab} in Fig. 3.7, we see from (2.12b) that for large u's

$$S_{ab} \sim u_m \cdots u_1 u_{1'} \cdots u_{m'} , \tag{3.20}$$

where the cut passes through the $(m+1)^{th}$ and $(m'+1)^{th}$ lines down from the peak on the left- and right-hand sides, respectively; $u_1, \ldots, u_m$ and $u_{1'}, \ldots, u_{m'}$ are associated with the intervening lines.

Now suppose that m and m′ are the total number of lines on either side of the peak, which we label by i. We can write

$$\int D_{j_1}^{-1} \cdots \int D_{j_m}^{-1} \int D_{j_{1'}}^{-1} \cdots \int D_{j_{m'}} \propto \int dz_m \prod_{k=1}^{m} d_{nn'}^{j_k}(z_k) \int dz_{m'} \prod_{k=1'}^{m'} d_{nn'}^{j_k}(z_k) \times$$

$$\times \int du_{i_1} \cdots du_{i_m} u_{i_1}^{-n_{i_1}-1} \cdots u_{i_m}^{-n_{i_m}-1} \int du_{i_{1'}} \cdots du_{i_{m'}} u_{i_{1'}}^{-n_{i_{1'}}-1} \cdots u_{i_{m'}}^{-n_{i_{m'}}-1} , \tag{3.21}$$

where $u_{ir} = u_1 u_2, \ldots, u_r$, and $u_{ir'}$ is similarly defined; $n_{ik} = n_k - n_{k+1}$ and $n_{m+1} = n_{m'+1} = 0$. Since each invariant cut S_{ab} asymptotically lies in a single u_{ir} or $u_{ir'}$ plane, or in the product of two such planes, it is clearly convenient to use the u_{ir} and $u_{ir'}$ variables as our dispersion variables.

If we now disperse $A_{s\underset{\sim}{\ell}}$ in the u_{ir} and $u_{ir'}$ variables, we will separate the cuts lying in $u_{ir} \gtrless 1$ into distinct spectral components. This ensures that if we define

$$A_{s\underset{\sim}{\ell}\underset{\sim}{k}} = \prod_k \int D_{j_k}^{-1} A_{s\underset{\sim}{\ell}} \tag{3.22}$$

and substitute the dispersion relation for $A_{s\underset{\sim}{\ell}}$ then move out the u_{ir}, $u_{ir'}$ contours in Fig. 3.6, we will pick up just the multiple discontinuities of $A_{s\underset{\sim}{\ell}}$ lying in $|u_{ir}| > 1 \; \forall \; r$, $|u_{ir'}| > 1 \; \forall \; r'$. This leads us to define a continuation of $\int D^{-1}$ from $n_{ir} \geq 0$, with $N_{ir} = j_r - n_r$ fixed, as follows. We define

$$\int D^{-1}_{\tau_{ir}N_{ir}}(n_{ir}) = \frac{1}{4\pi(2N_{ir}+2n_r+1)} \int_{-1}^{+1} dz_r \, d^{N_{ir}+n_r}_{n_r,n_{r+1}}(z_r) \left\{ \int_{\Delta_R} du_{ir}(u_{ir})^{-n_{ir}-1} - \tau_{ir} \int_{\Delta_L} du_{ir}(-u_{ir})^{-n_{ir}-1} \right\}, \tag{3.23}$$

where now the Δ_R and Δ_L integrations are given by the spectral regions of $A_{s\underset{\sim}{\ell}}$ and must be determined before any of the z_r integrations are performed. This is a bit cumbersome but the advantages of some sort of "factorized" notation should be clear. If (3.23) is substituted for $\int D^{-1}_{jk}$ in (3.11), then a continuation satisfying the Carlson condition in all helicities is defined provided that all the differences of angular momenta and helicities are held fixed at integer values. Again this follows from (3.16)-(3.18).

At this stage we have sets of $(N-3-N_T)$ cuts of A_s contributing to (3.15) and (3.23), where N_T is the number of T's in the hexagraph (note that $N_T = N_V + 1$, where N_V = number of V's). The only cuts still not accounted for are in those invariants linearly related to the z_i's associated with the T_i's. The discussion of the $\int T_i^{-1}$ projection is now straightforward. We extend the definition of $A_{s\underset{\sim}{\ell}\underset{\sim}{k}}$ by writing

$$A_{s\underset{\sim}{\ell}\underset{\sim}{r}\underset{\sim}{r}'}(\underset{\sim}{z}_i) = \prod_{m=r,r'} \int D^{-1}_{\tau_{im}N_{im}}(n_{im}) \int V^{-1}_{\tau_\ell \underset{\sim}{N}_\ell}(n_\ell) \, A_s \; ; \tag{3.24}$$

$A_{s\underset{\sim}{\ell}\underset{\sim}{r}\underset{\sim}{r}'}(\underset{\sim}{z}_i)$ will, of course, be a function of the τ, n, and N labels associated with the D^{-1}'s and V^{-1}'s. However, we are interested in it as a function of the z_i's. Again there are no fixed-cuts in any of the z_m-planes, and all the important cuts generated by the $\underset{\sim}{z}_m$, $\underset{\sim}{z}_\ell$, and $\underset{\sim}{u}$ integrations are end-point singularities. The cuts of $A_{s\underset{\sim}{\ell}\underset{\sim}{r}\underset{\sim}{r}'}(\underset{\sim}{z}_i)$ can thus be located simply by contracting all lines of the Toller diagram except the z_i-lines, because of properties 2(d) and 2(e) of the angular variables. Since there is only one T_i associated with each "piece" of our flow graph or hexagraph, we are effectively discussing a product of hexagraphs of the form shown in Fig. 3.8. From property 2(f), all cuts in the z_i-plane are now simply linear functions of z_i and in fact lie along the real axes in the right- and left-half z_i-planes.

We can now proceed in the usual manner to define a continuation of $\int T^{-1}_{j_i}$ to complex j_i. We write (for $n > n'$):

$$\frac{1}{2}\int_{-1}^{+1} dz_i(1+z_i)^{-(n+n')/2}(1-z_i)^{-(n-n')/2} \, d^{j_i}_{nn'}(z_i) = \int_C dz_i(1+z_i)^{n+n'/2}(1-z_i)^{n-n'/2} \, e^{j_i}_{nn'}(z_i) \, , \tag{3.25}$$

where $e^{j}_{nn'}(z)$ is the usual second-type representation function and C is the contour shown in Fig. 3.9. It can be checked that the kinematic singularities in the full relations between the angular variables and the invariants naturally gives $A_{s\underset{\sim}{\ell}\underset{\sim}{k}}(\underset{\sim}{z}_i)$ the necessary kinematic singularities to allow us to use (3.25).

Now we simply move the C contour out to lie around the cuts of $A_{s\underset{\sim}{\ell}\underset{\sim}{r}\underset{\sim}{r}'}$ as is also shown in Fig. 3.9. Consequently, we define (for $n > n'$):

$$\int T^{-1}_{\tau}(j_i) = \frac{1}{(2j_i + 1)} \left\{ \int_{\Delta_R} dz_i \; e^{j_i}_{nn'}(z_i)(1 + z_i)^{n+n'/2} \; (1 - z_i)^{n-n'/2} - \right.$$
$$\left. - \tau_i \int_{\Delta_L} dz_i \; e^{j_i}_{nn'}(-z_i)(1 + z_i)^{n-n'/2} \; (1 - z_i)^{n+n'/2} \right\}, \tag{3.26}$$

where $\tau_i = \pm 1$ for $j_i - n$ even or odd, respectively.

Putting together (3.15), (3.23), and (3.26) we can write the final formula for the Froissart-Gribov continuation of the partial-wave amplitude $f_{\underset{\sim}{j}\underset{\sim}{n}}$:

$$f_{\underset{\sim}{\tau}\underset{\sim}{N}}(\underset{\sim}{j},\underset{\sim}{n}) = \prod_i \int T^{-1}_{\tau_i}(j_i) \prod_{m=r,r'} \int D^{-1}_{\tau_{im} N_{im}}(n_{im}) \prod_{\ell} \int V^{-1}_{\tau_\ell \underset{\sim}{N}_\ell}(n_{\ell_1}) \; A_s \; , \tag{3.27}$$

where $\underset{\sim}{j},\underset{\sim}{n}$ stand for the angular momenta and helicity labels that have been taken complex; $\underset{\sim}{N}$ denotes the differences of helicity labels or of angular momenta and helicity labels, that have been kept fixed at integer values; $\underset{\sim}{\tau}$ denotes the signature labels we have had to introduce. Note we should also specify the relative magnitudes of some of the helicities and their signs at the integer values we continue from ($\underset{\sim}{<}$ labels). We shall avoid a label for this since the context should always make clear what such a label would be.

That (3.27) will satisfy the Carlson condition in the final j_i continuations, in addition to the helicity continuations that we have already discussed, follows from the usual result

$$e^{j}_{mm'}(z) \underset{|j|\to\infty}{\sim} j^{-1/2} \; e^{j \; \ln \left[z-(z^2-1)^{1/2}\right]} \; . \tag{3.28}$$

Note, however, that j_i's can only be continued independently after the n continuations have been performed.

Having established the existence of Froissart-Gribov continuations we shall now be able to prove a large number of properties of multiparticle amplitudes. We begin with the Sommerfeld-Watson transformation of the general partial-wave expansion.

3.3 Sommerfeld-Watson Representations

Using an appropriate modification of our earlier symbolic notation we can write the general partial-wave expansion of a spectral component A_s in the form

$$A_s = \sum_{\substack{\underset{\sim}{j},\underset{\sim}{n} \\ \underset{\sim}{N}}} \prod_i T_{j_i} \prod_k D_{N_k n_k} \prod_\ell V_{N_\ell n_\ell} f_{\underset{\sim}{j}\underset{\sim}{n}\underset{\sim}{N}} . \tag{3.29}$$

The notation now matches that used in defining Froissart-Gribov continuations, and indicates that the $\underset{\sim}{j}$ and $\underset{\sim}{n}$ labels are those that can be continued in the complex plane.

We discuss the Sommerfeld-Watson transformation of (3.29) by breaking the implied summations down into parts. Firstly we keep only that part of the sum which satisfies $n,n' \geq 0 \ \forall \ n,n'$ (we justify this later). Clearly we must also have

$$n,n' \leq j_s, \qquad s = i,j,k . \tag{3.30}$$

For each T_{j_i} we write $n_i = n_{i1} + n_{i2}$, $n_i' = n_{i1}' + n_{i2}'$ and define

$$\sum_i = \sum_{\substack{n_{i1},n_{i2} \\ n_{i1}',n_{i2}' \\ n_i \geq n_i'}} \sum_{j_i - n_i = 0}^{\infty} . \tag{3.31}$$

Similarly we write

$$\sum_{i'} = \sum_{n_i' > n_i} \sum_{j_i - n_i' = 0}^{\infty} . \tag{3.32}$$

For each $D_{N_k n_k}$ we write ($k \neq 1$)

$$\sum_k = \sum_{n_k = n_{k+1}}^{\infty} \sum_{N_k = 0}^{\infty} , \tag{3.33}$$

where k and $k+1$ are ordered along some chain of D's linked to a T. [For $k = 1$, $\sum_{n_1 = n_2}^{\infty}$ is included in (3.31) or (3.32).] For each $V_{\underset{\sim}{N}\ell n_\ell}$ we write

$$\sum_\ell = \sum_{n_{\ell_1} = 0}^{\infty} \sum_{N_\ell = 0}^{\infty} \sum_{N_{\ell_1}' = 0}^{\infty} \tag{3.34}$$

and define $\sum_{\ell'}$ similarly. To Sommerfeld-Watson transform (3.29) we proceed as follows. In $\sum_i$ we write

$$\sum_{j_i-n_i=0}^{\infty} (-1)^{j_i-n_i} = \frac{1}{2i} \int_{n_i-1/2-i\infty}^{n_i+1/2+i\infty} \frac{dj_i}{\sin \pi(j_i - n_i)} \tag{3.35}$$

$$\sum_{n_i \geq n_i'} (-1)^{n_{i1}+n_{i2}} = \frac{1}{8} \int_{-1/2-i\infty}^{-1/2+i\infty} \frac{dn_{i1}\, dn_{i2} \sin \pi(n_{i1} + n_{i2})}{\sin \pi n_{i1} \sin \pi n_{i2}} \int_{-1/2-i\infty}^{-1/2+i\infty} \frac{dn_{i1'}\, dn_{i2'}}{\sin \pi n_{i1'} \sin \pi n_{i2'}} \times$$

$$\times \frac{1}{\sin \pi(n_{i_1} + n_{i2} - n_{i1'} - n_{i2'})} . \tag{3.36}$$

We also write

$$\sum_{k} (-1)^{n_k - n_{k+1}} = \frac{1}{2i} \int_{n_{k+1}-1/2-i\infty}^{n_{k+1}-1/2+i\infty} \frac{dn_k}{\sin \pi(n_k - n_{k+1})} \tag{3.37}$$

$$\sum_{\ell} (-1)^{n_{\ell 1}} = \frac{1}{2i} \int_{-1/2-i\infty}^{-1/2+i\infty} \frac{dn_{\ell 1}}{\sin \pi n_{\ell 1}} \sum_{n_\ell=0}^{\infty} \sum_{N_{\ell 1'}=0}^{\infty} . \tag{3.38}$$

If we could ignore signature, (3.35)-(3.38) could be substituted directly into (3.29). Before treating signature, however, we introduce some simple modifications of our formalism which will simplify our further analysis. We define $P^j_{nn'}(z)$ by writing

$$d^j_{nn'}(z) = \frac{(1+z)^{n+n'/2} (1-z)^{n-n'/2} 2^j \Gamma(j+1/2) \left[\Gamma(j+1)\right]^2 P^j_{nn'}(z)}{\pi^{1/2} \left[\Gamma(j+n+1)\, \Gamma(j+n'+1)\, \Gamma(j-n+1)\, \Gamma(j-n'+1)\right]^{1/2}} ; \tag{3.39}$$

$P^j_{nn'}(z)$ is now a polynomial in z [essentially the Jacobi polynomial $P^{(n+n',n-n')}_{j-n}$] and has the simple asymptotic behaviour

$$P^j_{nn'}(z) \underset{|z|\to\infty}{\sim} \frac{z^j}{\Gamma(j+1)} + \sin \pi(j-n)\, O(z^{-j-1-n}) \quad |n| \geq |n'| . \tag{3.40}$$

The use of the $P^j_{nn'}(z)$ functions will considerably simplify our discussion of asymptotic behaviour. We absorb the factors $(1+z)^{n+n'/2} (1-z)^{n-n'/2}$ by defining new variables y_ℓ, y_{ir}, etc., which are related to the u-variables as follows:

$$y_{\ell_1} = (1 - z_\ell^2)^{1/2} (1 - z_{\ell_1}^2)^{1/2} u_{\ell_1} \tag{3.41}$$

$$y_{\ell_1'} = (1 - z_\ell^2)^{1/2} (1 - z_{\ell_1'}^2)^{1/2} u_{\ell_1'} \tag{3.42}$$

$$y_\ell = (1 - z_{\ell_1}^2)^{1/2} (1 + z_\ell)(1 - z_{\ell_1'}^2)^{1/2} u_\ell \tag{3.43}$$

$$y_{ir} = (1 - z_i^2)^{1/2} (1 + z_1) \ldots (1 + z_{r-1})(1 + z_r^2)^{1/2} u_{ir} , \tag{3.44}$$

where z_i is the z associated with the T_i from which the u_{ir} variables are defined. From (2.12b) we see that asymptotically the y_{ir} are linearly related to invariant variables. In fact it is by rewriting (3.15) and (3.23) in terms of y-variables that we can simply extract the kinematic factors necessary to use (3.25).

We absorb the j- and n-dependent factors in (3.39) into a new partial-wave amplitude $a_{\underset{\sim}{\tau}\underset{\sim}{N}}$. We can then write the complete Sommerfeld-Watson representation of a spectral component A_s (the sum over all hexagraphs related by a signature twist) in the compact form

$$A_s(z,y) = \sum_{\underset{\sim}{\tau}} \prod_i (\xi_i + \xi_{i'})\, T_{\tau_i}(j_i) \prod_k (\xi_k)\, D_{\tau_{ik}}(n_{ik}) \times$$
$$\times \prod_\ell (\xi_\ell + \xi_{\ell'})\, V_{\tau_\ell}(n_\ell)\, a_{\underset{\sim}{\tau}\underset{\sim}{N}}(\underset{\sim}{j},\underset{\sim}{n}) \ , \tag{3.45}$$

with ξ_ℓ, etc., now given by (3.28)-(3.30) and

$$T_{\tau_i}(j_i) = \frac{P^{j_i}_{n_{i1},n_{i1'}}(-z_i) + \tau_i P^{j_i}_{n_{i1},n_{i1'}}(z_i)}{2} \tag{3.46}$$

$$D_{\tau_{ik}}(n_{ik}) = \frac{\left[(-y_{ik})^{n_{ik}} + \tau_{ik}(y_{ik})^{n_{ik}}\right]}{2} P^{n_k+N_{ik}}_{n_k,n_{k+1}}(z_{ik}) \tag{3.47}$$

$$V_{\tau_{\ell_1}}(n_{\ell_1}) = \frac{\left[(-y_{\ell_1\ell_1'})^{n_{\ell_1}} + \tau_{\ell_1}(y_{\ell_1\ell_1'})^{n_{\ell_1'}}\right]}{2} y_{\ell_1'}^{N_\ell} P^{n_{\ell_1}+N_{\ell_1}}_{n_{\ell_1},n_{\ell_1'}}(z_\ell) \ . \tag{3.48}$$

We have now incorporated signature completely and, if we also sum over all hexagraphs, (3.31)-(3.38) together with (3.45)-(3.48) give a complete Sommerfeld-Watson representation of a general multiparticle amplitude.

In Section 5 we shall give some simple examples of the above general expressions. We close this section with some technical remarks. First we note that in the multi-Regge limit, z_i, z_{ir}, $z_{ir'}$, $z_\ell \to \infty$ $\forall$ i,r,r',ℓ, it follows from (3.41)-(3.44) that y_{ℓ_1}, $y_{\ell_1'}$, $y_{\ell_1\ell_1'}$, y_{ir}, $y_{ir'} \to \infty$ $\forall$ i,r,r',ℓ.

Therefore we can obtain an asymptotic expansion for A_s from (3.45) by pulling all the n and j contours to the left, provided that all the sums converge uniformly in the multi-Regge limit. All the summations are either expansions in a complete set of polynomials or Fourier expansions. They will converge provided only that no singularities are encountered in the planes of the associated z's and y's (at fixed values of the remaining z's and y's). However, our definition of the Froissart-Gribov continuations succeeded precisely because the asymptotic cuts of a spectral

component are in just those variables whose conjugate sums have been Sommerfeld-Watson transformed in (3.45). There are no fixed-cuts in the z_{ir}, $z_{ir'}$, z_{ℓ}, and $y_{\ell\ell'}$ planes. Provided that the Regge limit is taken in the complex plane, all of the cuts in these planes move out to infinity. [This can be checked in detail by adding the non-leading terms to (2.12a). In fact we must also take $|\cos \omega_{ij}| > \cosh \zeta_{ij}$ to ensure that the cuts move out sufficiently fast.] Consequently the sums do converge and we can use (3.45) to study Regge behaviour. Clearly we can also use this representation to study helicity limits in which u-variables go to infinity. First we must determine the location of the singularities in the helicity and angular momentum planes. This we shall do in the next section.

Finally, we remark that we have neglected the sums over negative n-labels in (3.29) precisely because we shall pull all the n-integration contours to the left in their respective half-planes. It can be shown that in this case the only function of the negative n terms is to cancel unwanted negative integer power behaviour coming from fixed poles in the left-half n-planes of (3.45). This effect is similar to the cancellation of the $O(z^{-j-1-n})$ term in (3.40), when we pull back the associated j-contour which is due to a generalized Mandelstam symmetry property [16].

SECTION 4 CROSS-CHANNEL UNITARITY I -- LOCATION OF REGGE AND HELICITY POLES AND FACTORIZATION OF RESIDUES

4.1 Two-particle Unitarity

In this section we begin our discussion of the implications of cross-channel unitarity for the Froissart-Gribov amplitudes defined in the last section. We begin with the two-particle unitarity relation and its diagonalization by the spectral components.

General discontinuity formulae have been given by Stapp in his lectures. The first formula we require is the most simple. The two-particle discontinuity formula in some channel of a multiparticle amplitude can be written in diagrammatic form:

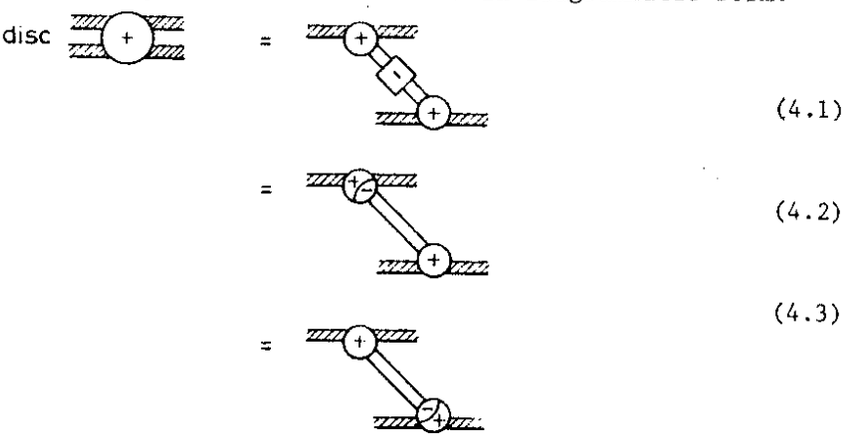

In this notation a circle represents the connected part of an S-matrix element, while a square denotes the full S-matrix (or its Hermitian conjugate). The channel in which the discontinuity has been taken is clear both from the grouping of the initial and final states shown on the left-hand side of (4.1) and the intermediate states displayed on the right-hand side. We shall also use the notation of (4.2) and (4.3) in which a minus sign inserted in a circle indicates that the amplitude is evaluated below the cuts associated with the states grouped with the minus sign.

Consider now the spectral components of an amplitude A defined with respect to some Toller diagram T in which one of the t-channels is the discontinuity channel of (4.1). If we cut the Toller diagram through this particular line it will define Toller diagrams T_L and T_R for each of the amplitudes A_L and A_R appearing on the right-hand side. This is illustrated in Fig. 4.1. Suppose now that we insert particular flow graphs for each of the amplitudes A_L and A_R as illustrated in Fig. 4.2. If the intermediate-state lines are contracted out of the resulting graph, as is also shown in Fig. 4.2, a unique flow graph for the complete amplitude A now results. We call this new flow graph the product flow graph of the two original flow graphs.

Clearly the unitarity integral represented by (4.1) will contain all the discontinuities of the product flow graph. These correspond to cuts through just one of the A_L and A_R or else to a cut through both amplitudes, which avoids the internal phase-space lines. The combination of cuts in each amplitude with the phase-space integration will certainly give this last form of cut in the complete integral. It follows, then, that the spectral components A_{SL} and A_{SR} of A_L and A_R, respectively, will contribute to that part of the discontinuity of A which comes from the product spectral component A_{SLR} defined by the product flow graph.

Before discussing whether the product of A_{SL} and A_{SR} can contribute to other spectral components, we must discuss the phase-space integration in more detail. The phase-space integration for two identical particles is

$$I_2(Q) = \frac{i}{8\pi^2} \int d^4P_1 \, d^4P_2 \, \delta^4(P_1 + P_2 - Q) \, \delta^+(P_1^2 - m^2) \, \delta^+(P_2^2 - m^2) \, . \qquad (4.4)$$

Change variables to $P = P_1 + P_2$ and P_1 so that

$$I_2 = \frac{i}{8\pi^2} \int d^4P_1 \, d^4P \, \delta^4(P - Q) \, \delta^+(P_1^2 - m^2) \, \delta^+(P_2^2 - m^2) \qquad (4.5)$$

$$= \frac{i}{8\pi^2} \int d^4P_1 \, \delta^+(P_1^2 - m^2) \, \delta^+((Q - P_1)^2 - m^2) \, , \qquad (4.6)$$

and so in a Lorentz frame S, where $Q = (\sqrt{t},0,0,0)$,

$$I_2 = \frac{i}{8\pi^2}\int \frac{d^3P_1}{2P_{10}}\,\delta^+(t - 2t^{1/2}P_{10}) \ . \tag{4.7}$$

Introducing polar coordinates (r,θ_Q,μ_Q) for P_1,

$$I_2 = \frac{i}{8\pi^2}\int \frac{drr^2}{2(r^2+m^2)^{1/2}}\int d(\cos\theta_Q)\,d\mu_Q\,\delta^+(t - 2t^{1/2}(r^2+m^2)^{1/2} \tag{4.8}$$

$$= \frac{i}{2^6\pi^2}\left(\frac{t-4m^2}{t}\right)^{1/2}\int_{-1}^{+1} dz_Q \int_0^{2\pi} d\mu_Q \tag{4.9}$$

$$= i\rho(t)\int dg_Q \ , \tag{4.10}$$

where

$$\rho(t) = \frac{1}{16\pi}\left(\frac{t-4m^2}{t}\right)^{1/2} \tag{4.11}$$

and

$$\int dg_Q = \frac{1}{8\pi^2}\int_{-1}^{+1} dz_Q \int_0^{2\pi} d\mu_Q \int_0^{2\pi} d\nu_Q \ . \tag{4.12}$$

We have introduced an azimuthal integration in a plane perpendicular to P_1 and P_2 for reasons that will soon become apparent. Amplitudes will be independent of ν, provided, of course, that they are amplitudes with spinless external particles.

Equation (4.9) is a familiar result, but we shall generalize its derivation later. The point we wish to make at the moment is that the parameters (θ,μ,ν) parametrize a rotation g_Q measured from a standard frame S in which Q lies along the time axis.

We could clearly choose S to be either of the standard frames associated with the vertices $V_L(S_L)$ or $V_R(S_R)$ in Fig. 4.1. Suppose we consider the multi-Regge limit associated with the Toller diagram T, in which all the z-variables are taken large. We can identify z-variables in T and T_L or T_R by identifying associated standard frames, except at the phase-space line Q. However, if we choose $S = S_L$ we can identify g_Q with the little group element g_L associated with Q in T_L. In this case the little group elements g_{LR} and g_R that are associated with Q in T and T_R, respectively, are related by

$$g_{LR} = g_L g_R \equiv g_Q g_R \ , \tag{4.13}$$

from which it follows that

$$z_R \underset{z_{LR} \to \infty}{\sim} z_{LR} \,. \tag{4.14}$$

Hence by choosing S appropriately, we can ensure that the "external" multi-Regge limit defined by T takes the phase-space integration region into the multi-Regge asymptotic region for A_L defined by T_L or into the analogous region for A_R defined by T_R (or both in fact -- by choosing S as an intermediate frame).

We return now to the question of whether other spectral components can be generated by A_{SL} and A_{SR} in (4.1). Note that we are assuming that the absence of double discontinuities in overlapping channels (in dispersion relations) continues to hold in the positive t's region where we are now working (outside of some finite domain in z- and u-space at least). In particular spectral components can still be specified by the sets of (N-3) non-overlapping cuts present in their flow graphs. If we then decompose both sides of (4.1) by writing a dispersion relation we will obtain the discontinuity of each spectral component on the left-hand side by isolating the corresponding component on the right-hand side. This we can do by determining the relevant multiple discontinuities on the right-hand side. We will obtain simple equations only if the spectral components of the integral on the right-hand side can be simply described in terms of the spectral components of the amplitudes that are integrated. We now argue that this is the case for the asymptotic singularity structure associated with Regge behaviour.

We first choose the form of the discontinuity formula given in (4.3) so that A_L is a physical amplitude. We then take $g_L = g_Q$ as discussed above. In this case the phase-space integration remains fixed in terms of the angular variables associated with A_L as $z_{LR} \to \infty$; that is, unless the integration region is distorted by the singularities of A_R (which move as z_{LR} varies). Now, as we discuss in the next section, since A_L is defined as a boundary-value beneath the cut in the Q^2 channel it will have asymptotic behaviour associated with Regge trajectory functions $\alpha_i^*(Q^2)$ (cuts or poles), where $\alpha_i(Q^2)$ are the trajectories associated with a positive boundary-value in the Q^2 channel. The $\alpha_i(Q^2)$ trajectories are those which will control the asymptotic behaviour of the physical amplitude on the left-hand side of (4.1). Therefore, if the integral (4.3) has asymptotic behaviour associated with $\alpha_i(Q^2)$ it can only arise from the integration region being pushed into the Regge asymptotic region for A_L by the cuts of A_R. That this happens can be seen by considering Fig. 4.3. This shows the ν_L-plane ($\nu_L = e^{i\theta_L}$, where $z_L = \cos\theta_L$). We can suppose that the integrations over ν_L and ν_L' have been performed, and that in these integrations branch-points are generated at $\nu_L, \nu_L' = 0, \pi$. At these points (4.13) simplifies to

$$\theta_{LR} = \theta_L \pm \theta_R \quad \text{or} \quad v_{LR} = v_L v_R, v_L/v_R \ , \tag{4.15}$$

and so for $\theta_{LR} \in (0,\pi)$ the "physical region" $\theta_R \in (0,\pi)$ maps into the v_L-plane as shown in Fig. 4.3. Cuts of A_L (which are all independent of z_{LR}) and cuts of A_R (which all depend on z_{LR}) are also shown.

If we now let $v_{LR} \to \infty$ in (4.15) then the cuts of A_R will move out in the v_R-plane pushing the integration contour out as shown in Fig. 4.4. Thus the integration region <u>is</u> pushed out into the Regge region for A_R. Furthermore, the only singularities of the integral which are generated out in the large v_L (or z_L) region are pinches of the integration contour between the cuts of A_R and A_L. If A_R and A_L are spectral components, the cuts generated in this manner are just those present in the product flow graph as described above.

The remaining singularities are those involving the end-points of the z_L integration (that is, $z_L = \pm 1$). These correspond to cuts not found in the product flow graph spectral component. However, these should not be associated with Regge behaviour of the integral since they are generated at small z_L. Therefore, for the purpose of analysing Regge behaviour we can work as if the spectral components diagonalized the discontinuity formulae (4.1)-(4.3) and write in symbolic form

$$A^+_{SLR} - A^-_{SLR} = \int A^+_{SL} A^-_{SR} = \int A^-_{SL} A^+_{SR} \ , \tag{4.16}$$

where $\pm$ denote boundary values with respect to the cuts associated with the phase-space integral $\int$, which in this case represents (4.4).

Next we move on to the partial-wave projection of (4.16). Note that above we implicitly used the fact that the cross-channel associated with the hexagraph for A_{SLR} will also contain the cross-channels for A_{SL} and A_{SR}. This follows because we can simply cut the hexagraph for A_{SLR} to obtain the hexagraphs for A_{SL} and A_{SR}. Consequently all our amplitudes have no physical region singularities and the use of partial-wave amplitudes is without ambiguities.

4.2 Diagonalization and Continuation of Unitarity

To describe the partial-wave diagonalization of (4.16) it is convenient to use a group-theoretic form for the partial-wave expansion (3.29). Using the full set of little group parameters g_i which we introduced in Section 2.1, we can write

$$A_{SLR}(\underset{\sim}{g},\underset{\sim}{t}) = \sum_{\underset{\sim}{j},\underset{\sim}{n},\underset{\sim}{m}} f^{LR}_{\underset{\sim}{j}\underset{\sim}{n}\underset{\sim}{m}} \prod_i D^{j_i}_{n_i m_i}(g_i) \ , \tag{4.17}$$

where now

$$D^{j_i}_{n_i m_i}(g_i) = e^{in_i\mu_i}\, d^{j_i}_{n_i m_i}(\theta_i)\, e^{m_i\nu_i} \tag{4.18}$$

with ν_i, θ_i, and μ_i defined by (2.2). The invariance conditions associated with (2.3)-(2.5) relate some of the n's and m's in (4.17) and enable us to re-express the expansion in the form (3.29). However, these will not concern us here.

The SO(3) representation functions $D^j_{nm}(g)$ have the completeness property

$$\int dg\; D^j_{nm}(g)\; D^{j'}_{n'm'}(g^{-1}) = \frac{1}{(2j+1)}\,\delta_{jj'}\delta_{nm'}\delta_{mn'} \,. \tag{4.19}$$

In effect we used this formula to write the partial-wave projection (3.11).

As we discussed above we can also use the parameters g_i for A_{SL} and A_{SR}, except at the phase-space line Q. There we choose g's related by (4.13). Thus if we write expansions of the form (4.17) for A_{SL} and A_{SR}, substitute into (4.16), and use (4.10) we will obtain

$$A^+_{SLR} - A^-_{SLR} = \sum_{\underset{\sim}{j},\underset{\sim}{n},\underset{\sim}{m}} \prod_{i\neq Q} D^{j_i}_{n_i m_i}(g_i)\, i\rho(t) \int dg_Q\; D^{j^L_Q}_{n^L_Q 0}(g_Q)\; D^{j^R_Q}_{0 m^R_Q}(g_Q^{-1} g_{LR}) \times$$

$$\times\; f^{L+}_{\underset{\sim}{j}\underset{\sim}{L}\underset{\sim}{m}^L\underset{\sim}{n}^L}\; f^{R-}_{\underset{\sim}{j}\underset{\sim}{R}\underset{\sim}{m}^R\underset{\sim}{n}^R} \tag{4.20}$$

(the zeros on the representation functions are because A_{SL} and A_{SR} have no dependence on ν_Q), where $(\underset{\sim}{j}^L,\underset{\sim}{m}^L,\underset{\sim}{n}^L) \cup (\underset{\sim}{j}^R,\underset{\sim}{m}^R,\underset{\sim}{n}^R) = (\underset{\sim}{j},\underset{\sim}{m},\underset{\sim}{n})$ except that we omit j_Q, j^R_Q, j^L_Q, m_Q, n^R_Q, and n^L_Q. Using the group representation property

$$D^j_{mn}(g_Q^{-1} g_{LR}) = \sum_{n'} D^j_{mn'}(g_Q^{-1})\; D_{n'n}(g_{LR}) \tag{4.21}$$

together with (4.19) gives

$$\int dg_Q\; D^{j^L_Q}_{n^L_Q 0}(g_Q)\; D^{j^R_Q}_{0 m^R_Q}(g_Q^{-}\, g_{LR}) = \frac{1}{(2j^R_Q+1)}\, D^{j^R_Q}_{n^L_Q m^R_Q}(g_{LR}) \,. \tag{4.22}$$

Therefore comparing (4.20) with (4.17) [and (4.16)] gives

$$f^{LR+}_{\underset{\sim}{J}_L j_Q \underset{\sim}{J}_R} - f^{LR-}_{\underset{\sim}{J}_L j_Q \underset{\sim}{J}_R} = i\tilde{\rho}_{J_Q}(t)\; f^{L\pm}_{\underset{\sim}{J}_L j_Q}\; f^{R\mp}_{j_Q \underset{\sim}{J}_R} \,, \tag{4.23}$$

where $\tilde{\rho}_J(t) = [1/(2J+1)]\rho(t)$ and $\underset{\sim}{J}_L$ now stand for all angular momentum and helicity labels associated with lines and vertices to the left of line Q in the hexagraph for A_{SLR}, and $\underset{\sim}{J}_R$ is similarly defined in terms of the right-hand side labels.

Since the hexagraph for A_{SLR} is the product of the hexagraphs for A_{SL} and A_{SR}, it follows that the angular momenta and helicities in the sets $\underset{\sim}{J}_L$ and $\underset{\sim}{J}_R$ that can be continued to complex values are the same on both sides of (4.23). Hence (4.23) can be continued directly to all such complex angular momenta and helicities. To rewrite (4.23) as an equation for our "renormalized" partial-wave amplitudes $a_{\underset{\sim}{N}}(\underset{\sim}{j},\underset{\sim}{n})$, we simply define

$$\rho_J(t) = \frac{\pi^{1/2}}{(2J+1)\ 2^J\Gamma(J+1/2)}\ \rho(t)\ . \tag{4.24}$$

The remaining Γ-functions in (3.39) will cancel out and we can write

$$a_\tau^{LR+}(J) - a_\tau^{LR-}(J) = i\rho a_\tau^{L\pm}(J)\ a_\tau^{R\mp}(J)\ , \tag{4.25}$$

where we have now left understood the labels $(\underset{\sim}{j}_L,\underset{\sim}{n}_L)$, $(\underset{\sim}{j}_R,\underset{\sim}{n}_R)$ which have been taken complex together with the associated signature labels, $\underset{\sim}{\tau}_L$ and $\underset{\sim}{\tau}_R$, and the integer-valued differences of angular momenta and helicities. We have also written $\rho \equiv \rho_J(t)$ and written J for J_Q. J is complex, but it may be a free angular momentum or it may be coupled to a helicity so that $J = N_L + n_L$ or $J = N_R + n_R$; τ is clearly the associated signature label.

4.3 Location and Factorization of Regge and Helicity Poles

Given the presence of a Regge singularity at $J = \alpha(t)$ in the signatured elastic Froissart-Gribov amplitude $a_\tau(J,t)$, we can use (4.25) to show that the same singularity must also occur in all multiparticle amplitudes. We cannot reverse the argument, however. We shall discuss Regge poles explicitly, although the arguments for the location of the Regge poles in angular momentum and helicity planes also go through for Regge cuts. In Section 6 we shall locate the Regge cuts directly from multiparticle unitarity in order to determine their discontinuities.

When (4.25) is applied to the elastic amplitude it immediately implies that $a_\tau^+(J)$ and $a_\tau^-(J)$ cannot have a pole at the same position. However, from the real-analyticity of the scattering amplitude it follows from the Froissart-Gribov formula that, when J is real, $a_\tau(J,t)$ is real below the threshold in t. Consequently $a_\tau(J,t)$ is a real analytic function and

$$a_\tau^-(J) = a_\tau^{+*}(J^*)\ . \tag{4.26}$$

If there is a Regge pole at $J = \alpha(t)$, then above threshold $\alpha(t)$ must have an imaginary part so that $a_\tau^-(J)$ has a pole at $J = \alpha^*(t)$ and (4.25) can be satisfied.

Next we apply (4.25) to the five-point function and consider the hexagraph shown in Fig. 4.5. This has a Froissart-Gribov-continuation $a_{\tau_1\tau' N_2}(j_1,n)$, where $N_2 = j_2 - n$ and the signatures τ_1 and τ' refer to j_1 and n. We first apply (4.25) in the j_1 channel in the form

$$a^{+}_{\underset{\sim}{\tau} N_2}(J,n) - a^{-}_{\underset{\sim}{\tau} N_2}(J,n) = i\rho a^{+}_{\tau_1}(J)\, a^{-}_{\underset{\sim}{\tau} N_2}(J,n) \ . \tag{4.27}$$

If

$$a^{+}_{\tau_1}(J) \underset{J \to \alpha}{\sim} \frac{\beta_L^{\tau_1}\ \beta_R^{\tau_1}}{(J-\alpha)} \ , \tag{4.28}$$

then we deduce from (4.27) that $a^{+}_{\underset{\sim}{\tau} N_2}(J,n)$ also has a pole at $J = \alpha$, with signature τ_1, and

$$a^{+}_{\underset{\sim}{\tau} N_2}(J,n) \underset{J \to \alpha}{\sim} \frac{\beta_L^{\tau_1}(i\rho\beta_R^{\tau_1}\ a^{-}_{\underset{\sim}{\tau} N_2}(\alpha,n))}{(J-\alpha)} \tag{4.29}$$

$$= \frac{\beta_L^{\tau_1}\ \beta^{\underset{\sim}{\tau}}_{RN_2}(n)}{(J-\alpha)} \ , \tag{4.30}$$

where, for the moment, (4.30) is just a definition.

We can also apply (4.25) in the j_2 channel to obtain

$$a^{+}_{\underset{\sim}{\tau} N_2}(j_1,J-N_2) - a^{-}_{\underset{\sim}{\tau} N_2}(j_1,J-N_2) = i\rho a^{-}_{\underset{\sim}{\tau} N_2}(j_1,J-N_2)\, a^{+}_{\tau_2}(J) \ , \tag{4.31}$$

where $\tau_2 = \pm\tau'$ according to whether N_2 is even or odd. Thus, although we have analytically continued in the helicity label, (4.31) implies that a Regge pole at $J = \alpha$ in the elastic amplitude appears at $n = \alpha - N_2$, which is, of course, $j_2 = \alpha$. Also the signature of the pole is associated with j_2 rather than n. So although our continuation procedure is unsymmetric in j_1 and j_2 the symmetry is restored when we look at Regge poles. Formula (4.31) also gives

$$a^{+}_{\underset{\sim}{\tau} N_2}(j_1,J-N_2) \underset{J \to \alpha}{\alpha} \frac{(i\rho a^{-}_{\underset{\sim}{\tau} N_2}(j_1,\alpha-N_2)\ \beta_L^{\tau_2})\ \beta_R^{\tau_2}}{(J-\alpha)} \tag{4.32}$$

$$\sim \frac{\beta^{\underset{\sim}{\tau}}_{LN_2}(j_1)\ \beta_R^{\tau_2}}{(J-\alpha)} \ . \tag{4.33}$$

Applying both (4.30) and (4.33) gives

$$a^{+}_{\underset{\sim}{\tau} N_2}(j_1,n) \underset{\substack{j_1 \to \alpha \\ n \to \alpha - N_2}}{\sim} \frac{\beta_L^{\tau_1}\ \beta^{\underset{\sim}{\tau}}_{N_2}\ \beta_R^{\tau_2}}{(J-\alpha)(n-\alpha+N_2)} \ . \tag{4.34}$$

Again we note that the factorization of our formalism is still just a matter of definition if we have no quantum numbers present. In fact we could introduce quantum numbers, and (4.29)-(4.34) would be a proof of factorization for $a^{+}_{\underset{\sim}{\tau}N_2}(j_1,n)$, given the factorization (4.28). Formula (4.28) is, of course, required by (4.25) if quantum numbers are introduced.

The full power of our formalism becomes apparent, however, if we move onto the six-point function. Consider the hexagraph shown in Fig. 4.6. Applying (4.25) in the j_3 channel gives

$$a^{+}_{\underset{\sim}{\tau}\underset{\sim}{N}}(j_3,n_1,n_2) - a^{-}_{\underset{\sim}{\tau}\underset{\sim}{N}}(j_3,n_1,n_2) = i\rho a^{+}_{\underset{\sim}{\tau}_1 N_1}(j_3,n_1)\; a^{-}_{\underset{\sim}{\tau}_2 N_2}(j_3,n_2)\;, \tag{4.35}$$

where $\underset{\sim}{\tau}_1 = (\tau_1,\tau_3)$, $\underset{\sim}{\tau}_2 = (\tau_3,\tau_2)$, $N_1 = j_3 - n_1$, $N_2 = j_3 - n_2$, and $\underset{\sim}{\tau} = (\tau_1,\tau_2,\tau_3)$, $\underset{\sim}{N} = (N_1,N_2)$. Continuing to $j_3 = \alpha$ gives

$$a^{+}_{\underset{\sim}{\tau}\underset{\sim}{N}}(j_3,n_1,n_2) \underset{j_3 \to \alpha}{\sim} \frac{\beta^{\underset{\sim}{\tau}_1}_{LN_1}(n_1)\; i\rho\beta^{\tau_3}_{R}}{(j_3-\alpha)}\; a^{-}_{\underset{\sim}{\tau}_2 N_2}(\alpha,n_2) \tag{4.36}$$

$$= \frac{\beta^{\underset{\sim}{\tau}_1}_{LN_1}(n_1)\;\beta^{\tau_2}_{RN_2}(n_2)}{(j_3-\alpha)}\;. \tag{4.37}$$

Now we really have <u>proved</u> a non-trivial <u>factorization</u>. In fact applying (4.25) also in the j_1 and j_2 channels and dropping signature labels for simplicity gives

$$a_{\underset{\sim}{N}}(j_3,n_1,n_2) \underset{\substack{j_3 \to \alpha \\ n_1 \to \alpha - N_1 \\ n_2 \to \alpha - N_2}}{\sim} \frac{\beta_L\;\beta_{N_1}\;\beta_{N_2}\;\beta_R}{(n_1-\alpha+N_1)(j_3-\alpha)(n_2-\alpha+N_2)}\;. \tag{4.38}$$

This final factorization could be read directly off from the hexagraph as shown in Fig. 4.7, since this tells us that n_1 couples to j_1 and n_2 couples to j_2. It should be clear that (4.25) can be applied successively to more and more complicated amplitudes to obtain the general result that the Regge pole at $j = \alpha$ appears in all channels with its location in a helicity plane determined by the coupled angular momentum. Also the signature is always determined by the signature appropriate for the total angular momentum in that channel, and never by a helicity signature or the signature referring to the difference of an angular momentum and a helicity.

In multiple Regge-pole residues there is a complete factorization. The explicit form of the factorization can be read off from the hexagraph by breaking it down into the original vertices of Fig. 2.4 and using the mapping shown in Fig. 4.8. This mapping introduces some new notation which is more general than that used above and allows for different Regge poles in each channel.

SECTION 5 MULTI-REGGE ASYMPTOTIC BEHAVIOUR -- STRUCTURE OF VERTEX FUNCTIONS AND PHYSICAL REGION FACTORIZATION

5.1 The Five-Point Function and the Two-Reggeon Vertex

We begin by considering the flow graph of Fig. 5.1a. The associated hexagraph and Toller diagram, defining the variables we use, are shown in Fig. 5.2. Defining also

$$u = e^{i\omega} , \quad y = (1 - z_1^2)^{1/2}(1 - z_2^2)^{1/2}\, u , \tag{5.1}$$

and writing A_1 to denote the spectral component of A_5, we can read its Sommerfeld-Watson representation directly from (3.45). There is just one T and one D in the hexagraph and so (temporarily omitting signature and t-labels for simplicity) we obtain

$$A_1(z_1,z_2,y) = \frac{-1}{4i}\int \frac{dn}{\sin \pi n}\,(-y)^n \int \frac{dj_1\, P_n^{j_1}(-z_1)}{\sin \pi(j_1 - n)} \sum_{N_2=0}^{\infty} P_n^{n+N_2}(z_2)\, a_{N_2}(j_1,n) \ . \tag{5.2}$$

To study the single Regge limit $z_1 \to \infty$, we pull back the j_1 contour. A Regge pole at $j_1 = \alpha_1$ in $a_{N_2}(j_1,n)$ gives, on using (3.40) for $P_n^{j_1}(-z_1)$ together with (4.30),

$$A_1 \underset{z_1 \to \infty}{\sim} (-z_1)^{\alpha_1}\, \Gamma(-\alpha_1)\, \beta_{\alpha_1}\, \frac{1}{2i}\int \frac{dn \sin \pi\alpha_1}{\sin \pi n \sin \pi(\alpha_1 - n)} \left(\frac{y}{z_1}\right)^n \sum_{N_2=0}^{\infty} P_n^{n+N_2}(z_2)\, \beta_{\alpha_1 N_2}(n) \ . \tag{5.3}$$

Alternatively, the single Regge limit $z_2 \to \infty$ is obtained by pulling back the n contour and picking up "helicity-poles" at $n = \alpha_2 + N_2$. Using (3.40) for $P_n^{n+N_2}(z_2)$ then gives

$$A_1 \underset{z_2 \to \infty}{\sim} (-z_2)^{\alpha_2}\, \Gamma(-\alpha_2)\, \beta_{\alpha_2} \sum_{N_2=0}^{\infty} \left(\frac{y}{z_2}\right)^{\alpha_2 - N_2} \left\{\frac{1}{2i}\int \frac{dj_1\, P_{\alpha_2 - N_2}^{j_1}(z_2)}{\sin \pi(j_1 - \alpha_2)}\, \beta_{N_2\alpha_2}(j_1)\right\} . \tag{5.4}$$

We note at this point that the function in the brackets { } in (5.4) can be regarded as a Reggeon + particle → particle + particle scattering amplitude. It has many of the characteristics of a four-point function and satisfies unitarity equations [16]. However, we shall not elaborate on this point here.

We can obtain the double Regge behaviour in the $z_1, z_2 \to \infty$ limit from either (5.3) or (5.4). Pulling back the n contour in (5.3) and again picking up the helicity poles at $n = \alpha_2 + N_2$ gives

$$A_1 \underset{\substack{z_1 \to \infty \\ z_2 \to \infty}}{\sim} (-z_1)^{\alpha_1}(-z_2)^{\alpha_2}(u)^{\alpha_2}\Gamma(-\alpha_1)\Gamma(-\alpha_2)\ \beta_{\alpha_1}\ \beta_{\alpha_2}\ V^1_{\alpha_1\alpha_2}(u)\ , \tag{5.5}$$

where

$$V^1_{\alpha_1\alpha_2}(u) = \frac{\sin \pi\alpha_1}{\sin \pi(\alpha_1 - \alpha_2)} \sum_{N_2=0}^{\infty} (-u)^{-N_2}\ \beta_{\alpha_1\alpha_2 N_2}\ . \tag{5.6}$$

If we include signature then from (3.46) and (3.47)

$$(-z_1)^{\alpha_1}(-z_2)^{\alpha_2}\ u^{\alpha_2} = (-z_1)^{\alpha_1-\alpha_2}(-y)^{\alpha_2} \tag{5.7}$$

$$\to z_1^{\alpha_1-\alpha_2}\left[e^{-i\pi(\alpha_1-\alpha_2)} + \tau_1\tau_2\right] y^{\alpha_2}\left[e^{-i\pi\alpha_2} + \tau_2\right] \tag{5.8}$$

$$= z_1^{\alpha_1-\alpha_2}\ y^{\alpha_2}\ \xi_{\alpha_1\alpha_2}\ \xi_{\alpha_2}\ , \tag{5.9}$$

where τ_1 and τ_2 are the signatures of α_1 and α_2, and $\xi_{\alpha_1\alpha_2}, \xi_{\alpha_2}$ are conventional signature factors. Making the replacement (5.7)-(5.9) in (5.5) gives the signatured form of (5.5). Equation (5.6) remains unchanged except that $\beta_{\alpha_1\alpha_2N_2} \to \beta^{\tau_1\tau_2}_{\alpha_1\alpha_2N_2}$. Note that there are only two signature labels. The $\beta^{\tau_1\tau_2}_{\alpha_1\alpha_2N_2}$ are not necessarily analytically related for different N_2 and so there is no separate vertex signature.

If we add to (5.5) the analogous result for the spectral component A_2 represented by the flow graph of Fig. 5.1b we obtain the familiar form of double Regge behaviour long known from models:

$$A_5(z_1,z_2,y) \underset{\substack{z_1,z_2 \to \infty \\ u \text{ fixed}}}{\sim} \Gamma(-\alpha_1)\Gamma(-\alpha_2)\ \beta_{\alpha_1}\ \beta_{\alpha_2}\left[z_1^{\alpha_1-\alpha_2}\ y^{\alpha_2}\ \xi_{\alpha_1\alpha_2}\ \xi_{\alpha_2}\ V^1_{\alpha_1\alpha_2}(u) + \right.$$

$$\left. + z_2^{\alpha_2-\alpha_1}\ y^{\alpha_1}\ \xi_{\alpha_1\alpha_2}\ \xi_{\alpha_2}\ V^2_{\alpha_1\alpha_2}(u)\right]\ , \tag{5.10}$$

where $V^2_{\alpha_1\alpha_2}(u)$ is given by (5.6) with 1 and 2 interchanged.

Note that (5.6) is an asymptotic expansion of $V^1_{\alpha_1\alpha_2}(u)$ for large u. It will therefore converge outside of some domain in the u-plane. We remarked in Section 3 that to ensure that the sum over N_2 in (5.2) converges for large z_1 and z_2, and that limits can be taken inside the sum, it is necessary to take cos ω sufficiently large. Equation (5.6) will probably not converge, therefore, in the physical

region $|u| = 1$. This is not a serious difficulty, however, since we shall always be able to perform our analysis and derive results for sufficiently large (but finite) u. The final results can be expressed in a form, such as (5.10), which can be continued to $|u| = 1$.

Next we remark that there are other singularities in the left-half n-plane of the integrand in (5.3). Firstly there are the fixed-poles at $\sin \pi n = 0$. As we pointed out in Section 3, asymptotic contributions from these poles are cancelled by the negative n contribution to the partial-wave expansion of A_1 which we omitted in writing (5.2). We can ignore the negative n sum if we adopt the convention that we always move n contours to the left. This corresponds to writing an asymptotic expansion in u rather than 1/u (although our justification is that we are taking z's rather than u large). In this case the negative n term gives only fixed-power behaviour. We could adopt the opposite convention, in which the negative n sum would always give the Regge behaviour.

A further more subtle effect arises in (5.3) from the poles at $\sin \pi(\alpha_1 - n) = 0$. These give non-Regge behaviour in the double Regge limit,

$$A_1 \underset{z_1, z_2 \to \infty}{\sim} (-y)^{\alpha_1} \sum_{N_2=0}^{\infty} P_{\alpha_1}^{\alpha_1+N_2}(z_2)\, C_{\alpha_1 N_2} + \ldots . \tag{5.11}$$

This would be single Regge behaviour in the limit $z_1 \to \infty$, z_2 fixed. In general we expect that (5.11) will give some sort of exponential behaviour as $z_2 \to \infty$, and will correspond to an essential singularity at $z_2 = \infty$. Such behaviour might be expected for the following reason. In the single Regge limit A_1 has no singularities in the finite z_2-plane at fixed (but "infinite") (y/z_1) and so must be an entire function. As should be clear it has been the purpose of our analysis to achieve this property for A_1. Even though the full amplitude is polynomially bounded (by assumption) and satisfies a dispersion relation of the form (2.13) it is natural that the break up of the amplitude into spectral components will introduce <u>some</u> "exponential" behaviour for the components.

Notice, however, that in defining Froissart-Gribov continuations we did not disperse A_1 in z_2. We dispersed in z_1 and u, in which we assume that A_1 remains polynomially bounded (this is borne out by models and I feel it should be provable). It is a general result that we never disperse a component in variables in which exponential behaviour may appear in the Sommerfeld-Watson representation.

Fortunately the exponential behaviour can be simply cancelled by the non-basic flow graphs or lower dimensional terms S in (2.13). We have ignored these terms almost completely in previous sections. The flow graph shown in Fig. 5.1c is just such a case. It can be obtained by contracting either Fig. 5.1a or 5.2b. It has just one cut as shown by the dotted line. We shall not develop the formalism for discussing contracted graphs in detail but we note that we can introduce a new i-j vertex with a straight line polygraph as shown in Fig. 5.3. The correspondence between a hexagraph and the flow graph of Fig. 5.1c is also shown. The hexagraph indicates that both angular momenta are coupled to the helicity. The corresponding spectral component A_0 has a helicity continuation only, and its Sommerfeld-Watson representation is (omitting signature)

$$A_0 = \frac{1}{2i} \int \frac{dn}{\sin \pi} [-y]^n \sum_{N_1, N_2 = 0}^{\infty} P_n^{n+N_1}(z_1)\, P_n^{n+N_2}(z_2)\, a_{N_1 N_2}(n) \,. \qquad (5.12)$$

Helicity poles occur in $a_{N_1 N_2}(n)$ at $n = \alpha_1 - N_1$ and $n_2 = \alpha_2 - N_2$. Hence A_0 gives single Regge behaviour in single Regge limits and gives exponential behaviour in the double Regge limit which can cancel with (5.11) (and must if the complete amplitude is polynomially bounded).

Note that the role of (5.12) depends on the order in which we take z_1 and $z_2 \to \infty$. Taking $z_1 \to \infty$ first, gives (5.3) plus a contribution analogous to (5.4) from A_2 and a contribution from A_0. Taking $z_2 \to \infty$ in (5.3) gives (5.5) together with (5.11). Formula (5.11) is (presumably) then cancelled by A_0. With the limits taken in this order, A_2 gives only Regge behaviour, since no exponential term arises from (5.4). Reversing the order of the limits would reverse the situation. In the following we shall keep only the Regge behaviour from basic graphs, knowing that any apparent exponential behaviour is always cancelled by contracted graphs.

Before finally leaving the five-point function we note that the "helicity-pole" limit $y \to \infty$, z_1, z_2 fixed, gives from (5.2)

$$A_1 \underset{y \to \infty}{\sim} (-y)^{\alpha_2}\, \Gamma(-\alpha_2)\, \beta_{\alpha_2} \left\{ \frac{1}{2i} \int \frac{dj_1\, P_{\alpha_2}^{j_1}(z_2)}{\sin \pi(j_1 - \alpha_2)}\, \beta_{\alpha_2 0}(j_1) \right\} . \qquad (5.13)$$

There is also a $(-y_1)^{\alpha_1}$ term which gave (5.11). However, if the exponential cancellation discussed above takes place, A_0 must also cancel this term in the helicity-pole limit. In effect then A_1 gives only α_2-type behaviour in this limit, while A_2 gives only α_1-type behaviour.

5.2 The Six-Point Function and Physical Region Factorization

We begin with the Toller diagram of Fig. 2.1 and consider the hexagraph labelled (1) in Fig. 2.4. There are two D's attached to a single leg of a T. Reading directly from (3.45) and omitting signature initially, we obtain

$$A_1 = \frac{-1}{8i}\int \frac{dn_2}{\sin \pi n_2}\int \frac{dn_1}{\sin \pi(n_1 - n_2)}\,(-y_{12})^{n_2}\,(-y_1)^{n_1-n_2}\int \frac{dj_1\; P^{j_1}_{n_1}(-z_1)}{\sin \pi(j_1 - n_1)} \times$$

$$\times \sum_{N_1=0}^{\infty} P^{N_1+n_1}_{n_1 n_2}(z_3) \sum_{N_2=0}^{\infty} P^{N_2+n_2}_{n_2}(z_2)\; a_{N_1N_2}(j_1,n_1,n_2)\;; \qquad (5.14)$$

y_1 and y_{12} are defined as in Section 3 with $y_1 \equiv y_{i1}$ and $y_{12} \equiv y_{i2}$, so

$$y_{12} \underset{z_1,z_2,z_3 \to \infty}{\sim} z_1 z_2 z_3 u_1 u_2\;, \qquad y_1 \underset{z_1,z_3 \to \infty}{\sim} z_1 z_3 u\;.$$

Regge poles occur in $a_{N_1N_2}(j_1,n_1,n_2)$ at $j_1 = \alpha_1$, $n_1 = \alpha_3 + N_1$, $n_2 = \alpha_2 + N_2$ and so in the multi-Regge limit $z_1,z_2,z_3 \to \infty$ we obtain

$$A_1 \sim (-z_1)^{\alpha_1}(-z_2)^{\alpha_2}(-z_3)^{\alpha_3}\;\Gamma(-\alpha_1)\Gamma(-\alpha_2)\Gamma(-\alpha_3)\;\beta_{\alpha_1}\beta_{\alpha_2}\;V^1_{\alpha_1\alpha_2\alpha_3} \qquad (5.15)$$

where, using the factorization property derived in the last section,

$$V^1_{\alpha_1\alpha_2\alpha_3}(u_1,u_2) = \frac{\sin \pi\alpha_1 \sin \pi\alpha_3}{\sin \pi(\alpha_1 - \alpha_3)\sin \pi(\alpha_3 - \alpha_2)} \sum_{N_1,N_2=0}^{\infty} (-u_1)^{-N_1}(-u_2)^{-N_2}\;\beta_{\alpha_1\alpha_3N_1}\beta_{\alpha_3\alpha_2N_2} \qquad (5.16)$$

$$= V^1_{\alpha_1\alpha_3}(u_1)\; V^1_{\alpha_3\alpha_2}(u_2)\;. \qquad (5.17)$$

Clearly A_2 defined by hexagraph (2) in Fig. 2.4, gives precisely the same form as (3.15) with $1 \leftrightarrow 2$.

The component A_3 has a little more complicated representation since now there is a T with D's attached on either side of a T. Consequently both the $\sum_i$ and $\sum_{i'}$ summations of (3.30) and (3.31) contribute and we obtain

$$A_3 = \frac{-1}{8i}\int \frac{dn_2}{\sin \pi n_2}\int \frac{dn_1}{\sin \pi(n_1 - n_2)}\,(-y_{12})^{n_2}(-y_1)^{n_1-n_2}\int \frac{dj_3\; P^{j_3}_{n_1 n_2}(z_3)}{\sin \pi(j_3 - n_1)} \times$$

$$\times \sum_{N_1,N_2=0}^{\infty} P^{n_1+N_1}_{n_1}(z_1)\; P^{n_2+N_2}_{n_2}(z_2)\; a_{N_1N_2}(j_3,n_1,n_2) + \qquad (5.18)$$

$$+ (1 \leftrightarrow 2)\ ,$$

where y_1 and y_{12} are defined as above.

The bracket $(1 \leftrightarrow 2)$ indicates that the preceding expression is rewritten with 1 and 2 interchanged. The first term arises from the $\sum_i$ summation and $(1 \leftrightarrow 2)$ term arises from the $\sum_{i'}$ summation. Inserting poles at $n_1 = \alpha_1 - N_1$, $n_2 = \alpha_2 - N_2$, $j_3 = \alpha_3$ gives

$$A_3 \underset{z_1,z_2,z_3 \to \infty}{\sim} (-z_1)^{\alpha_1}(-z_2)^{\alpha_2}(-z_3)^{\alpha_3}\,\Gamma(-\alpha_1)\Gamma(-\alpha_2)\Gamma(-\alpha_3) \times$$

$$\times \beta_{\alpha_1}\beta_{\alpha_2}\, u_1^{\alpha_1}u_2^{\alpha_2}\left[V^{31}_{\alpha_1\alpha_2\alpha_3} + V^{32}_{\alpha_1\alpha_2\alpha_3}\right], \qquad (5.19)$$

where $V^{31}_{\alpha_1\alpha_2\alpha_3}(u_1,u_2)$ comes from the first term of (5.18) and $V^{32}_{\alpha_1\alpha_2\alpha_3}(u_1,u_2)$ comes from the second term. The factorization of Section 4 gives

$$V^{31}_{\alpha_1\alpha_2\alpha_3}(u_1,u_2) = \frac{\sin \pi\alpha_1 \sin \pi(\alpha_3 - \alpha_2)}{\sin \pi\alpha_3 \sin \pi(\alpha_1 - \alpha_2)}\, V^2_{\alpha_1\alpha_3}(u_1)\; V^1_{\alpha_3\alpha_2}(u_2) \qquad (5.20)$$

$$V^{32}_{\alpha_1\alpha_2\alpha_3}(u_1,u_2) = \frac{\sin \pi\alpha_2 \sin \pi(\alpha_3 - \alpha_1)}{\sin \pi\alpha_3 \sin \pi(\alpha_2 - \alpha_1)}\, V^2_{\alpha_1\alpha_3}(u_1)\; V^1_{\alpha_3\alpha_2}(u_2)\ . \qquad (5.21)$$

The final hexagraph is number (4) of Fig. 2.4. We also give the Sommerfeld-Watson representation of this, since it contains a V. It has no D's and two T's. Consequently (3.45) gives

$$A_4 = \frac{-1}{8i}\int \frac{dn_1}{\sin \pi n_1}\sum_{N_2=0}^{\infty}(-y_{12})^{n_1}(-y_2)^{N_2}\int \frac{dj_1\; P^{j_1}_{n_1}(-z_1)}{\sin \pi(j_1 - n)} \times$$

$$\times \int \frac{dj_2\; P^{j_2}_{n_1+N_2}(-z_2)}{\sin \pi(j_2 - n_1 - N_2)}\sum_{N_1=0}^{\infty} P^{n_1+N_2+N_1}_{n_1+N_2,n_1}(z_3)\; a_{N_1N_2}(j_1,j_2,n_1) + \qquad (5.22)$$

$$+ (1 \leftrightarrow 2)\ ,$$

where again the two terms come from the $\sum_i$ and $\sum_{i'}$ terms in (3.45). Regge poles occur at $j_1 = \alpha_1$, $j_2 = \alpha_2$, $n_1 - (N_1 + N_2) = \alpha_3$, and after addition of both terms we obtain

$$A_4 \underset{z_1,z_2,z_3 \to \infty}{\sim} (-z_1)^{\alpha_1}(-z_2)^{\alpha_2}(-z_3)^{\alpha_3}\, \Gamma(-\alpha_1)\Gamma(-\alpha_2)\Gamma(-\alpha_3) \times$$

$$\times\, \beta_{\alpha_1}\beta_{\alpha_2}\, u_1^{\alpha_3} u_2^{\alpha_3}\, V^4_{\alpha_1\alpha_2\alpha_3}\ , \tag{5.23}$$

where

$$V^4_{\alpha_1\alpha_2\alpha_3}(u_1,u_2) = V^1_{\alpha_1\alpha_3}(u_1)\ V^2_{\alpha_3\alpha_2}(u_2)\ . \tag{5.24}$$

While (5.17) and (5.24) seem consistent with factorization of the complete amplitude $A_6 (= A_1 + A_2 + A_3 + A_4)$ in the "linear" triple Regge limit we have been discussing, (5.20) and (5.21) appear to violate factorization. In fact (5.20) and (5.21) tell us that the unsignatured triple Regge amplitude does not factorize. This was emphasized some years ago by Weis [17] and by Halliday [18]. However, as was found by Weis and Halliday, (5.17), (5.20), (5.21), and (5.24) are precisely the conditions needed for factorization of the complete amplitude <u>with signature</u> included. We have now proved these conditions directly from analyticity and unitarity, via our Sommerfeld-Watson representations.

The reader can check that incorporation of signature factors into (5.15), (5.19), and (5.23) as in (5.10) will lead to factorization of the complete amplitude in the form

$$A_6 \sim (z_1)^{\alpha_1}(z_2)^{\alpha_2}(z_3)^{\alpha_3}\, \Gamma(-\alpha_1)\Gamma(-\alpha_2)\Gamma(-\alpha_3)\ \beta_{\alpha_1}\beta_{\alpha_2}\, [\ ]_{13}\, [\ ]_{32}\ , \tag{5.25}$$

where each of the square brackets in (5.25) has the form of the square bracket in (5.10). It is important for this result that the signature factors in expressions such as (5.10) give the complete phase of amplitudes. This is only the case when the Regge limit is taken along the real axis in the z's. There is no factorization for general complex z's. Nevertheless this form of factorization is sufficient to give <u>physical region factorization</u> of multi-Regge pole amplitudes. In general, factorization of the form of (5.17)-(5.24) for vertex functions is a necessary and sufficient requirement for physical region factorization of amplitudes [19].

Finally we note that the signature phase factors associated with the two terms in (5.19) suggest these terms be associated with the two sets of non-overlapping discontinuities which are present in the flow graph of A_3. These two sets of discontinuities give two separate contributions to (2.13). As we noted in Section 2, and Stapp has described in detail, it is possible to define multiple "discontinuity functions" which satisfy the generalized Steinmann relations and to use these in (2.13). The above results suggest that if we take "discontinuities" in our formalism by giving opposite boundary-values to our asymptotic angular variables we will obtain the functions described by Stapp. As Weis has emphasized, these "discontinuities" also factorize [20].

5.3 The Three-Reggeon Vertex

As a final example we briefly consider the six-point function using the Toller diagram of Fig. 5.4a. Our convention has been to choose the unsymmetric set of variables shown, to study the hexagraph and flow graphs of Figs. 5.4b and 5.4c.

Writing A_{12} for the spectral component associated with Fig. 5.4c, we note that the hexagraph contains one T and two D's, and the Sommerfeld-Watson representation is (without signature)

$$A_{12} = \frac{-1}{8i} \int \frac{dn_1\, dn_2}{\sin \pi n_1 \sin \pi n_2} (-y_1)^{n_1} (-y_2)^{n_2} \int \frac{dj_3\, P^{j_3}_{n_1+n_2}(z_3)}{\sin \pi(j_3 + n_1 + n_2)} \times$$
$$\times \sum_{\substack{N_1=0 \\ N_2=0}}^{\infty} P^{n_1+N_1}_{n_1}(z_1)\, P^{n_2+N_2}_{n_2}(z_2)\, a_{N_1N_2}(j_3,n_1,n_2) \,. \tag{5.26}$$

Regge poles occur at $n_1 = \alpha_1 + N_1$, $n_2 = \alpha_2 + N_2$, and $j_3 = \alpha_3$, and so using factorization we obtain

$$A_{12} \underset{z_1,z_2,z_3 \to \infty}{\sim} (-z_1)^{\alpha_1}(-z_2)^{\alpha_2}(-z_3)^{\alpha_3}\, \Gamma(-\alpha_1)\Gamma(-\alpha_2)\Gamma(-\alpha_3) \times$$
$$\times \beta_{\alpha_1}\beta_{\alpha_2}\beta_{\alpha_3}\, V^{12}_{\alpha_1\alpha_2\alpha_3}(u_1,u_2) \,, \tag{5.27}$$

where

$$V^{12}_{\alpha_1\alpha_2\alpha_3}(u_1,u_2) = \frac{\sin \pi\alpha_3\, u_1^{\alpha_1} u_2^{\alpha_2}}{\sin \pi(\alpha_3 + \alpha_2 + \alpha_1)} \sum_{N_1,N_2=0}^{\infty} (-u_1)^{N_1}(-u_2)^{N_2}\, \beta_{\alpha_1\alpha_2\alpha_3 N_1 N_2} \,. \tag{5.28}$$

Signature factors should be added to (5.27) as in the other examples above. However, these arise from the set of hexagraphs obtained from Fig. 5.4b by twist operations. We must initially add to (5.27) the two other hexagraphs obtained by cyclically rotating Fig. 5.4b in the plane. This will give the complete unsignatured triple Regge vertex.

First we must consider the variables we are using more carefully. In terms of the variables u_{12}, u_{23}, and u_{31} (introduced in Section 2) which satisfy (2.5), we have

$$u_1 = u_{13} = \frac{1}{u_{31}} = e^{-i\omega_{31}} , \quad u_2 = u_{23} = e^{i\omega_{23}} . \tag{5.29}$$

To parallel the above discussion of A_{12}, for A_{23} -- the spectral component defined by the hexagraph of Fig. 5.5 -- we choose variables u_2' and u_3', where

$$u_2' = u_{21} = \frac{1}{u_{12}} = e^{-i\omega_{12}} , \quad u_3' = u_{31} = e^{i\omega_{31}} . \tag{5.30}$$

From (2.5) we see that

$$u_2' = \frac{u_2}{u_1} , \quad u_3 = \frac{1}{u_1} . \tag{5.31}$$

Therefore if we write A_{23} in the form (5.27) we can write

$$V^{23}_{\alpha_1\alpha_2\alpha_3}(u_1,u_2) = \frac{\sin \pi\alpha_1}{\sin \pi(\alpha_3 + \alpha_2 + \alpha_1)} u_2^{\alpha_2} u_1^{-\alpha_2-\alpha_3} \sum_{\substack{N_2=0 \\ N_3=0}}^{\infty} \left(\frac{-u_2}{u_1}\right)^{-N_2} \left(\frac{1}{u_1}\right)^{-N_3} \beta_{\alpha_1\alpha_2\alpha_3 N_2 N_3} . \tag{5.32}$$

Note that (5.27) and (5.32) do not have a common domain of validity, since (5.27) holds for large u_1 and u_2, while (5.32) holds for large u_2/u_1 and large $1/u_1$. Nevertheless we can extract the residues of the spurious poles at $\alpha_1 + \alpha_2 + \alpha_3 = N$ in both expressions and see that a cancellation between V^{12}, V^{23}, and V^{31} can take place. We could also have obtained different asymptotic expansions for these vertices which would have exposed different spurious poles.

Clearly the complete triple Regge vertex is a subtle object and there is no simple symmetric way of writing it. If only one term is of interest, as is the case when a discontinuity is taken to obtain an inclusive cross-section, then the form (5.27) can be used without difficulty. In fact the inclusive "triple Regge limit" is really a helicity-pole limit and picls out just the first term in (5.27).

Note that we have only three terms in the triple-Regge vertex, whereas De Tar and Weis found four in the dual model [21]. This is because they did not impose the constraint (2.5) and so allowed u_{12}, u_{31}, and u_{23} to be independent variables. They interpreted their fourth term as being due to singularities in a combination of three channels which cannot all be above threshold in any physical region. Hence, there will not be a corresponding contribution to the dispersion relation (2.13). In effect we have distributed the fourth term amongst the other three.

SECTION 6 CROSS-CHANNEL UNITARITY II -- REGGE CUTS AND THEIR DISCONTINUITIES

6.1 Multiparticle Unitarity

The analysis of Regge cuts in the cross-channel multiparticle unitarity relation [11], [22] is notoriously complicated. However, the formalism that we have developed in previous sections will enable us to give an outline discussion which does not get too involved with technical detail.

We begin with the multiparticle discontinuity formula given by Stapp. In a similar notation to that of Section 4

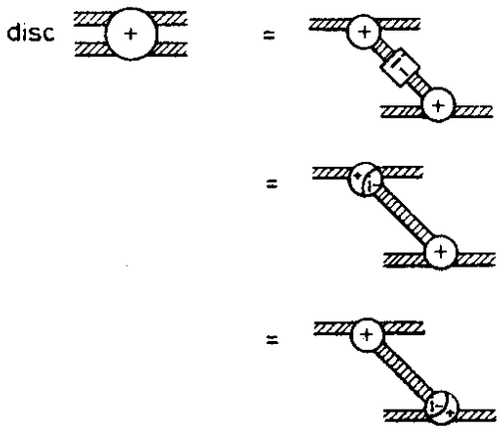

(6.1)

(6.2)

(6.3)

The i- in the square-box in (6.1) indicates that the discontinuity is that due to a particular intermediate state i in the discontinuity channel; $=\boxed{i^-}=$ is the inverse of the physical S-matrix defined with respect to this state (which in our case will be a general 2N-particle state). The discontinuity taken is then the local discontinuity around the cut due to the state i. The intermediate integrations are over the phase-space for this state. The (i^-) in (6.2) and (6.3) indicates that an amplitude is evaluated below the i-cut and all sub-channel cuts associated with the phase-space.

We wish to show that asymptotically our spectral components also diagonalize the above multiparticle unitarity equations. We proceed in analogy with our discussion of the two-particle integral in Section 4.

We first write the phase-space integration in terms of Toller variables. To draw a Toller diagram T_i for the phase-space we draw a tree-diagram connecting an initial-line representing the incoming momentum Q to final particles representing the phase-space state. This is illustrated in Fig. 6.1. Starting from some standard frame S for Q we can introduce little group parameters g_j for each of the internal lines of the tree-diagram, a g_Q for Q, and boosts ζ_{jk} for the internal vertices as in Section 2. A generalization of (4.4)-(4.12) then gives

$$I_i(Q) = i \int d\rho(t,t_j) \int dg_Q \prod_j \!\!\!\!\!\!\int dg_j \ . \tag{6.4}$$

Detailed derivations of this result for three- and four-particle phase-space can be found in Ref. [22]. The integral $\int d\rho(t,t_j)$ is an integration over the vertex boosts ζ_{jk}. All we shall need to know about this integration is that one boundary of the integration region is the phase-space boundary (B_{T_i}) given by $\lambda(t_i,t_j,t_k) = 0 \ \forall$ i,j,k, where λ is defined in (2.7). In particular it is given by

$$t_i^{1/2} = t_j^{1/2} + t_k^{1/2} \ , \tag{6.5}$$

where t_i is the largest of t_i,t_j,t_k. In a cross-channel such a t_i is always picked out at each i-j-k vertex (it is the horizontal line of the associated hexagraph).

Proceeding as in Section 4 we introduce a Toller diagram T for the amplitude A whose discontinuity we are considering. Again we choose the discontinuity channel as one of the internal lines Q of the Toller diagram and denote the sub-amplitudes in (6.1) by A_L and A_R. Cutting the Toller diagram T at Q and joining the phase-space diagram T_i to each of the parts of T gives Toller diagrams T_L and T_R which coincide with those for all lines of T except Q by choosing the same standard frames in each case. We can also use the same g_j for T_L and T_R at all internal phase-space lines. So the only difference in the parameters of A, A_L, and A_R is in their respective little group elements g_{LR}, g_L, g_R associated with Q. These will again be related by

$$g_{LR} = g_L g_R \ , \tag{6.6}$$

and by choosing the standard frame S appropriately we can take $g_Q = g_L$ or g_R^{-1}.

If we now insert flow graphs associated with spectral components A_{SL} and A_{SR} into the right side of (6.1) we can form the product flow graph as before by contracting out all structure associated with the intermediate state lines. However, since there are now several particles in the intermediate state, this process contracts out some non-trivial part of the flow graphs. Thus it appears that in general many spectral components will contribute to a single spectral component of A. This is the case, except when we look for asymptotic behaviour of the unitarity integral which depends on internal Regge singularities of A_L or A_R. We now give a brief outline argument (which is very similar to that given in Section 4) to show that we only need consider the product of two spectral components when discussing Regge cuts.

Suppose we look for asymptotic behaviour in (6.2) associated with Regge poles $\alpha(t_k)$ $k = 1, \ldots, N$, where each $t_k = Q_k^2$ with Q_k an internal momentum of the phase-space Toller diagram. Further, suppose that each Q_k is the momentum of a pair of phase-space particles so that we are discussing a 2N-particle intermediate state. (We will discuss this specialization later.) First we note that since A_R is evaluated below all cuts associated with the intermediate state i, and all the Regge trajectories $\alpha(t_k)$ acquire imaginary parts at the two-particle thresholds in the t_k-channels, A_R will have asymptotic behaviour associated with $\alpha^*(t_k)$ and not $\alpha(t_k)$ $\forall$ k. Therefore any Regge behaviour associated with the $\alpha(t_k)$ must come from A_L. However, we can again choose $g_Q = g_L$, in which case the internal phase-space parameters g_j of A_L apparently remain finite even in the external Regge limit $z_{LR} \to \infty$.

Clearly, although A_R does not have the appropriate Regge behaviour it must have cuts which lead to a distortion of the phase-space in the asymptotic limit. That is, there must be a "pinch" of the integration $\Pi_j \int dg_j$ with some part of the integration region necessarily pushed into the Regge asymptotic region for A_L. (This is essentially a generalization of Mandelstam's original discussion [5] of the presence of Regge cuts in the three-particle unitarity integral.) In particular, if we are to ensure that we expose all of the Regge poles $\alpha(t_k)$, there must be a pinch of a complete set of internal integrations g_j which couple the internal momenta Q_k and the external momenta. (We are assuming here that if such a complete set of integrations is not pinched then we can always distort the unpinched integration contours to avoid the internal Regge region.)

Now each spectral component has simultaneous discontinuities in only a limited set of the internal angular variables. Hence a simultaneous pinching of <u>all</u> internal

angular integrations is certainly not possible. Each component has the potential to pinch only a particular set of internal integrations. Initially we might suppose that we should discuss spectral components with cuts in the z_k-variables associated with the Q_k's. The aim would then be to show that the cuts of such components necessarily push the integration contour into the Regge asymptotic region in the z_k-variables. In fact such components have too many cuts in channels associated purely with the internal phase-space particles. They do not have a sufficient number of cuts in channels involving the external particles to give a complete pinch of the integration variables coupling the internal and external particles.

Following this argument through in detail, we find that the only possibility is to expose the internal Regge poles in helicity limits by pinches of the u-integrations. The requirement that there be cuts in all u-variables adjacent to the Q_k-lines in the hexagraph is equivalent to requiring all Q_k-lines to have a sloping part. The requirement that there also be enough cuts in channels linking the external and internal particles then leads to a unique spectral component A_{Sk} -- given a spectral component A_{SLR} for A.

The unique hexagraph (unique up to a signature twist) is constructed as follows. We place the internal particles in a vertical column and then couple them according to the Toller diagram T_i by moving to the right only, as shown in Fig. 6.2, until we reach Q. The rest of the hexagraph for A_{Sk} is the same as that for A_{SLR}.

It should be clear from the associated flow graph (an example of which is shown in Fig. 6.3) that we have introduced the maximum degree of non-planarity into the scattering processes producing particles in the direct channel. In the cross-channel this maximizes the number of cuts in channels linking the external and internal particles and so produces the best possibility for a pinch of the complete phase-space integration. (The observant reader will also notice the parallel with the non-planar Feynman diagram used to couple Regge poles in the Reggeon Calculus.)

We similarly argue for the uniqueness of A_{SL} as follows. Firstly all the necessary helicity poles must be present. As should be clear from (5.13), this requires all of the angular momenta associated with the Q_k to be coupled to helicities. This requires that the Q_k-lines in the hexagraph of A_{SL} have a sloping part. To show that the rest of the graph must be the same as for A_{SR} we take $g_Q = g_R^{-1}$ so that the internal parameters of A_{SL} remain fixed. The pinching of the remaining integration variables must now be produced by the cuts of A_{SL}. Hence it must have the same hexagraph structure as A_{SR}.

Once again we have an effective diagonalization of the discontinuity formulae (6.1)-(6.3) for the purpose of studying Regge asymptotic behaviour. If we drop the i-notation in (6.1)-(6.3) and replace it by a minus we can write symbolically

$$A^{+}_{SLR} - A^{-}_{SLR} = \sum_{T_i} \int_i A^{+}_{SL} A^{-}_{SR} \tag{6.7}$$

$$= \sum_{T_i} \int_i A^{-}_{SR} A^{+}_{SL} \, . \tag{6.8}$$

This equation is best illustrated in terms of hexagraphs as in Fig. 6.4. The summation $\sum_{T_i}$ is a sum over all Toller diagrams for the phase-space i where the corresponding phase-space boundaries B_{T_i} are distinct. The distinction of the phase-space boundaries ensures that there is no double counting in evaluating Regge cut contributions to (6.1)-(6.3).

As we have implied, the Regge cuts generated by the Regge poles associated with a particular Toller diagram are generated near the phase-space boundary B_{T_c} for the t's of the Toller diagram. These boundaries lie in distinct parts of the physical phase-space for the i-state. (In fact the definition of Froissart-Gribov continuations for the unique hexagraph associated with a Toller diagram breaks down at some distance from the boundary B_{T_i}.)

A more detailed version of the above argument for spectral component diagonalization is clearly desirable. That we have isolated just those hexagraphs for A_L and A_R corresponding to the cross-channel in which we are working does add strength to the argument. The point that we really wish to emphasize, however, is that we believe the above argument should be made before we go into the angular momentum plane. The following angular momentum analysis of a single "diagonal" product of hexagraphs is very clean. We can prove that these components do generate Regge cuts. The point of the above argument was to remove all other components from consideration.

The angular momentum analysis now proceeds in close analogy with Section 4 and so we can minimize the details. First we select a Toller diagram T and write partial-wave expansions of the form (4.17) for A_{SL}, A_{SR}, and A_{SLR}. Next we insert these expansions into (6.2) and (6.3). Then writing the phase-space integration in the form (6.4), we can use (4.19), (4.21), and (4.22) as before to write both sides of (6.2) and (6.3) in comparable form. The uniqueness of the partial-wave expansion then enables us to write an equation for the partial-wave coefficients analogous to (4.23):

$$f^{LR+}_{\underset{\sim}{J}_L j_Q \underset{\sim}{J}_R} - f^{LR-}_{\underset{\sim}{J}_L j_Q \underset{\sim}{J}_R} = i \sum_{\underset{\sim}{N}_j, \underset{\sim}{n}_j} \int d\rho_{j_Q \underset{\sim}{N}_j} f^{L+}_{\underset{\sim}{J}_L j_Q \underset{\sim}{N}_j \underset{\sim}{n}_j} f^{R-}_{\underset{\sim}{N}_j \underset{\sim}{n}_j j_Q \underset{\sim}{J}_R}, \qquad (6.9)$$

where, as before, $\underset{\sim}{J}_L$ and $\underset{\sim}{J}_R$ refer to helicity and angular momentum labels on the left and right of the line Q in the Toller diagram T; $\underset{\sim}{n}_j$ and $\underset{\sim}{N}_j$ refer to helicities and differences of angular momenta and helicities associated with the phase-space Toller diagram T_i. The notation is consistent with the fact that the hexagraphs that represent A_{SL} and A_{SR} contain only D subgraphs associated with the internal phase-space lines. Hence all N_j's must be kept fixed at integer values and only the n_j's can be taken complex. This is, however, precisely what we require.

Next we re-express (6.9) in terms of our renormalized amplitudes $a_{\underset{\sim}{N}}(j,\underset{\sim}{n})$. This time not all of the renormalization factors implied by (3.39) can be harmlessly absorbed into the phase-space factor ρ as in (4.24). In particular we must keep track of the nonsense singularities at $j - n + 1 = 0$ and $j - n' + 1 = 0$ which arise from the Γ-functions in the square-root factor of (3.39). To this effect we write a factor $(j - n + 1)^{-1}$ or $(j - n' + 1)^{-1}$ multiplying the product $a^L_{\underset{\sim}{N}}(j,\underset{\sim}{n}) a^R_{\underset{\sim}{N}}(j,\underset{\sim}{n})$ whenever $(j - n)$ or $(j - n')$ is not a positive integer. The remaining factors will play no role in the following. They will be analytic at points where we discuss the generation of singularities and so we can safely absorb them in ρ and omit specific labels.

We also wish to express (6.9) in a form where it can be directly continued to complex j_Q. The summations over $\underset{\sim}{N}_j$ will converge even for complex j_Q. They correspond directly to the sub-angular momentum summations in the Sommerfeld-Watson representations discussed in Section 3, which we showed remained convergent in Regge limits. This implied that the continued partial-wave amplitudes have good convergence properties in the $\underset{\sim}{N}_j$ variables and hence these sums will converge.

The $\underset{\sim}{n}_j$ sums, however, will not converge for complex j_Q. In (6.9) these sums are bounded by either j_Q or the internal angular momenta. It can be shown that simply allowing these sums to be come unbounded for complex j_Q leads to divergences. The trick we use is to write these sums as helicity integrals.

For the helicity bounded by j_Q we note that

$$\sum_{j=0}^{\infty} \sum_{n\leq j} a_{jn} = \sum_{n=0}^{\infty} \sum_{j=n}^{\infty} a_{jn} \tag{6.10}$$

$$= -\frac{1}{4} \int_{-\frac{1}{2}-i\infty}^{-\frac{1}{2}+i\infty} \frac{dn(-1)^n}{\sin \pi n} \int_{-\frac{1}{2}-i\infty}^{-\frac{1}{2}+i\infty} \frac{dj(-1)^{j-n}}{\sin \pi(j-n)} a(j,n) \tag{6.11}$$

$$= \frac{1}{2i} \int_{-\frac{1}{2}-i\infty}^{-\frac{1}{2}+i\infty} \frac{dj(-1)^j}{\sin \pi j} \left\{ \frac{\sin \pi j}{2i} \int_{-\frac{1}{2}-i\infty}^{-\frac{1}{2}+i\infty} \frac{dn\, a(j,n)}{\sin \pi n \sin \pi(j-n)} \right\}, \tag{6.12}$$

where we have simply interchanged the orders of integration in going from (6.11) to (6.12). However, if a_{jn} falls off when $n \to \infty$ and when $j - n \to \infty$, so that we can write (6.11), then from (6.12)

$$\frac{\sin \pi j}{2i} \int_{-\frac{1}{2}-i\infty}^{-\frac{1}{2}+i\infty} \frac{dn\, a(j,n)}{\sin \pi n \sin \pi(j-n)} \tag{6.13}$$

must fall-off in the j-plane. This is necessary so that we can close the j-contour in (6.12) and reproduce the original sum over j in (6.10).

Note that as j moves into the right-half j-plane, the n-contour in (6.13) is distorted as shown in Fig. 6.5. At integer j the two sets of poles in the n-plane pinch the n-contour giving a pole of the integral. The residue of this pole is picked out by the sin πj factor in (6.13), and is just the require finite sum over helicities.

A further point is that we must separate the sums over even and odd (j - n), (n), etc., which in this context we can refer to as even- and odd-signatured sums. As we know, the Froissart-Gribov continuations of the corresponding partial-wave amplitudes are different. When all signatures are even we write

$$\sum_{Q} = \sum_{n_Q \leq j_Q} = \frac{\sin \pi/2\, j_Q}{4i} \int \frac{dn_Q}{\sin \pi/2\, n_Q \sin \pi/2(j_Q - n_Q)(j_Q - n_Q + 1)}, \tag{6.14}$$

where we have now introduced explicitly the nonsense fixed-pole factor which arises from the product of two normalization factors referred to above. The modification of (6.14) to be used for odd-signature sums should be obvious.

We also pick out that part of the internal helicity sums which satisfies $n_j > n_{j'}$, for each D_j subgraph (see Fig. 3.2 for notation), for analogous reasons to those we gave when discussing Sommerfeld-Watson representations. However, since we are in effect now reversing orders of summation, we must explicitly take account of the two helicities $n_{j_1'}$ and $n_{j_2'}$ which sum to form $n_{j'}$. Therefore, we write (taking account of even signature sums only),

$$\sum_{n_{j'}} = \sum_{n_{j_1'}+n_{j_2'}\leq n_j} = \frac{\sin \pi/2\, n_j}{-16} \int \frac{dn_{j_1'}\, dn_{j_2'}}{\sin \pi/2\, n_{j_1'} \sin \pi/2\, n_{j_2'} \sin \pi/2(n_j - n_{j_1'} - n_{j_2'})} \times$$

$$\times \frac{1}{(n_j + N_j - n_{j_1'} - n_{j_2'} + 1)} , \tag{6.15}$$

where the factor $n_j + N_j - n_{j_1'} - n_{j_2'} + 1 = j_j - n_{j'} + 1$ again arises from the nonsense fixed-pole normalization factor.

We can now rewrite (6.9) in a form which, from our previous proof of the existence of Froissart-Gribov continuations, can be directly continued to complex j_Q and all allowed complex j's and n's in $\underset{\sim}{J}_R$ and $\underset{\sim}{J}_L$. Dropping the L, R, LR, $\underset{\sim}{J}_L$, $\underset{\sim}{J}_R$ labels for simplicity we write

$$a^+(j_Q) - a^-(j_Q) = i \sum_Q \sum_{\underset{\sim}{n}_{j'}} \sum_{\underset{\sim}{N}_j} \int d\rho\; a^+_{\underset{\sim}{N}_j}(j_Q, \underset{\sim}{n}_j)\; a^-_{\underset{\sim}{N}_j}(j_Q, \underset{\sim}{n}_j) , \tag{6.16}$$

where $\sum_Q$ is given by (6.14) and $\sum_{\underset{\sim}{n}_{j'}}$ is a product of expressions of the form of (6.15). We have omitted signature labels since we have taken all signatures positive.

It is now straightforward to discuss the generation of Regge cuts in (6.16). Suppose that $j_1' \equiv 1$, $j_2' \equiv 2$, where 1 and 2 denote two pairs of the internal particles. In this case there are helicity poles at $n_1 = \alpha(t_1) \equiv \alpha_1$, $n_2 = \alpha(t_2) \equiv \alpha_2$. Inserting $1/(n_1 - \alpha_1)$ and $1/(n_2 - \alpha_2)$ into (6.15), writing $n_{12} = n_j$, and taking $N_j = 0$, we see that there is a pole of the integral generated by the helicity poles and the nonsense pole and

$$\sum_{n_{12}'} \sim \frac{(-1)\, \sin \pi/2(\alpha_1 + \alpha_2 - 1)}{\sin \pi/2\, \alpha_1 \sin \pi/2\, \alpha_2} \frac{1}{n_{12} - \alpha_1 - \alpha_2 + 1} . \tag{6.17}$$

Next we move on into the hexagraph to the next i-j-k vertex where two D's couple to a third. Either line Q_3 enters this vertex or line Q_{34} ($Q_{34} = Q_3 + Q_4$). If Q_3 enters we write $n_{j_1'} \equiv n_{12}$, $n_{j_2'} \equiv n_3$, and $n_j \equiv n_{123}$. Inserting (6.17) into (6.15) together with a helicity pole $1/(n_3 - \alpha_3)$ gives

$$\sum_{n'_{123}} \sim \frac{(-1)^2 \sin \pi/2(\alpha_1 + \alpha_2 - 1) \sin \pi/2(\alpha_1 + \alpha_2 + \alpha_3 - 2)}{\sin \pi/2\, \alpha_1 \sin \pi/2\, \alpha_2 \sin \pi/2\, \alpha_3} \frac{1}{n_{123} - \alpha_1 - \alpha_2 - \alpha_3 + 2} . \tag{6.18}$$

Clearly if we had taken $n_{j_2'} = n_{34}$ and inserted a form (6.17) we would have obtained a corresponding result.

We can proceed through the hexagraph in the above manner until we arrive at the final $\sum_Q$ integration of (6.14). However, this has the same form as (6.15) and so the final result will be

$$\sum_Q \sum_{\underset{\sim}{n}_{j'}} \sim (-1)^{N-1} \xi_{T_N}(\alpha_1, \ldots, \alpha_N) \frac{1}{j_Q - 1 - \sum_{k=1}^{N} (\alpha_k - 1)} , \tag{6.19}$$

where $\xi_{T_N}(\alpha_1, \ldots, \alpha_N)$ is a form of signature factor, whose exact form depends on the nature of the hexagraph we are studying. Its general form can be seen from (6.17) and (6.18). Its most important property is

$$\xi_{T_N}(1, \ldots, 1) = 1 . \tag{6.20}$$

Another important point to note is the $(-1)^{N-1}$ factor in (6.19), where N is the number of Regge poles we are considering.

The final step is to make the replacement (6.19) in (6.16). We must also, of course, take the residue of $a^+_{\underset{\sim}{N}_j}(j_Q, \underset{\sim}{n}_j)$ at the helicity poles that we have used to generate (6.19). We have taken $\underset{\sim}{N}_j = 0$ everywhere, which means every helicity is coupled to its angular momentum at its "maximum value". [Not to have done so would have shifted the position of the pole in (6.19).] We have also used a nonsense pole at every i-j-k vertex. (If we were to consider all signatures, then to obtain a non-zero residue in this case we would have to impose a signature condition, but we shall not elaborate on this here.) Since we have extracted kinematic square-root factors to obtain the nonsense fixed-poles, we simply have to evaluate $a^+_{\underset{\sim}{N}_j}(j_Q, \underset{\sim}{n}_j)$

and $a^{-}_{\underset{\sim}{N}_j}(j_Q,\underset{\sim}{n}_j)$ at the nonsense point. However, these functions are often referred to as fixed-pole residues.

To evaluate $a^{-}_{Q}(j_Q,\underset{\sim}{\alpha}_k) \equiv a^{-}_{\underset{\sim}{\alpha}}(j_Q)$ we use the two-particle unitarity relation (4.25). [Note that $\pm$ in (4.25) refer only to the two-particle state whereas the - attached to $a^{-}_{\underset{\sim}{\alpha}_k}(j_Q)$ applies to all t_k-channels.] However, by using (4.25) extensively it can be shown that

$$\prod_k (i\rho_k)\; a^{+}(j_Q,\underset{\sim}{n})\; a^{-}(j_Q,\underset{\sim}{n}) \underset{\underset{\sim}{n}_k \to \underset{\sim}{\alpha}_k}{\sim} \frac{A_{\underset{\sim}{\alpha}}(j_Q)\; A^{i}_{\underset{\sim}{\alpha}}(j_Q)}{\prod_k (n_k - \alpha_k)}\,, \tag{6.21}$$

where $A_{\underset{\sim}{\alpha}}(j_Q)$ is the multiple residue of $a^{+}(j_Q,\underset{\sim}{n})$ at $\underset{\sim}{n} = \underset{\sim}{\alpha}$ and $A^{i}_{\underset{\sim}{\alpha}}(j_Q)$ is $A_{\underset{\sim}{\alpha}}(j_Q)$ evaluated below just the cut in the $t = Q^2$ channel due to the state i; ρ_k is the two-particle phase-space factor for the Q_k channel.

Using (6.21) and (6.19) in (6.16) gives (dropping $\pm$ labels and using an i where appropriate):

$$a(j_Q) - a^{i}(j_Q) = (-1)^{N-1}\; i \sin \pi/2\; j \int \frac{d\rho'\; \xi_N\; A_{\underset{\sim}{\alpha}}(j_Q)\; A^{i}_{\underset{\sim}{\alpha}}(j_Q)}{j - 1 - \sum_{k=1}^{N} (\alpha_k - 1)}\,, \tag{6.22}$$

where $d\rho' = d\rho/\Pi_k\, \rho_k$. Now we note that if (6.5) is satisfied

$$t_{12}^{1/2} = t_1^{1/2} + t_2^{1/2}\,, \quad t_{123}^{1/2} = t_1^{1/2} + t_2^{1/2} + t_3^{1/2}\,, \quad t^{1/2} + t_{12\ \ldots\ N}^{1/2} = t_1^{1/2} + \,, \ldots, t_N^{1/2} \tag{6.23}$$

which has the symmetric solution

$$t_1 = t_2 = \ldots t_N = \left(\frac{t}{N}\right)^2\,. \tag{6.24}$$

So if $\alpha_k(t_k) = \alpha(t_k)\ \forall\ k$, that is, we insert the same Regge pole in all channels, the pole at $j = 1 + \sum_{k=1}^{N} (\alpha_k - 1)$ will be tangent to the phase-space boundary at the symmetric point (6.24) and a Regge cut will be generated at

$$j = \alpha_N(t) = 1 + N\left[\alpha\left(\frac{t}{N^2}\right) - 1\right]\,. \tag{6.25}$$

This is the N-Reggeon cut.

The discontinuity is extracted by noting that (6.25) is real below the 2N-particle threshold but picks up an imaginary part at this threshold. Hence, $a^i(j_Q)$ will have a cut at $j = \alpha_N^*(t)$ and will not have a cut at $j = \alpha_N(t)$. Consequently (6.22) has the formal structure

$$a(j) - a^i(j) = \Gamma(j)\, a(j)\, a^i(j) \,, \tag{6.26}$$

where $\Gamma(j)$ denotes the phase-space which generates the cut and $a^i(j)$ has no cut. Therefore we can write

$$\delta a(j) = a(j^+) - a(j^-) = \left[\Gamma(j^+)\, a(j^+) - \Gamma(j^-)\, a(j^-)\right] a^i(j) \tag{6.27}$$

$$= \left[\Gamma(j^+)\, \delta a(j) + \delta\Gamma(j)\, a(j^-)\right] a^i(j) \tag{6.28}$$

$$\Rightarrow \left[1 - \Gamma(j^+)\, a^i(j)\right] \delta a(j) = \delta\Gamma(j)\, a(j^-)\, a^i(j) \tag{6.29}$$

$$= \left[1 - \Gamma(j^+)\, a^i(j)\right] \delta\Gamma(j)\, a(j^+)\, a(j^-) \tag{6.30}$$

which has the solution

$$\delta a(j) = \delta\Gamma(j)\, a(j^+)\, a(j^-) \tag{6.31}$$

where $\delta\Gamma(j)$ is the discontinuity given by the phase-space $\Gamma(j)$.

This discontinuity is most simply taken by continuing (6.22) to negative t's. To make this continuation we extract all kinematic threshold factors from $A_{\underset{\sim}{\alpha}}(j_Q)$. It has thresholds at $\lambda(t_i,t_j,t_k) = 0$ for all i-j-k vertices. Since we evaluate $A_{\underset{\sim}{\alpha}}(j_Q)$ at a nonsense point at each vertex it can be shown from the Froissart-Gribov formula that these are just square-root branch-points and they can thus be combined with the phase-space factor $\int d\rho'$.

Therefore if we define $M(j_Q)$ from $A(j_Q)$ by removing all threshold factors and absorbing all other irrelevant kinematic factors, it can be shown that for negative t's we can write

$$\Gamma(j) = \int \frac{d\rho'}{j - 1 - \sum_{r=1}^{N} (\alpha_r - 1)} \to \int_{\lambda<0} \frac{\prod_j dt_j}{\prod_{i,j,k} \left[-\lambda(t_i,t_j,t_k)\right]^{1/2}} \frac{1}{j - 1 - \sum_{r=1}^{N} (\alpha_r - 1)} \,. \tag{6.32}$$

$\delta\Gamma(j)$ is now evaluated by replacing the pole factor in (6.32) by a δ-function. Hence, adding the contribution from all phase-space Toller diagrams T_N we obtain the complete discontinuity across the N-Reggeon cut in the form

$$M(j_Q^+) - M(j_Q^-) = (-1)^{N-1}\, i \sin \pi/2\, j_Q \sum_{T_N} \xi_{T_N} \int_{\lambda<0} \frac{\prod_j dt_j}{\prod_{i,j,k} \left[-\lambda(t_i,t_j,t_k)\right]^{1/2}} \times$$

$$\times \delta\left[j_Q - 1 - \sum_{r=1}^{N} (\alpha_r - 1) \right] M(j_Q^+)\, M(j_Q^-) \,. \qquad (6.33)$$

Note that we have suppressed arbitrary external angular momentum and helicity labels on $M(J_Q)$ so this is a very general result.

We have also suppressed many of the details of the last stages of the derivation of this result simply because of their complexity. For example, we should have taken care of boundary-values onto Regge cuts in internal channels besides the t_k channels in which we inserted Regge poles. We chose these channels for simplicity. The N-Reggeon cut trajectory first picks up an imaginary part at the 2N particle threshold, and the associated unitarity integral is the simplest place to isolate and study this cut. However, as in momentum space, cuts in sub-channel angular momenta also contribute to a cut in the total angular momentum and we should have studied this point.

Fortunately, details of sub-channel boundary-values and all other features of (6.33) are compactly summarized by noting that when summed over all N-Reggeon cuts (6.33) is analogous to a quasi-unitarity relation for intermediate states associated with quasi-particles carrying two-dimensional momentum $\underset{\sim}{k}_i$, where $\underset{\sim}{k}_i^2 = t_i$ $\forall$ i and energy $E_i = 1 - j_i$ with the non-relativistic energy momentum relation $E = 1 - \alpha(\underset{\sim}{k}^2)$:

$$\delta\left[j_Q - 1 - \sum_{k=1}^{N} (\alpha_k - 1) \right] \leftrightarrow \int \prod_K dE_K\, \delta\left(E - \sum_{k=1}^{N} E_K\right) \delta(E_K - 1 + \alpha_k)$$

$$\Rightarrow \text{energy conservation + "energy shell" conditions}$$

$$\int \frac{dt_j\, dt_k}{\left[-\lambda(t_i,t_j,t_k)\right]^{1/2}} \leftrightarrow \int d^2\underset{\sim}{K}_k\, d^2\underset{\sim}{K}_j\, \delta^2(\underset{\sim}{K}_i - \underset{\sim}{K}_k - \underset{\sim}{K}_j)$$

$$\Rightarrow \text{momentum conservation + phase-space integration} \,.$$

We have arrived at these last results after a long study of analyticity, unitarity, and Regge theory. It will be the purpose of the following course of lectures to solve (6.33) for the Pomeron using the above analogy as a basis.

The function of the sin $\pi/2$ j signature factor in (6.33) is simply to ensure that Regge cuts do not give singularities in t-channel partial waves. The $(-1)^{N-1}$ factor is, however, crucial when studying the Pomeron. It says that multi-Pomeron cuts have alternating sign imaginary parts. This makes (6.33) a very unconventional unitarity relation.

REFERENCES

[1] T. Regge, Nuovo Cimento 14, 951 (1959); 18, 947 (1960).

[2] G.F. Chew and S. Frautschi, Phys. Rev. Letters 7, 394 (1961).

[3] V.N. Gribov, Soviet Phys. JETP 14, 478 and 1395 (1962).

[4] D. Amati, A. Stanghellini and S. Fubini, Nuovo Cimento 26, 896 (1962).

[5] S. Mandelstam, Nuovo Cimento 30, 1127 and 1148 (1963).

[6] J.C. Polkinghorne, J. Math. Phys. 4, 1396 (1963).

[7] V.N. Gribov, Soviet Phys. JETP 26, 414 (1968).

[8] J. Coster and H.P. Stapp, LBL-2427, to be published in J. Math. Phys.
K.E. Cahill and H.P. Stapp, LBL-2428, to be published in Ann. Phys.
Early results were also obtained by M.J.W. Bloxham, D.I. Olive and
J.C. Polkinghorne, J. Math. Phys. 10, 494, 545 and 553 (1969).

[9] J. Bros, Trieste seminar on High-Energy Physics and Elementary Particles
(ed. A. Salam) (IAEA, Vienna, 1965), p. 85.

[10] M. Toller, Riv. Nuovo Cimento 1, 403 (1969); Nuovo Cimento 62A, 341 (1969).

[11] V.N. Gribov, I. Ya Pomeranchuk and K.A. Ter-Martirosyan, Phys. Rev. B 139,
184 (1965).

[12] P. Goddard and A.R. White, Nuovo Cimento 1A, 645 (1971).
A.R. White, Nuclear Phys. B39, 432 (1972).

[13] N. Bali, G.F. Chew and A. Pignotti, Phys. Rev. 163, 1572 (1967).

[14] R.C. Brower, C.E. De Tar and J.H. Weis, Physics Reports 14C, 257 (1974).

[15] P. Goddard and A.R. White, Nuclear Phys. B17, 45 (1970).

[16] A.R. White, Nuclear Phys. B67, 189 (1973).

[17] J.H. Weis, Phys. Rev. D 6, 1977 (1971); D 5, 1043 (1972).

[18] I.G. Halliday, Nuclear Phys. B33, 285 (1971).

[19] J. Bartels, Phys. Rev. D 11, 2977 and 2989 (1975).

[20] J.H. Weis, Phys. Letters 43B, 487 (1973).

[21] C.E. De Tar and J.H. Weis, Phys. Rev. D 6, 3161 (1971).

[22] A.R. White, Nuclear Phys. B50, 93 and 130 (1972); Phys. Rev. D 10, 1236
(1974).

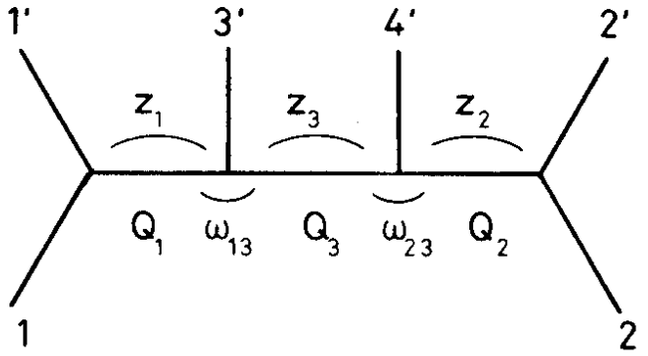

Fig. 2.1 A Toller diagram for the six-point function

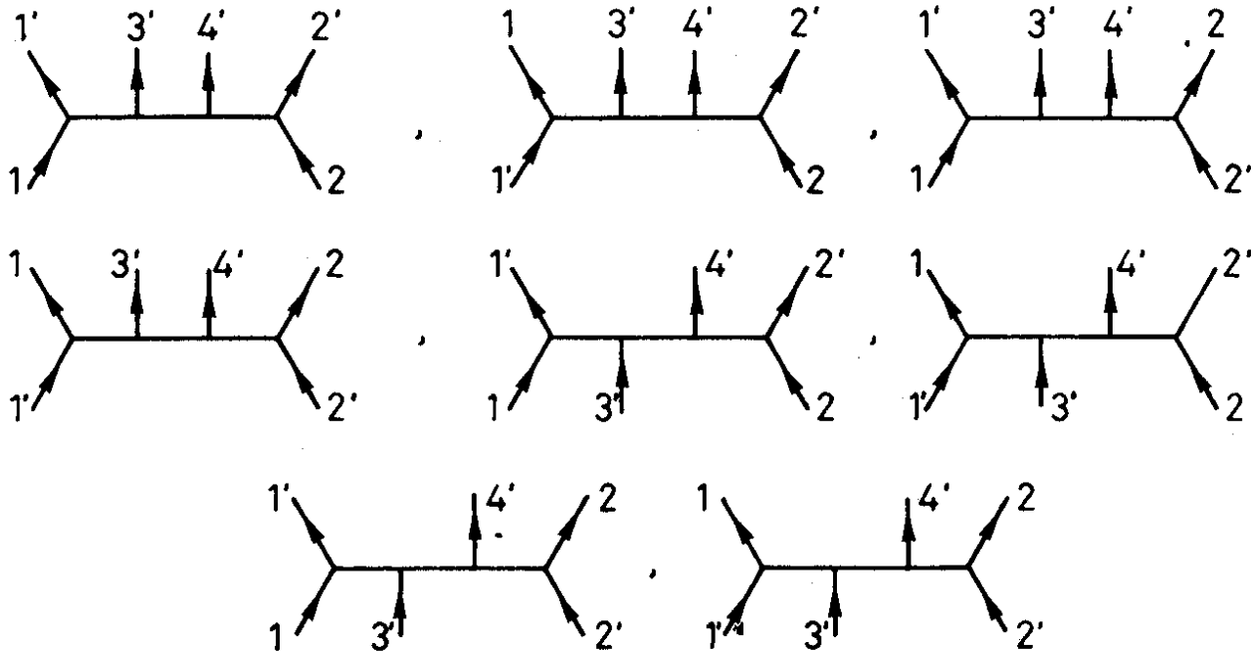

Fig. 2.2 Direct channels for the Toller diagram of Fig. 2.1

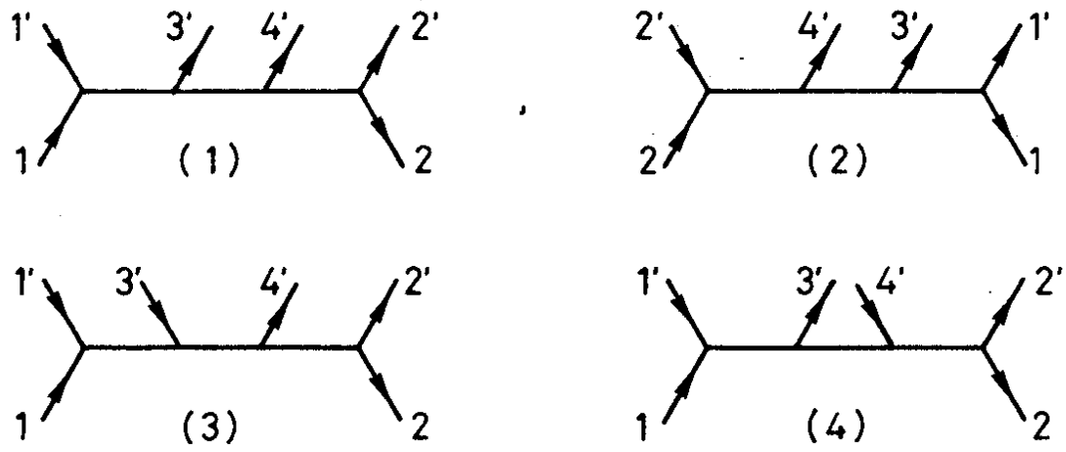

Fig. 2.3 Cross-channels for the Toller diagram of Fig. 2.1

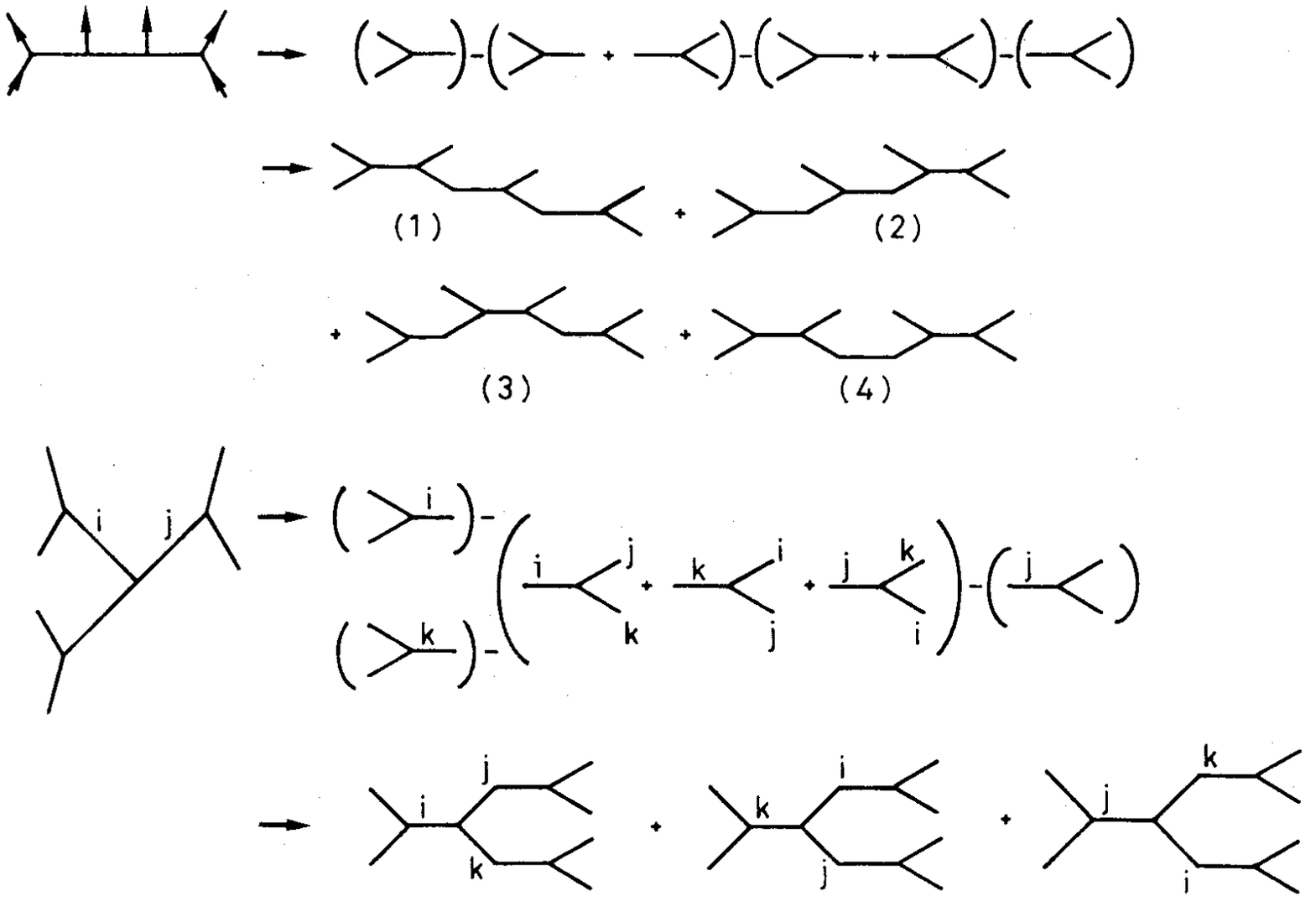

Fig. 2.4 The construction of hexagraphs for the six-point function

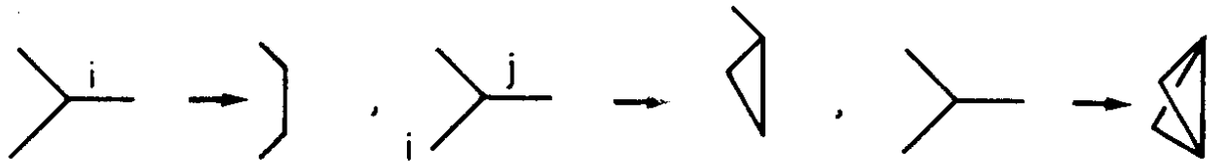

Fig. 2.5 The mapping of hexagraphs into flow graphs

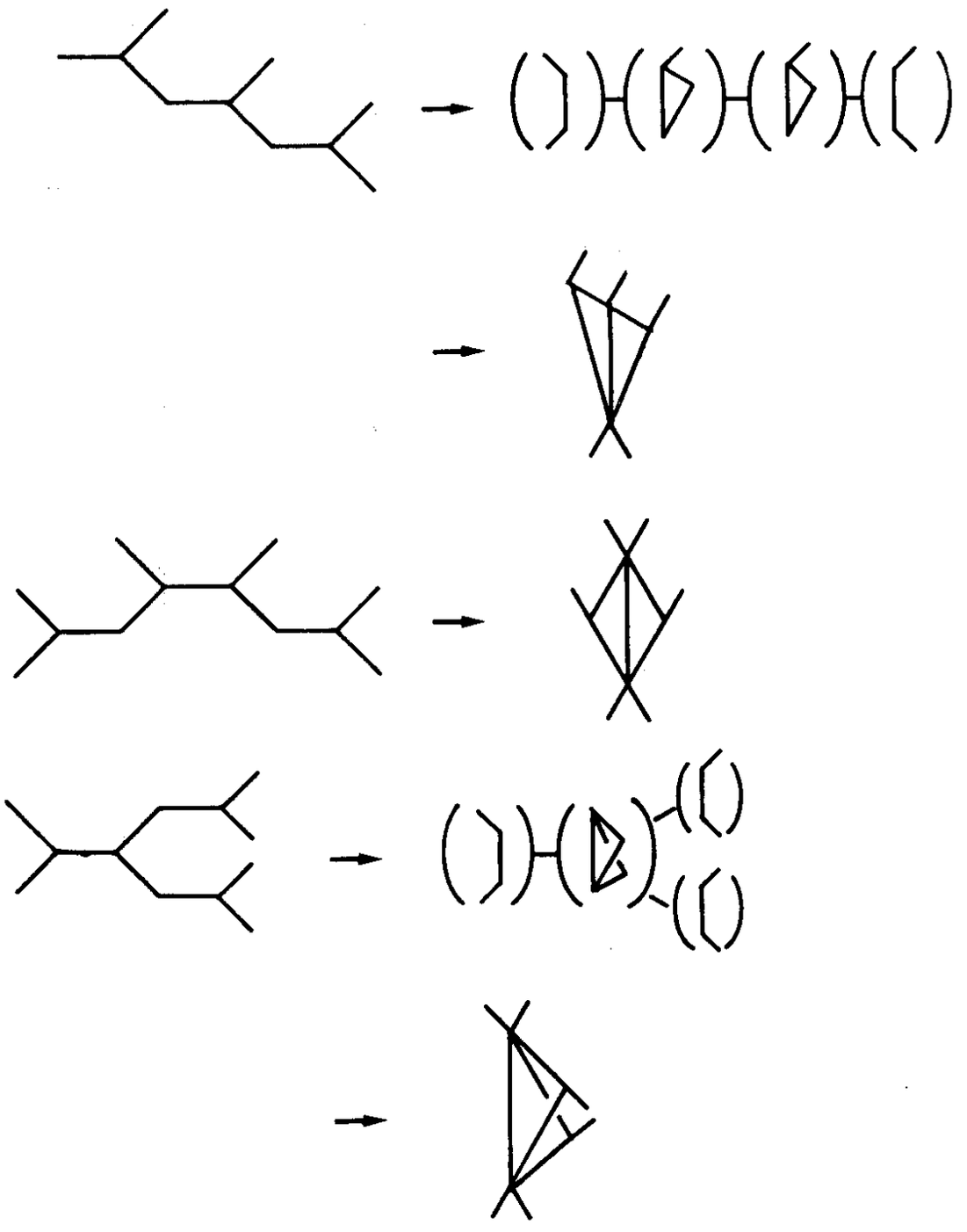

Fig. 2.6 The formation of flow graphs

Fig. 2.7 Complex cuts protruding from normal threshold cuts

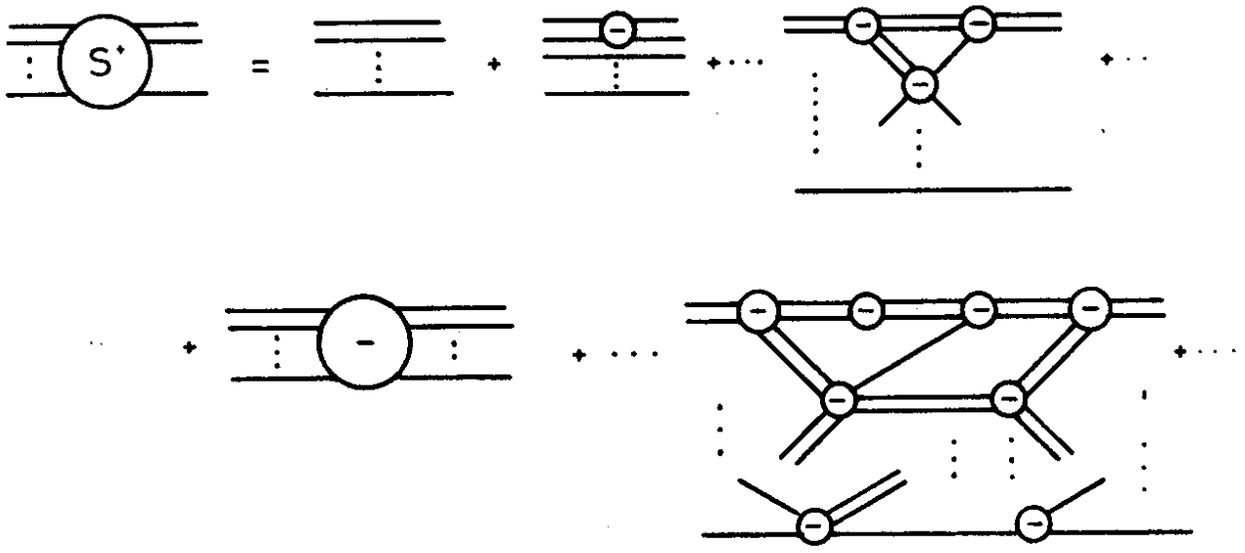

Fig. 2.8 The bubble diagram scattering expansion

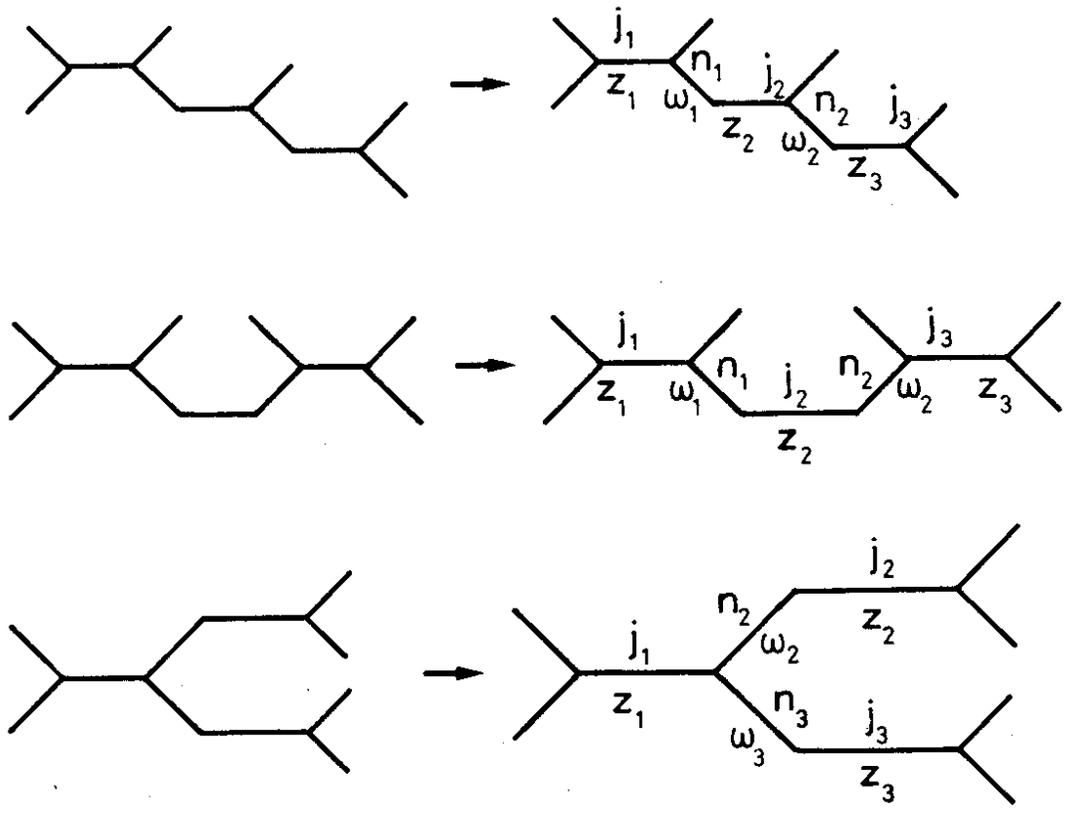

Fig. 3.1 Examples of the assignment of variables to the lines of hexagraphs

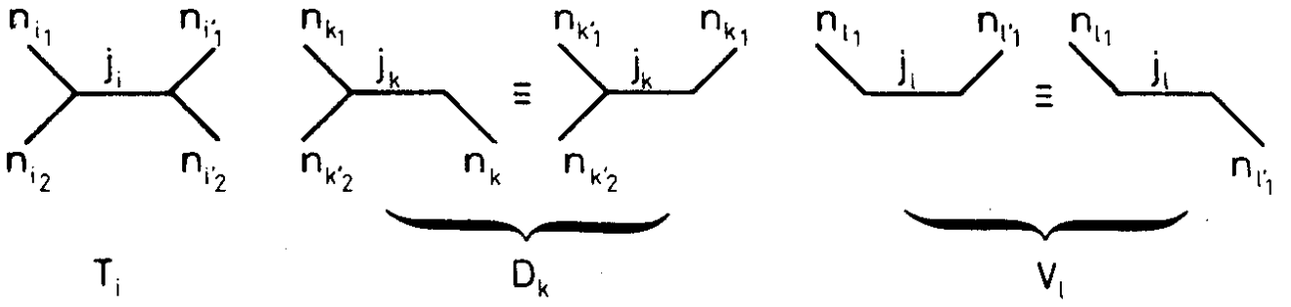

Fig. 3.2 The subgraphs of a hexagraph

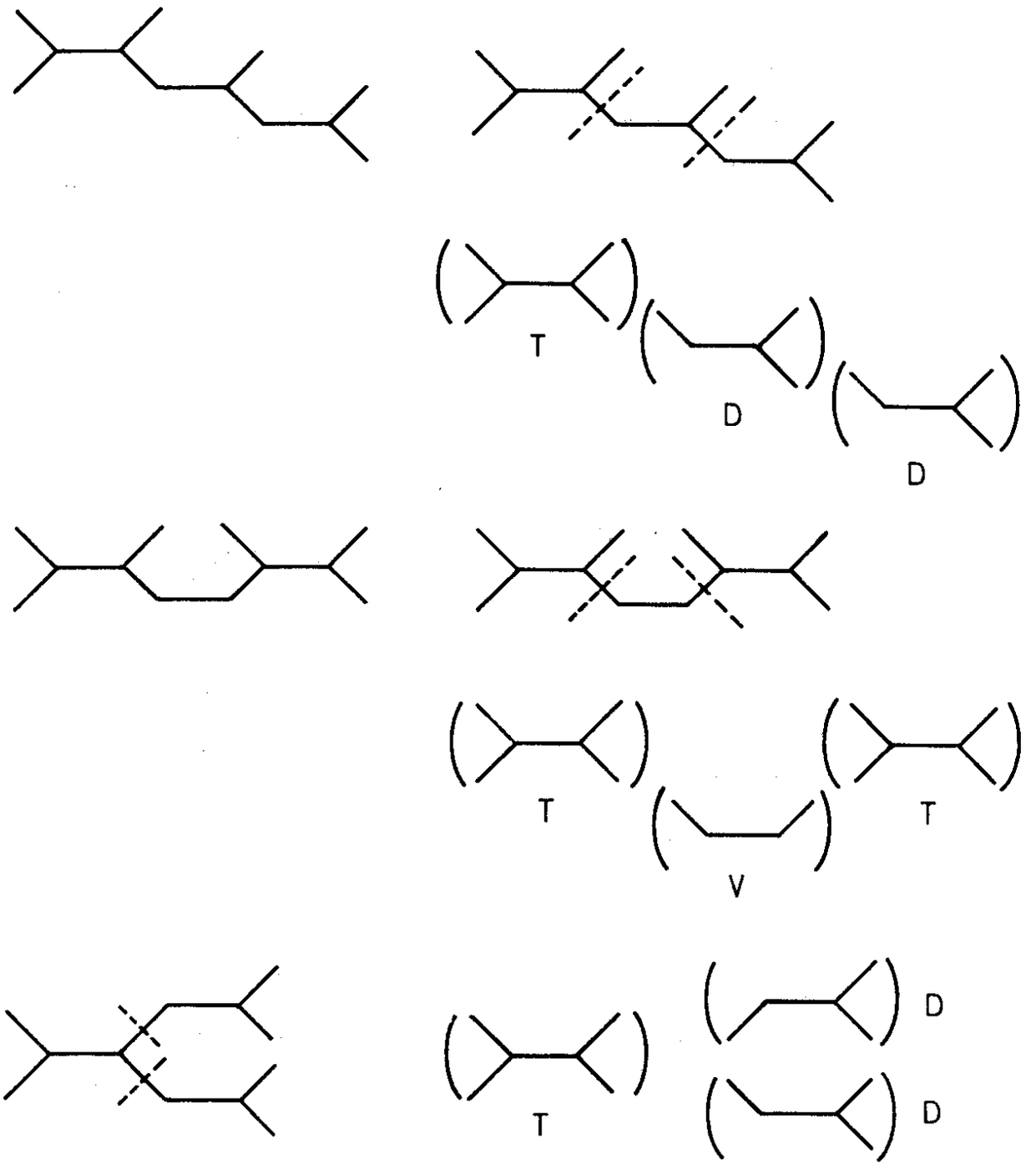

Fig. 3.3 Examples of the breakdown of hexagraphs into subgraphs

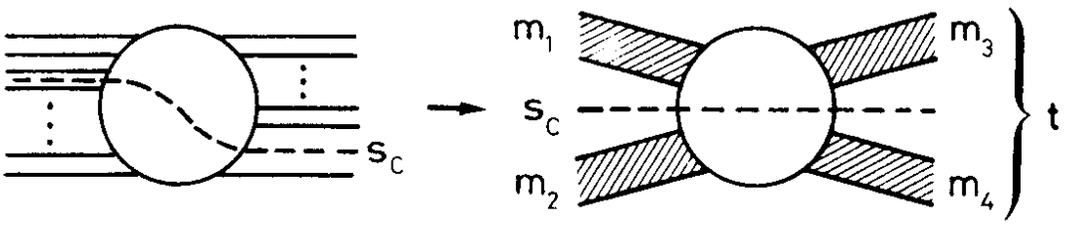

Fig. 3.4 A general amplitude treated as a four-point function

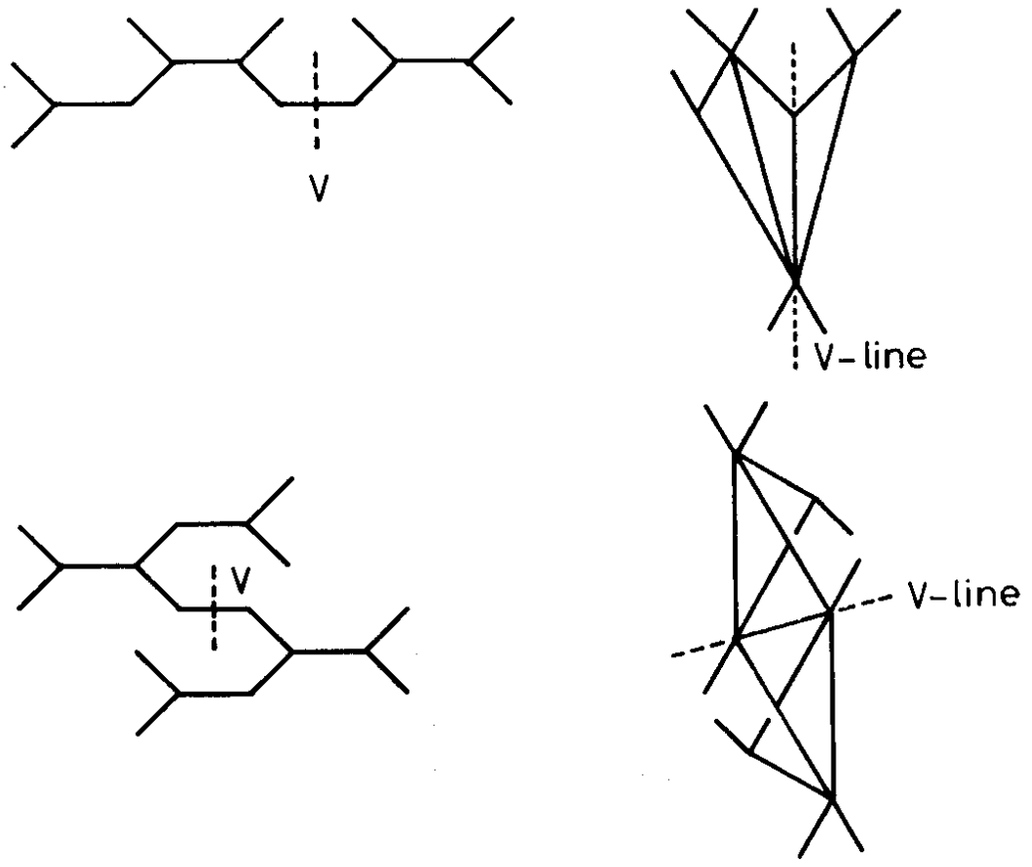

Fig. 3.5 Examples of V-lines of hexagraphs

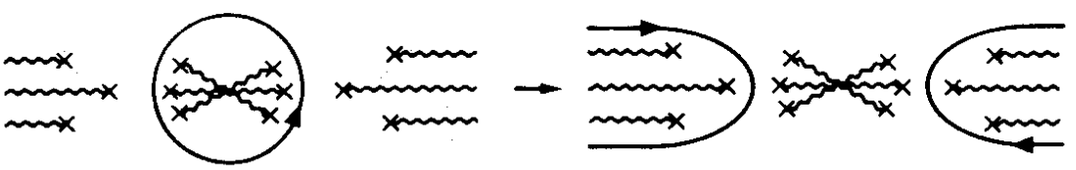

Fig. 3.6 The manipulation of a contour in a u-plane

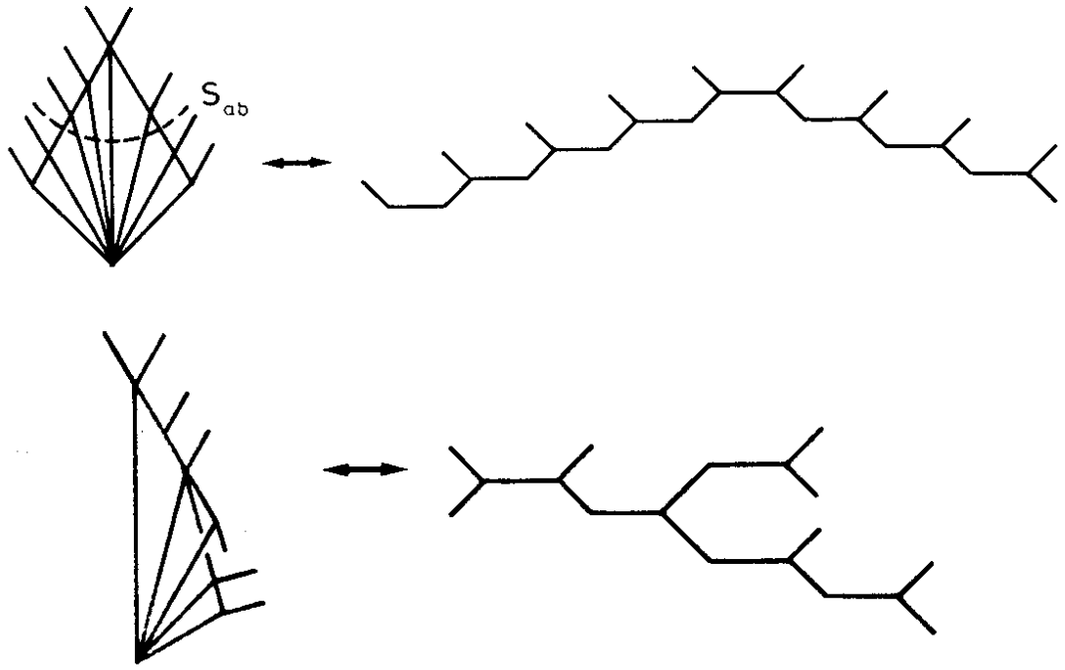

Fig. 3.7 Examples of pieces and their hexagraphs

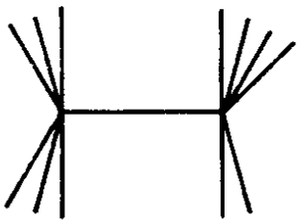

Fig. 3.8 The contraction of a hexagraph to a single internal line

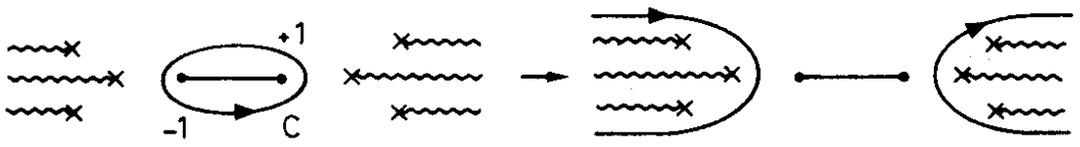

Fig. 3.9 The manipulation of a contour in the z-plane

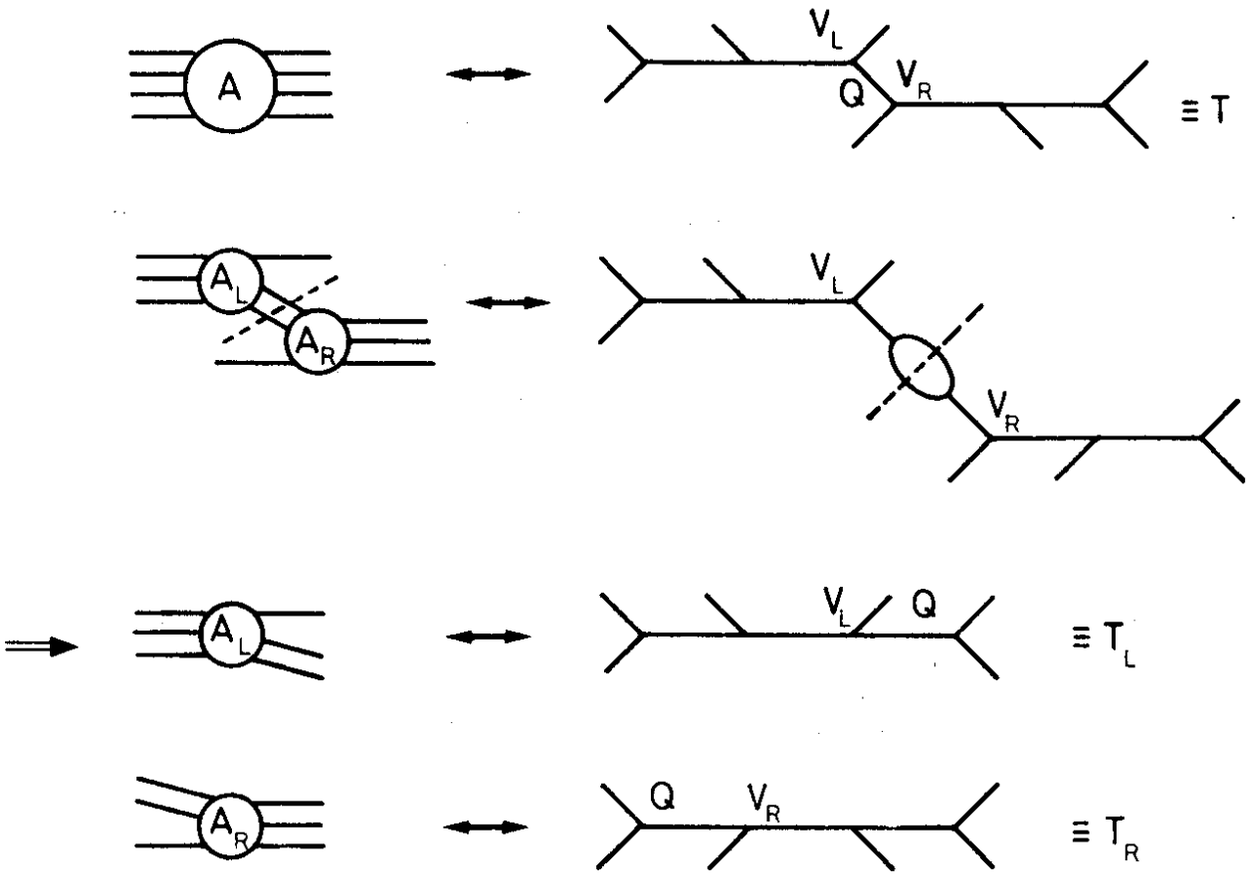

Fig. 4.1 The cutting of a Toller diagram T into Toller diagrams T_L and T_R

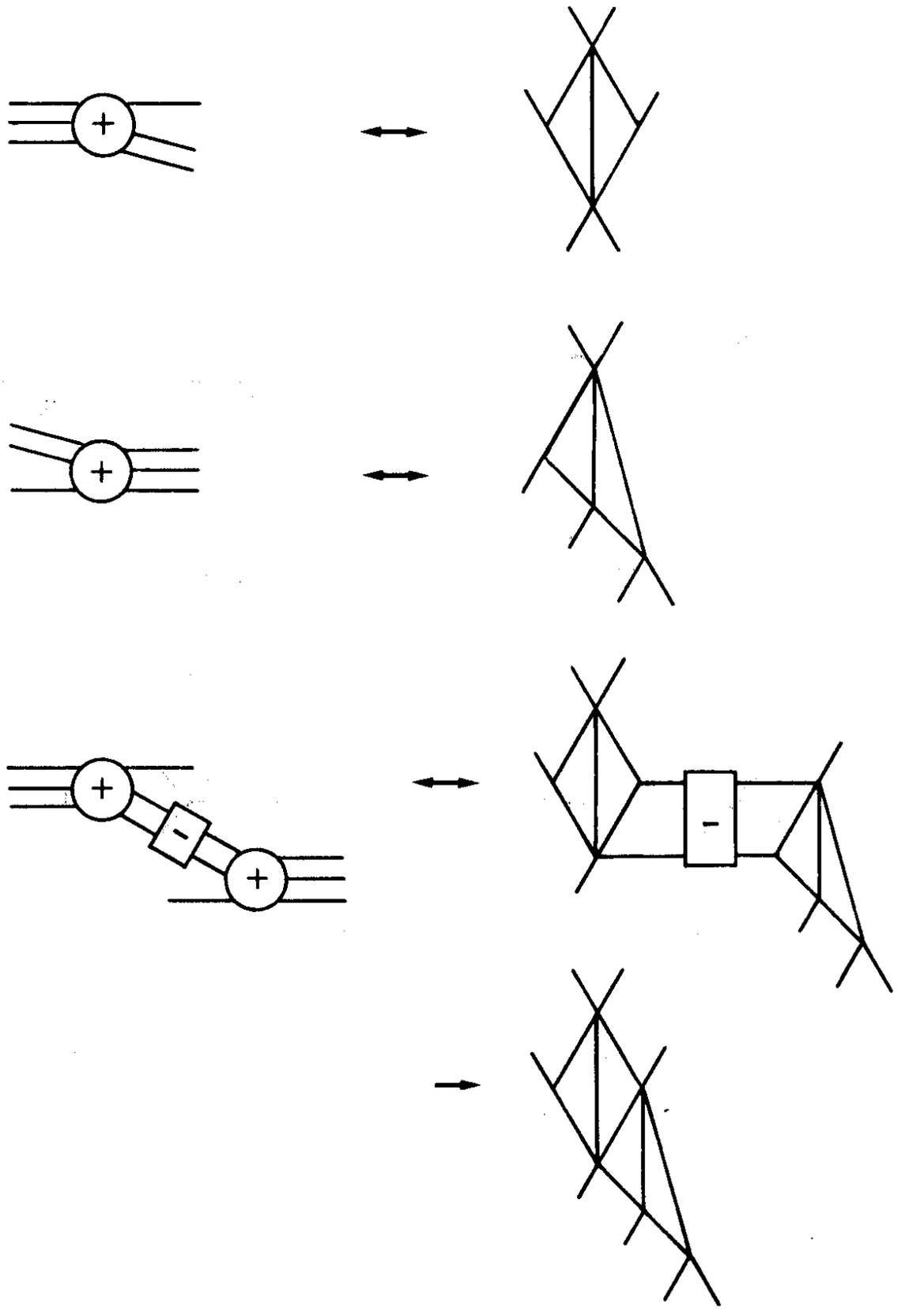

Fig. 4.2 The formation of a product flow graph

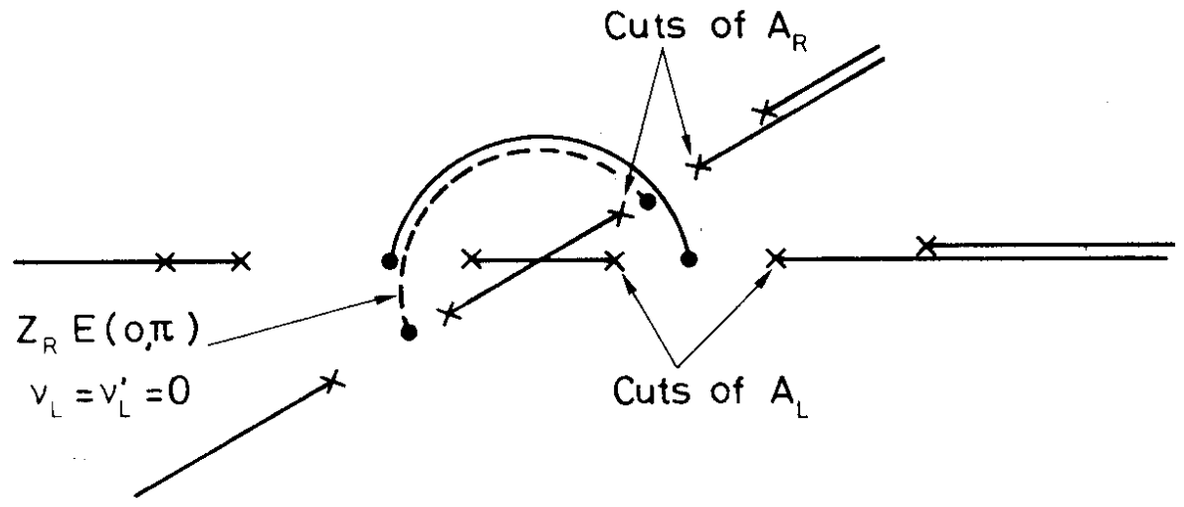

Fig. 4.3 The ν_L-plane

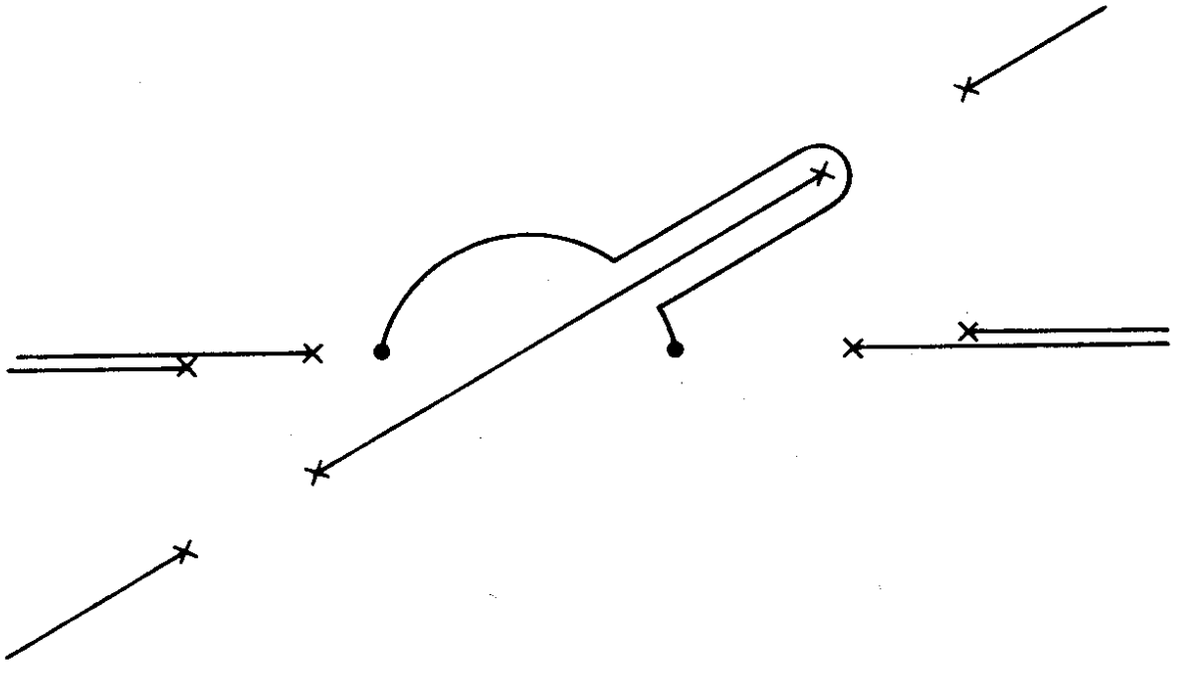

Fig. 4.4 The distortion of the ν_L contour as $\nu_{LR} \to \infty$

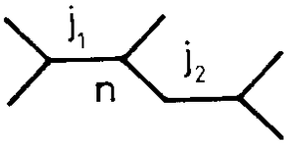

Fig. 4.5 A hexagraph for the five-point function

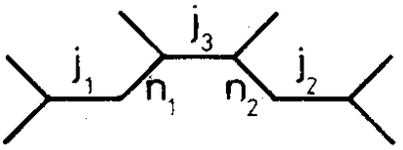

Fig. 4.6 A hexagraph for the six-point function

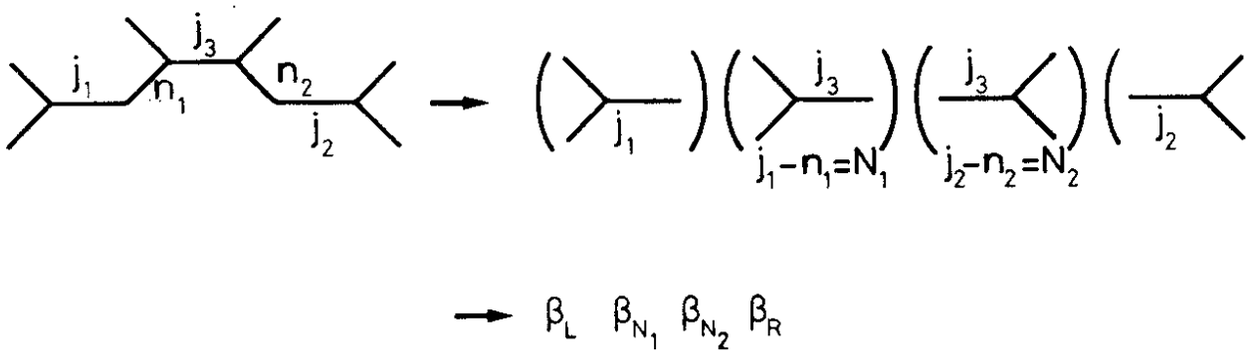

Fig. 4.7 Factorization of Regge pole residues associated with the hexagraph of Fig. 4.6

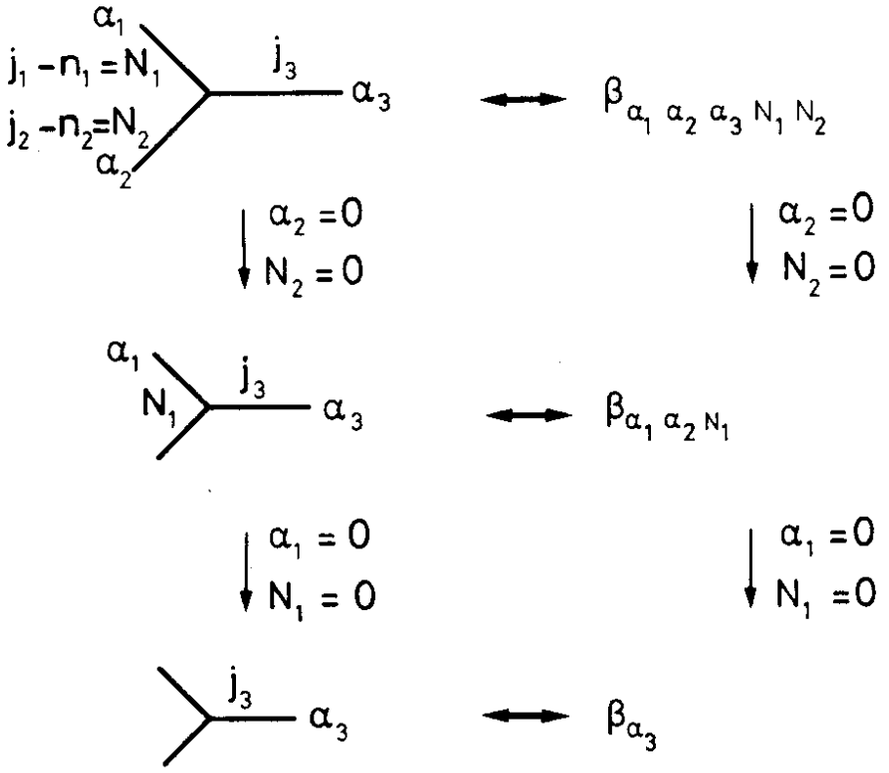

Fig. 4.8 The general mapping of a hexagraph into a factorized residue function

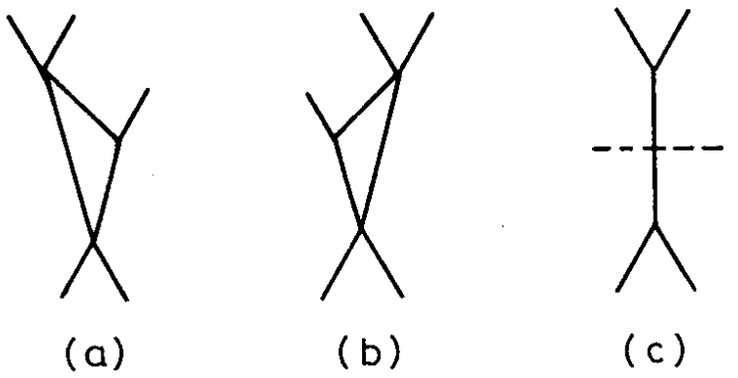

Fig. 5.1 Flow graphs for the five-point function

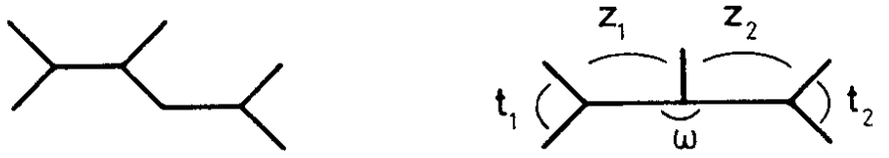

Fig. 5.2 A hexagraph and a Toller diagram for the five-point function

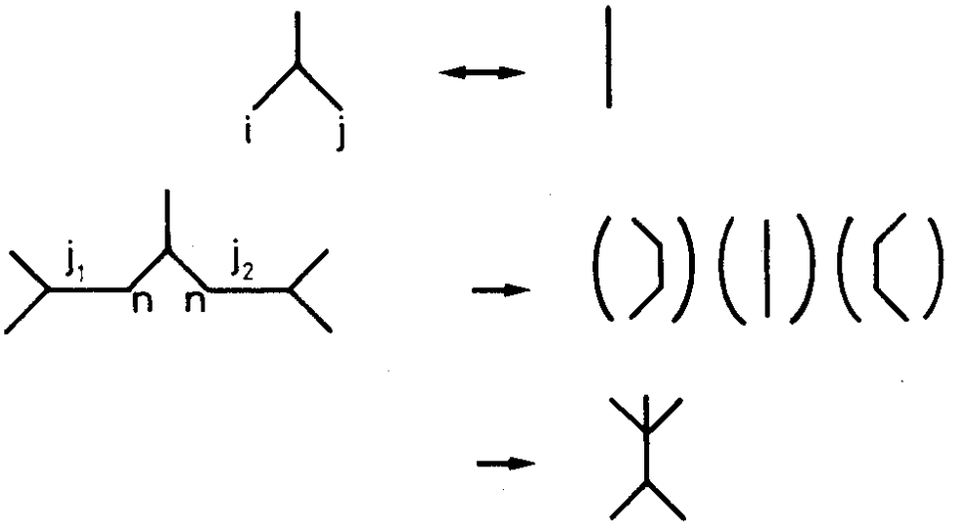

Fig. 5.3 The formation of flow graphs from hexagraphs for non-basic graphs

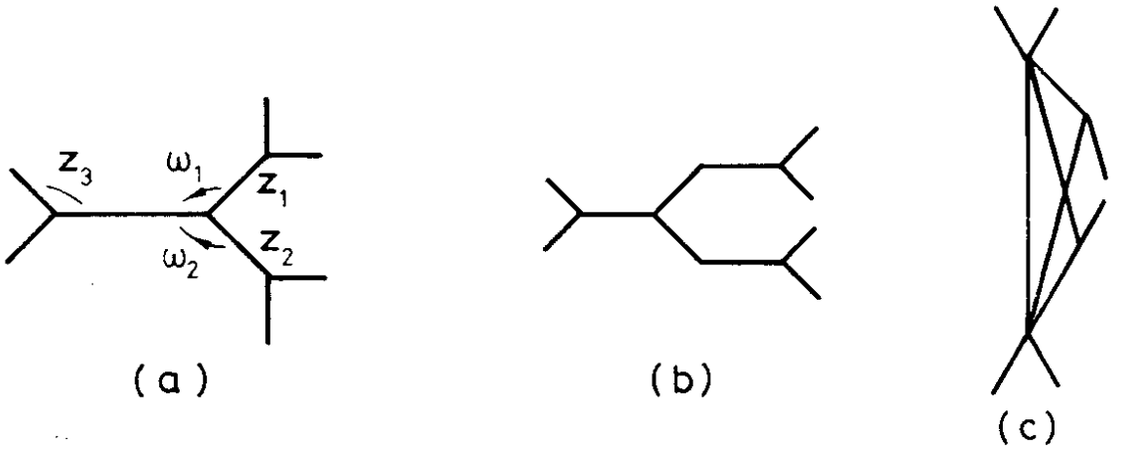

Fig. 5.4 A Toller diagram, a hexagraph, and a flow graph for the six-point function

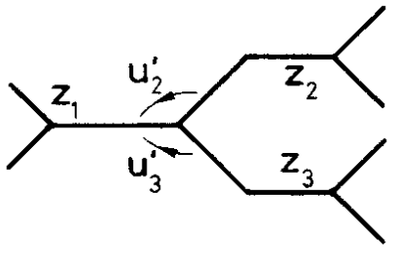

Fig. 5.5 A hexagraph for the six-point function

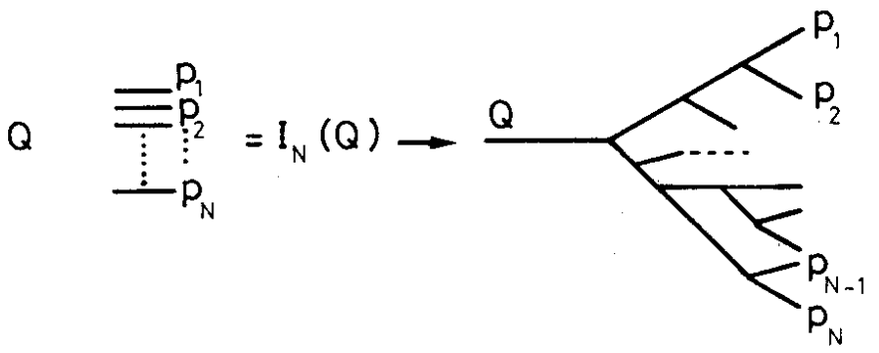

Fig. 6.1 A Toller diagram for N-particle phase-space

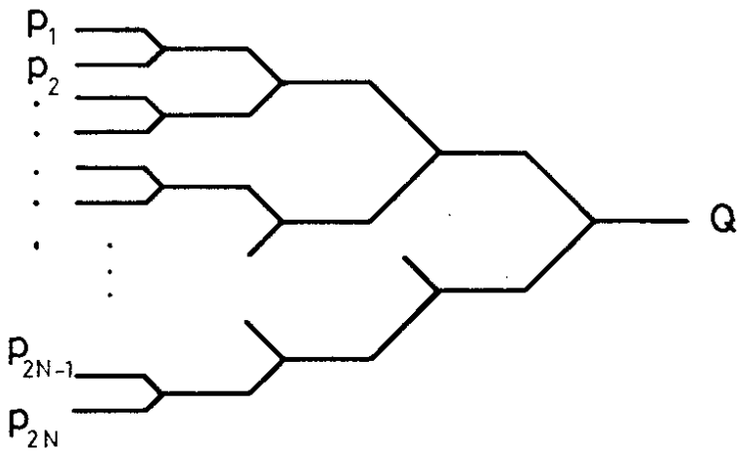

Fig. 6.2 The hexagraph for the spectral component which generates an N-Reggeon cut in the 2N-particle phase-space

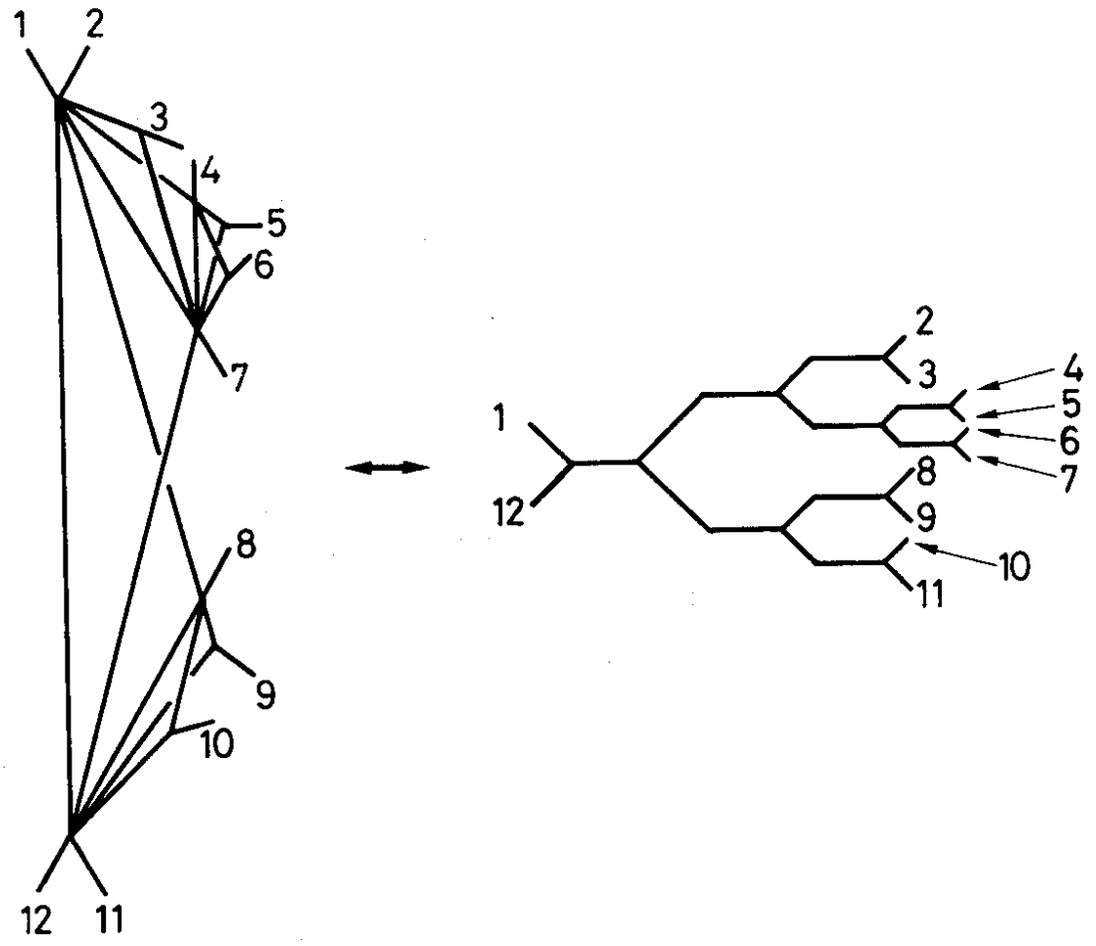

Fig. 6.3 A flow graph and hexagraph associated with the generation of Regge cuts

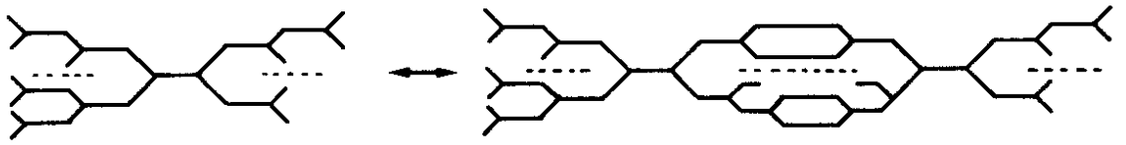

Fig. 6.4 The diagonalization of a unitarity integral by spectral components illustrated with hexagraphs

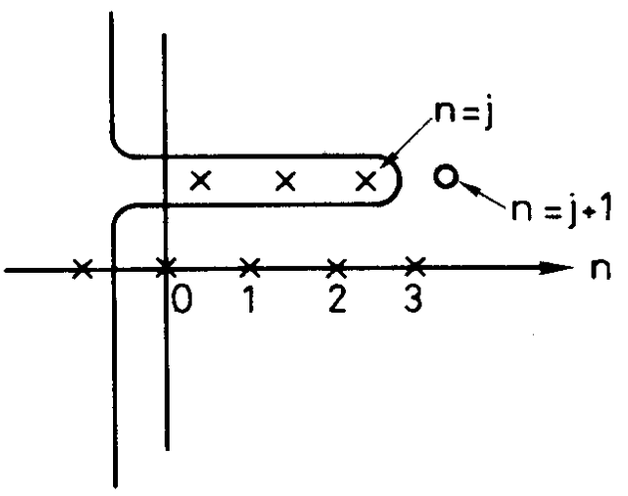

Fig. 6.5 The helicity contour in a unitarity integral continued in the complex angular momentum plane